CalVal Jason
CLS.DOS/NT/07-254
Version : 1rev0, December 21, 2007
Nomenclature : SALP-RP-MA-EA-21484-CLS

Ramonville, December 21, 2007

Jason-1 validation and cross calibration activities

Contract No 60453/00 - lot2.C

	AUTHORS	COMPANY	DATE	INITIALS
WRITTEN BY	M. Ablain S. Philipps	CLS CLS		
APPROVED BY	J. Dorandeu	CLS		
QUALITY VISA	DT/AQM	CLS		
APPLICATION AUTHORISED BY				

CLS - 8-10 Rue Hermès - Parc Technologique du Canal - 31520 Ramonville St-Agne - FRANCE
Telephone 33 5 61 39 47 00 / Fax 33 5 61 75 10 14

CHRONOLOGY ISSUE

Control Initials	ISSUE	DATE	REASON FOR CHANGE
	1.0		Creation

LIST OF ACRONYMS

TBC	To Be Confirmed

List of Tables

List of Figures

Contents

APPLICABLE DOCUMENTS / REFERENCE DOCUMENTS

1 Introduction

This document presents the synthesis report concerning validation activities of Jason-1 GDRs under SALP contract (N° 60453/00 Lot2.C) supported by CNES at the CLS Space Oceanography Division. It is divided into two parts: CAL/VAL Jason-1 activities - Jason-1 / T/P cross-calibration.

Since the beginning of the mission, Jason-1 data have been analyzed and monitored in order to assess the quality of Jason-1 GDR products (AVISO and PODAAC User handbook, [51]) for oceanographic applications. This report is basically concerned with long-term monitoring of the Jason-1 altimeter system, from all GDR products available to date, that is for almost 6 years of data (cycles 1 to 214). This includes careful monitoring of all altimeter and radiometer parameters, performance assessment, geophysical evaluation and cross-calibration with T/P measurements. Moreover specific studies are presented in this document :

- the comparisons of the new GDRs release (version "b") with the former GDRs (version"a")
- the comparisons between the mean sea level and the sea surface temperature for all operational altimeter missions.

This work is routinely performed at CLS and in this frame, besides continuous analyzes in terms of altimeter data quality, Jason-1 GDR Quality Assessment Reports (e.g. Ablain et al. 2007 [4]) are produced and associated to data dissemination. Even if only low order statistics are mainly presented here, other analyzes including histograms, plots and maps are continuously produced and used in the quality assessment process. The work performed in terms of data quality assessment also includes cross-calibration analyzes mainly with the T/P mission until November 2005 (end of the T/P mission). Even if T/P mission is finished, cross-calibration analyzes are useful for the reprocessing activities in order to study the sea state bias or the SSH bias for instance.
Indeed, it is now well recognized that the usefulness of any altimeter data only makes sense in a multi-mission context, given the growing importance of scientific needs and applications, in particular for operational oceanography. One major objective of the Jason-1 mission is to continue the T/P high precision altimetry and to allow combination with other missions (ENVISAT, GFO). This kind of comparisons between different altimeter missions flying together provides a large number of estimations and consequently efficient long term monitoring of instrument measurements. Of course, other sources of comparisons are also needed, using independent datasets (e.g. Queffeulou et al. 2004 [54], Ray and Beckley 2003 [57], Arnault et al. 2004 [8], Provost et al. 2004 [52]). [69] and [70] show comparisons between altimeter data and in-situ data (respectively tide gauge measurements and T/S profilers).

2 Processing status

2.1 GDR and CAL/VAL Processing

Jason-1 GDRs (in version "b") from cycle 1 to 214 (till 28/10/2007), are used in this report. Since cycle 136, Jason-1 products are produced by CMA ground processing software in version "b" (see section 2.3). During 2006 and 2007 the previous cycles (1 to 135) were reprocessed at NASA and CNES and delivered in version "b". Therefore the whole mission is now available in a homogeneous time-series. The purpose of this document is to report the major features of the data quality from the Jason-1 mission. Moreover, the document is associated with comparison results from T/P GDRs. All these cycle reports are available on AVISO website: http://www.jason.oceanobs.com. In addition to these reports, several meeting (CAVE, OSTST) have been performed to inform the Jason-1 GDR's users about the main results and the studies in progress.

2.2 CAL/VAL status

2.2.1 Missing measurements

This section presents a summary of major satellite events that occurred from cycle 1 to 214. Table 1 gives a status about the number of missing passes (or partly missing) for GDRs version "b" and the associated events for each cycle.
For some cycle this table may be different from the table shown in the previous report, as reprocessing helped to recover some passes missing due to ground processing issues in GDRs version "a".
Gyro calibration, Star Tracker unavailability and ground processing issues were the main events which produced missing data from cycle 1 to 64 (2002 and 2003).
During year 2004 (cycle 65 to 109), 2 safe hold mode incidents have produced 15 days of missing data due to a wheel anomaly. As result of this incident, only 3 wheels have been available but this has had no impact on scientific applications.
During year 2005 (110-146), most of incidents are due to SEU on C Band. Few passes have only been impacted every time. During year 2006 (cycles 147 - 183) Jason-1 experienced a safe hold mode (cycle 177 to 179) producing 17 days of missing data due to mass memory error. In addition 2 altimeter SEU occurred. It also happened that small data gaps occur (less than a minute duration).
During 2007 (cycles 183 to 214) Jason-1 had experienced several altimeter SEU.

Jason-1 Cycles	Number of Missing passes	Number of partly missing passes	Events
001	5	7	Science telemetry unavailability
002	16	0	On board Doris anomaly
003	0	2	Gyro-calibration
004	2	5	Gyro-calibration and Science telemetry unavailability
			.../...

Jason-1 Cycles	Number of Missing passes	Number of partly missing passes	Events
006	1	4	Altimeter echo data unavailability
007	0	2	Science telemetry unavailability
008	2	5	Ground processing issue
009	3	4	Poseidon-2 altimeter SEU and Gyro-calibration
010	0	2	Gyro-calibration
015	0	1	Ground processing issue
019	0	1	Ground processing issue
021	0	1	Star tracker unavailability
023	0	1	Ground processing issue
026	0	2	Gyro-calibration
027	0	2	Gyro-calibration
031	0	1	Star tracker unavailability
038	0	4	Ground processing issue
039	0	1	Gyro-calibration
042	5	2	Poseidon-2 altimeter SEU
045	0	3	Gyro-calibration
046	0	1	Poseidon-2 altimeter SEU
048	0	1	Gyro-calibration
062	0	1	Ground processing issue
064	0	2	Exceptional calibrations
075	4	0	Poseidon-2 altimeter SEU
077	69	0	Safe hold mode (15/02/04 to 21/02/04)
078	82	0	Safe hold mode (15/02/04 to 21/02/04)
080	0	1	Calibration over ocean
082	54	1	Failure in module 3 of PLTM2
087	0	1	Calibration over ocean

.../...

Jason-1 Cycles	Number of Missing passes	Number of partly missing passes	Events
091	2	4	DORIS instrument switch to redundancy and altimeter incident (no C band information)
094	0	1	Under investigation : altimeter incident or star tracker unavailability
099	0	1	Under investigation : altimeter incident or star tracker unavailability
101	0	1	Under investigation : altimeter incident or star tracker unavailability
102	1	0	Altimeter SEU (no C band information)
103	0	2	Altimeter SEU (no C band information)
104	0	1	No data between 21:29:18 and 21:30:07 on November 8th pass 189
106	3	2	Altimeter SEU (no C band information)
108	0	2	Altimeter SEU (no C band information)
114	3	1	Altimeter SEU (no C band information)
115	0	4	2 altimeter SEU incidents (C band) and altimeter initialization procedure.
118	6	2	Altimeter SEU (no C band information)
131	0	7	TRSR2 "elephant packets" anomaly
132	0	1	Altimeter SEU (no C band information)
133	0	2	Altimeter SEU (no C band information)
136	104	2	Altimeter SEU (no C band information), Platform incident (20/09/05 to 28/09/05)

.../...

Jason-1 Cycles	Number of Missing passes	Number of partly missing passes	Events
137	91	2	Platform incident (20/09/05 to 28/09/05)
161	0	5	TRSR elephant packets
165	0	1	(planned) Poseidon calibration (board filter)
173	0	3	Altimeter SEU (no C band information)
177	141	1	Safehold mode (30/10/2006 to 16/11/2006)
178	254	0	Safehold mode (30/10/2006 to 16/11/2006)
179	45	1	Safehold mode (30/10/2006 to 16/11/2006)
181	5	2	Altimeter SEU
185	0	3	calibration over ocean
191	0	2	Altimeter SEU
192	0	1	calibration over ocean
198	1	1	Altimeter SEU
200	0	1	Altimeter SEU
206	0	3	calibration over ocean

Table 1: *M*issing pass status

2.2.2 Edited measurements

Table 2 indicates the cycles which have a larger amount of removed data due to editing criteria (see section 3.2.1). Most of the occurrences correspond to dual-ionospheric correction at default value (altimeter SEU) or missing radiometer wet troposphere correction (following safehold modes).
Notice that since cycle 78, the satellite operates with only 3 wheels: the maneuver impact (burn maneuver, yaw transition) is greater than before on the attitude control. Consequently, some measurements could previously be edited due to higher mispointing values when a maneuver occurs. Improvements in ground retracking algorithm have been set up in place and are applied in the GDR "b" release, and improvements on Star Tracker behavior are performed in 2006. Therefore only few measurements were edited by mispointing criterion.

Jason-1 Cycles	Comments
001	Passes 252 to 254 are edited due to radiometer wet troposphere correction at default value.
006	Pass 56 (in the Pacific ocean) is partly edited due to the bad quality of data. Indeed, the altimetric parameters values are out of the thresholds.
008	All the altimetric parameters are edited for 10% of pass 252 due to the bad quality of all the altimetric parameters as a result of a Star Tracker incident leading to a quite high off nadir angle. Half of pass 252 edited by radiometer wet troposphere correction at default value.
009	Passes 004 and 005 partly edited by dual-ionospheric correction at default value (no c-band information).
019	Most of pass 010 is edited by radiometer wet troposphere correction at default value. Passes 19 to 21 are edited due to datation anomaly.
021	Small part of pass 210 is edited after checking the square of the mispointing angle criterion.
069	Passes 209 to 211 are edited due to the JMR set to default value. This is linked to the safe hold mode on cycle 69 : the JMR has been set on 2 hours after the altimeter.
078	Passes 83 to 85 are edited due to the JMR set to default value. This is linked to the safe hold mode on cycle 88 : the JMR has been set on 2 hours after the altimeter.
091	Passes 126, 127 and partly 130 are edited by dual-ionospheric correction at default value (no c-band information).
102	Passes 187, 188 and partly 189 are edited by dual-ionospheric correction at default value (no c-band information).
103	Passes 29 to 31 are edited by dual-ionospheric correction at default value (no c-band information).
108	Passes 16 and 17, as well as part of passes 15 and 18 are edited by dual-ionospheric correction at default value (no c-band information).
115	Passes 19 to 21 and 29 to 31 are edited by dual-ionospheric correction at default value (no c-band information).
133	Pass 13 is partly edited due to dual-ionospheric correction at default value (no c-band information).
137	Passes 92, 93 and partly 94 are edited by radiometer wet tropospheric correction, since the radiometer was later switched on than the other instruments.

.../...

Jason-1 Cycles	Comments
173	As the altimeter is only restarted during pass 68, the dual-frequency ionospheric correction is partially missing for passes 65 and 68 and fully for passes 66 and 67.
175	Pass 9 is partly edited by mispointing criterion out of threshold (probably aberrant quaternion).
179	As radiometer was only switch on later, passes 046 to 058, as well as part of pass 059 are edited by radiometer wet troposphere correction at default values.
181	Pass 247 is partly edited by dual-frequency ionosphere at default value (no C-band information).
198	Pass 073 is partly edited by dual-frequency ionosphere at default value (no C-band information).
212	Pass 187 is entirely edited: one half by altimetric parameters at default value, other half by apparent squared mispointing values out of thresholds. Pass 186 is partly edited by apparent squared mispointing values out of thresholds.

Table 2: *E*dited measurement status

2.3 Jason-1 product version "b"

2.3.1 Models and Standards History

Two versions of the Jason-1 Interim Geophysical Data Records (IGDRs) and Geophysical Data Records (GDRs) have been generated to date. These two versions are identified by the version numbers "a" and "b" in the name of the data products. For example, version "a" GDRs are named "JA1_GDR_2Pa" and version "b" GDRs are named "JA1_GDR_2Pb". Both versions adopt an identical data record format as described in Jason-1 User Handbook and differ only in the models and standards that they adopt. Version "a" I/GDRs were the first version released soon after launch. Version "b" I/GDRs were first implemented operationally from the start of cycle 140 for the IGDRs and cycle 136 for the GDRs. Reprocessing to generate version "b" GDRs for cycles 1-135 were performed in 2006 and 2007 in order to generate a consistent data set. The table 3 below summarizes the models and standards that are adopted in these two versions of the Jason I/GDRs. More details on some of these models are provided in Jason-1 User Handbook document.

Model	Product Version "a"	Product Version "b"
Orbit	JGM3 Gravity Field DORIS tracking data for IGDRs DORIS+SLR tracking data for GDRs	EIGEN-CG03C Gravity Field DORIS tracking data for IGDRs DORIS+SLR+GPS tracking data for GDRs
Altimeter Retracking	MLE3 + 1st order Brown model (mispointing estimated separately)	MLE4 + 2nd order Brown model : MLE4 simultaneously retrieves the 4 parameters that can be inverted from the altimeter waveforms: epoch, SWH, Sigma0 and mispointing angle. This algorithm is more robust for large off-nadir angles (up to 0.8°).
Altimeter Instrument Corrections	Consistent with MLE3 retracking algorithm.	Consistent with MLE4 retracking algorithm.
Jason Microwave Radiometer Parameters	Using calibration parameters derived from cycles 1-30.	Using calibration parameters derived from cycles 1-115.
Dry Troposphere Range Correction	From ECMWF atmospheric pressures.	From ECMWF atmospheric pressures and model for S1 and S2 atmospheric tides.
Wet Troposphere Range Correction from Model	From ECMWF model	From ECMWF model.
		.../...

Model	Product Version "a"	Product Version "b"
Back up model for Ku-band ionospheric range correction.	Derived from DORIS measurements.	Derived from DORIS measurements.
Sea State Bias Model	Empirical model derived from cycles 19-30 of version "a" data.	Empirical model derived from cycles 11-100 of MLE3 altimeter data with version "b" geophysical models.
Mean Sea Surface Model	GSFC00.1	CLS01
Along Track Mean Sea Surface Model	None (set to default)	None (set to default)
Geoid	EGM96	EGM96
Bathymetry Model	DTM2000.1	DTM2000.1
Inverse Barometer Correction	Computed from ECMWF atmospheric pressures	Computed from ECMWF atmospheric pressures after removing model for S1 and S2 atmospheric tides.
Non-tidal High-frequency Dealiasing Correction	None (set to default)	Mog2D ocean model on GDRs, none (set to default) on IGDRs. Ocean model forced by ECMWF atmospheric pressures after removing model for S1 and S2 atmospheric tides.
Tide Solution 1	GOT99	GOT00.2 + S1 ocean tide . S1 load tide ignored.
Tide Solution 2	FES99	FES2004 + S1 and M4 ocean tides. S1 and M4 load tides ignored.
Equilibrium long-period ocean tide model.	From Cartwright and Taylor tidal potential.	From Cartwright and Taylor tidal potential.
Non-equilibrium long-period ocean tide model.	None (set to default)	Mm, Mf, Mtm, and Msqm from FES2004.
Solid Earth Tide Model	From Cartwright and Taylor tidal potential.	From Cartwright and Taylor tidal potential.
Pole Tide Model	Equilibrium model	Equilibrium model.
Wind Speed from Model	ECMWF model	ECMWF model
Altimeter Wind Speed	Table derived from TOPEX/POSEIDON data.	Table derived from version "a" Jason-1 GDR data.

.../...

Model	Product Version "a"	Product Version "b"
Rain Flag	Derived from TOPEX/POSEIDON data.	Derived from version "a" Jason-1 GDRs.
Ice Flag	Climatology table	Climatology table

Table 3: *M*odels and standards adopted for the Jason-1 product version "a" and product version "b"

2.3.2 Impact of product version "b"

The main changes between GDRs version "a" and "b" are the new orbit, the retracking of the wave forms with MLE4 algorithm, and new geophysical corrections. This has not only an impact on editing procedure, but also on crossover performances. In the following sections these issues are briefly addressed. For further information, please refer to [50] or [6].

2.3.2.1 Editing procedure

The new MLE4 retracking algorithm based on a second-order altimeter echo model is more robust for large off-nadir angles (up to 0.8 degrees). For product version "a" (previous CMA version 6.3), the maximum threshold on square off-nadir angle proposed in Jason-1 User Handbook document was set to 0.16 deg^2. Henceforth, this threshold is too restrictive and has to be set to 0.64 deg^2.

However, this editing criteria had the side effect of removing some bad measurements impacted by rain cells, sigma0 blooms or ice. With the new threshold (0.64 deg^2), these measurements are not rejected any more even though the estimated SSH is not accurate for such waveforms.
Therefore 2 new criteria have to be added to check for data quality:

- Standard deviation on Ku sigma0 $\leq$ 1 dB
- Number measurements of Ku sigma0 $\geq$ 10

The Jason-1 User Handbook suggests the following editing criteria for the version "a" GDRs:

- -0.2 $deg^2 \leq$ square of off-nadir angle from waveforms (off_nadir_angle_ku_wvf) $\leq$ 0.16 deg^2
- sigma0_rms_ku $<$ 0.22 dB (optional criterion)

For the version "b" GDRs these two edit criteria should be replaced by:

- -0.2 $deg^2 \leq$ square of off-nadir angle from waveforms (off_nadir_angle_ku_wvf) $\leq$ 0.64 deg^2
- and sigma0_rms_ku $\leq$ 1.0 dB
- and sig0_numval_ku $\geq$ 10

With these new criteria, the editing gives similar results for both product versions. Most of anomalous SSH measurements are rejected. Please note that some of them are still not detected, in particular close to sea ice. This is due to the ice flag which is not perfect.

2.3.2.2 Quantity of data

In GDRs version "a" data could be missing, apart from platform problems, due to acquisition errors, ground processing issues, datation problems or following altimeter SEU. In GDRs version "b" most of these data have been recovered. In addition, measurements which previously were edited due to squared apparent mispointing out of thresholds, are now thanks to the MLE4 retracking algorithm (using 2nd order Brown model) mostly valid.

Figure 1 shows the difference of measurements (GDR "b" - GDR "a") after validation step. Positive value means that GDRs version "b" data have more valid measurements than GDRs version "a" data.

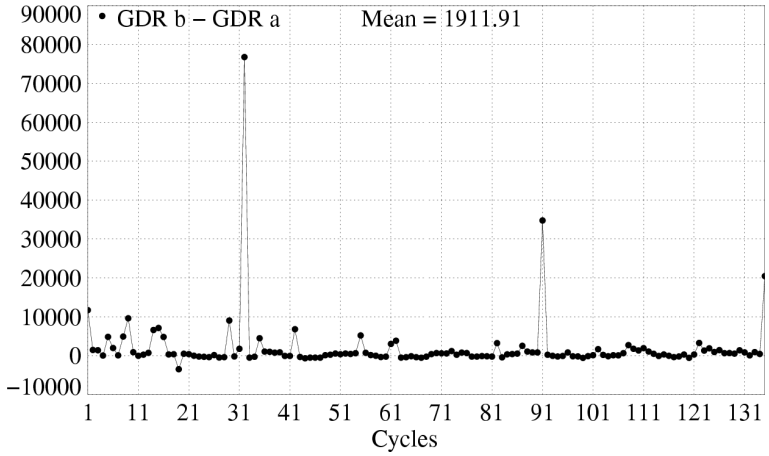

Figure 1: *Cycle per cycle difference of number of valid measurements between the two GDRs version (GDR "b" - GDR "a").*

2.3.2.3 Impact of new orbit

The new orbit of the GDRs version "b" is a tri-technic orbit, using gravity field of EIGEN-CG03C, whereas GDRs version "a" orbit is a bi-technic (SLR/DORIS) orbit using JGM-3 gravity field.
Figure 2 shows the mean of SSH crossover differences (difference between ascending and descending passes) for cycles 1 to 135 using orbit of GDRs version "a" (left) and "b" (right). The left figure (GDRs "a" orbit) shows broad structures of positive or negative differences in the order of 3 to 4 cm, whereas the right figure (GDRs "b" orbit) shows differences in the magnitude of $\pm$ 1cm, which are more homogeneous.

2.3.2.4 Monitoring of performances at crossovers

Standard deviation of SSH differences at crossover points is reduced using GDRs version "b", compared to GDRs version "a" (left of figure 3). It drops from 5.87 cm to 5.19 cm.
Mean of SSH differences at crossover points (right of figure) is increased (absolute values) when using GDRs version "b", nevertheless it is more stable in the time.

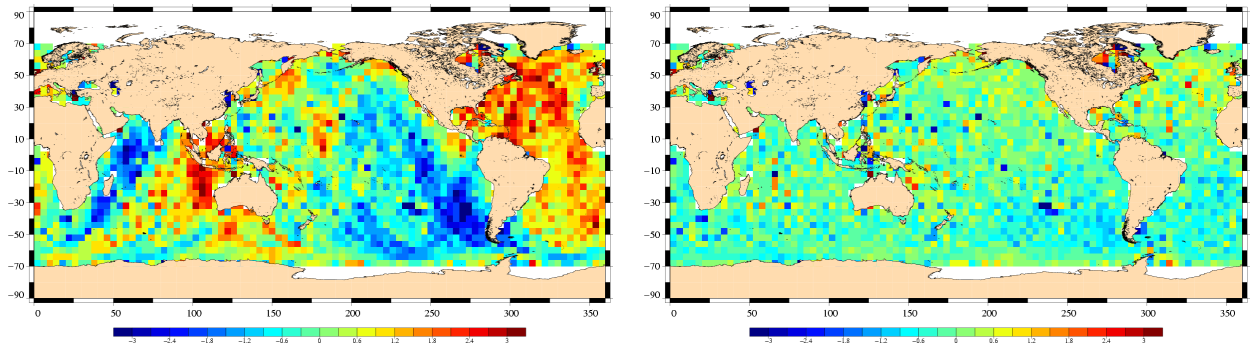

Figure 2: *Mean of SSH crossover differences for cycles 1 to 135, using GDRs version "a" orbit (left) or GDRs version "b" orbit (right).*

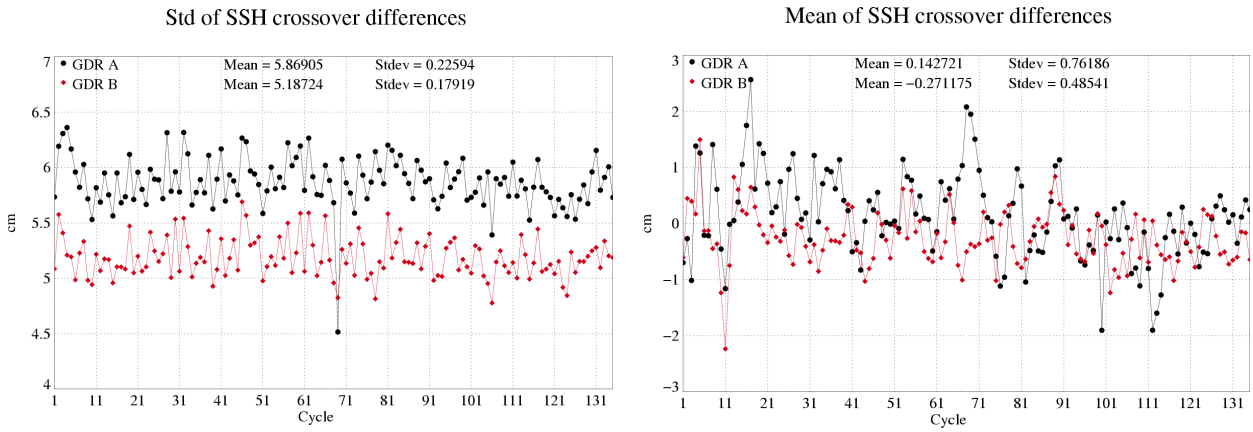

Figure 3: *Cycle per cycle standard deviation (left) and mean (right) of SSH differences at crossover points using GDRs version "a" (black) or GDRs version "b" (red).*

3 Data coverage and edited measurements

3.1 Missing measurements

3.1.1 Over ocean

Determination of missing measurements relative to the theoretically expected orbit ground pattern is used to detect missing telemetry in Jason-1 datasets due to altimetry events for instance. This procedure is applied cycle per cycle and leads to results plotted on the left figure 4. It represents the percentage of missing measurements relative to the theory, when limited to ocean surfaces. The mean value is about 3.6% but this figure is not significant due to several events where the measurements are missing. All these events are described on table 1.
On figure 4 on the right, the percentage of missing measurements is plotted without taking into account the cycles where instrumental events or other anomalies occurred. Moreover shallow waters and high latitudes have been removed. This allows us to detect small data gaps in open ocean. The mean value is about 0.02%. This weak percentage of missing measurements is mainly explained by the rain cells, ice sea or sigma0 blooms. These sea states can disturb significantly the Ku band waveform shape leading to a non significant measure.
Another reason for these small data gaps in open ocean, are datation gaps, which occur occasionally.

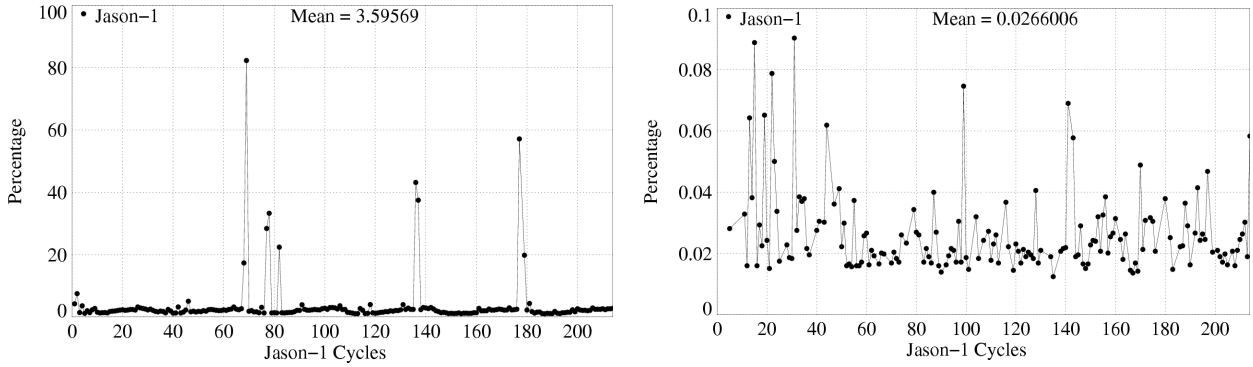

Figure 4: *Cycle per cycle percentage of missing measurements over ocean*

3.1.2 Over land and ocean

Figure 5 shows the percentage of missing measurements for Jason-1 and T/P (all surfaces) computed with respect to a theoretical possible number of measurements. Due to differences between tracker algorithms, the number of data is greater for T/P (excepted when T/P experienced problems, especially since the tape recorders were no longer in service (T/P cycle 444, Jason-1 cycle 101)) than for Jason-1. Differences appear on land surfaces as is shown in figure 6.

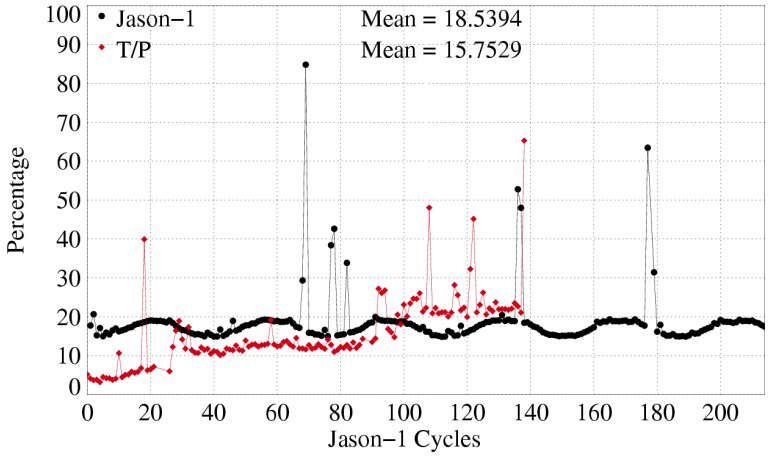

Figure 5: *Percentage of missing measurements over ocean and land for J1 and T/P*

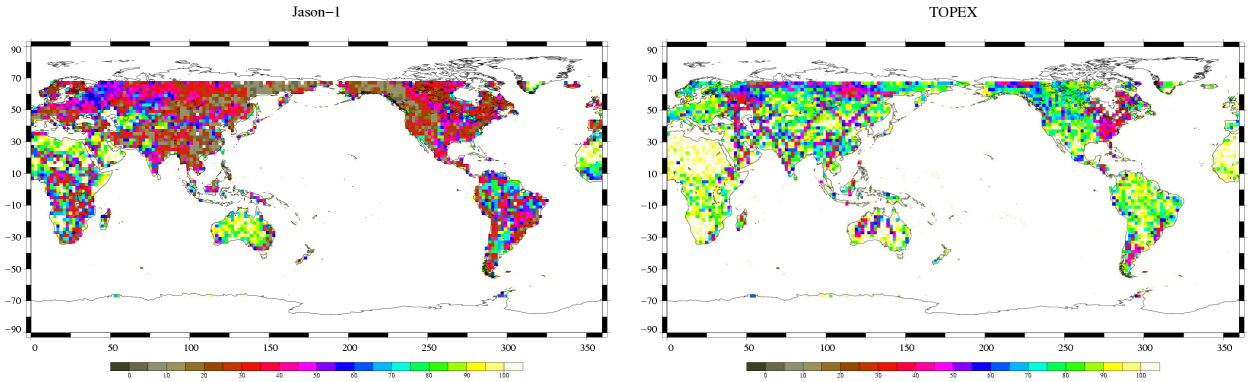

Figure 6: *Map of percentage of available measurements over land for Jason-1 on cycle 61 (left) and for TOPEX on cycle 404 (right)*

3.2 Edited measurements

3.2.1 Editing criteria definition

Editing criteria are used to select valid measurements over ocean. The editing process is divided into 4 parts. First, only measurements over ocean and lake are kept (see section 3.2.2). Second, the quality criteria concern the flags which are described in section 3.2.3 and 3.2.5. Then, threshold criteria are applied on altimeter, radiometer and geophysical parameters and are described in the table 4. Moreover, a spline criterion is applied to remove the remaining spurious data. These criteria defined for the GDR products "b" are also defined in AVISO and PODAAC User handbook. For each criterion, the cycle per cycle percentage of edited measurements has been monitored. This allows detection of anomalies in the number of removed data, which could come from instrumental, geophysical or algorithmic changes.

Parameter	Min thresholds	Max thresholds	mean edited
Sea surface height	$-130\ m$	$100\ m$	0.75%
Sea level anomaly	$-10\ m$	$10.0\ m$	1.39%
Number measurements of range	10	*Not applicable*	1.09%
Standard deviation of range	0	$0.2\ m$	1.28%
Square off-nadir angle	$-0.2\ deg^2$	$0.64\ deg^2$	0.48%
Dry troposphere correction	$-2.5\ m$	$-1.9\ m$	0.00%
Inverted barometer correction	$-2.0\ m$	$2.0\ m$	0.00%
JMR wet troposphere correction	$-0.5m$	$-0.001\ m$	0.15%
Ionosphere correction	$-0.4\ m$	$0.04\ m$	1.08%
Significant waveheight	$0.0\ m$	$11.0\ m$	0.55%
Sea State Bias	$-0.5\ m$	$0.0\ m$	0.91%
Number measurements of Ku-band Sigma0	10	*Not applicable*	1.08%
Standard deviation of Ku-band Sigma0	0	$1.0\ dB$	1.62%
Ku-band Sigma0 [1]	$4.6\ dB$	$27.6\ dB$	0.51%
Ocean tide	$-5.0\ m$	$5.0\ m$	0.04%
Equilibrium tide	$-0.5\ m$	$0.5\ m$	0.00%
Earth tide	$-1.0\ m$	$1.0\ m$	0.00%
Pole tide	$-15.0\ m$	$15.0\ m$	0.00%

.../...

Parameter	Min thresholds	Max thresholds	mean edited
Altimeter wind speed	0 $m.s^{-1}$	30.0 $m.s^{-1}$	0.91%
All together	-	-	2.94%

Table 4: *E*diting criteria

3.2.2 Selection of measurements over ocean and lakes

In order to remove data over land, a land-water mask is used. Only measurements over ocean or lakes are kept. Indeed, this allows us to keep more data near the coasts and then detecting potential anomalies in these areas. Furthermore, there is no impact on global performance estimations since the most significant results are derived from analyzes in deep ocean areas. Figure 7 (left) shows the cycle per cycle percentage of measurements eliminated by this selection. It shows a seasonal signal. This is due to the varying number of measurements available in the GDRs, which varies not only over ocean, but also over land. After removing the annual signal, there is no trend noticeable Figure 7 (right).

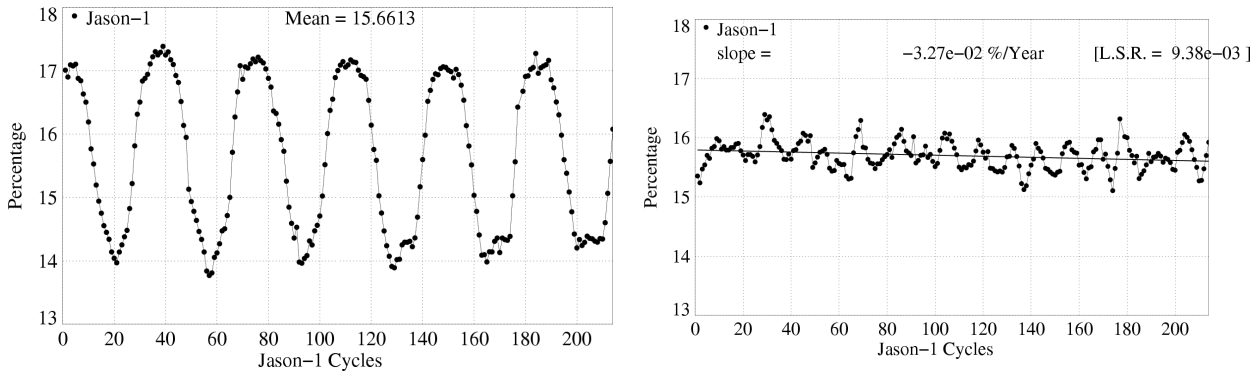

Figure 7: *Cycle per cycle percentage of eliminated measurements during selection of ocean/lake measurements (left). Trend of eliminated measurements after removing annual signal (right).*

[1]The thresholds used for the Ku-band Sigma0 are the same than for T/P, but the sigma0 bias between Jason-1 and T/P (about 2.4 dB) is applied.

3.2.3 Flagging quality criteria: Ice flag

The ice flag is used to remove the sea ice data. Figure 8 shows the cycle per cycle percentage of measurements edited by this criterion. No anomalous trend is detected (figure 8 right) but an annual cycle is visible. Indeed, the maximum number of points over ice is reached during the northern fall. As Jason-1 takes measurements between 66° north and south, it does not detect thawing of sea ice (due to global warming), which takes place especially in northern hemisphere beyond 66°N. The ice flag edited measurements are plotted in Figure 9 for one cycle. It shows that the ice flag is not perfectly tuned especially in the northern hemisphere, for instance the Hudson Bay is divided into 2 parts (figure 9, left). By using an empirical ice flag similar to the one used for ERS satellite (which involves the difference between bifrequency radiometer wet troposphere and model wet troposphere), the detection of ice is improved (see section 3.2.4).

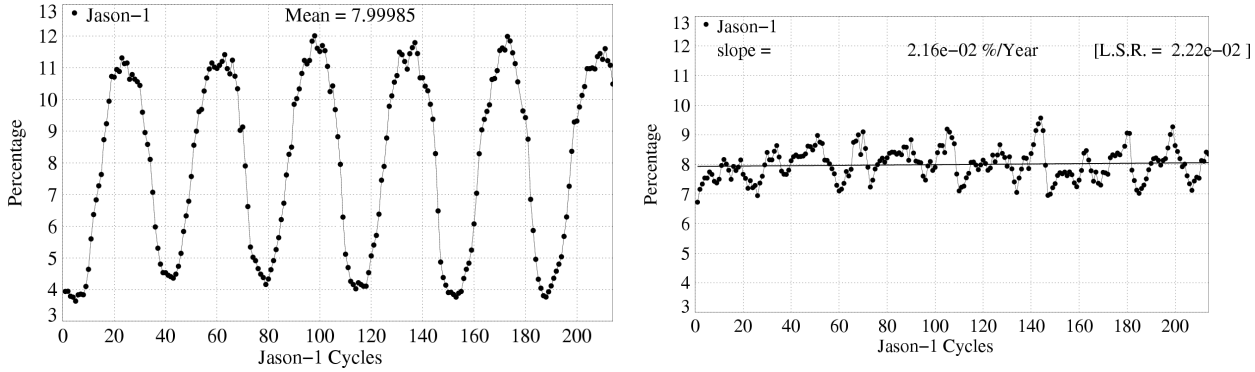

Figure 8: *Cycle per cycle percentage of edited measurements by ice flag criterion (left), after subtracting annual signal (right).*

3.2.4 Flagging quality criteria: Ice flag with ERS method

The ice flag of ERS uses the difference between the dual-frequency radiometer wet troposphere and the ECMWF model wet troposphere correction. This difference is small over ocean, but important over ice. In [27] this method was adapted for Jason-1. The dual-frequency wet troposphere is calculated by

Tropo_bifr = $-0.01 * (142.932 - 56.2442 * LOG(280 - TEMP\_BRI\_C2) + 28.5724 * LOG(280 - TEMP\_BRI\_C3))$

Ice is detected when for latitudes higher than 50° the following 2 conditions are fullfilled:

- Number of elementary measurements < 10
- |dual-frequency wet troposphere - ECMWF model wet troposphere| > 10 cm

This criteria works fine, and detects ice in the entire Hudson Bay. Nevertheless ice cover can also be found south of 50°N as for example in the northern part of Caspian sea, in the Aral Sea or in the La Perouse strait (north of Japon). Therefore the ERS ice flag should be extended to a latitude of 40°N within a coast distance of 500 km (to avoid erroneous ice detection in open sea). Figure 9 (right) shows ice detected on cycle 185 using the extended ERS ice flag. It shows that ice is detected in the entire Hudson Bay, as well as in the Aral sea and in the northern part of the Caspian Sea.
This ice flag is an empirical method, which certainly does also have erroneous ice detection or ice which is not detected, but statistically is works better than the current ice flag present in the GDRs.

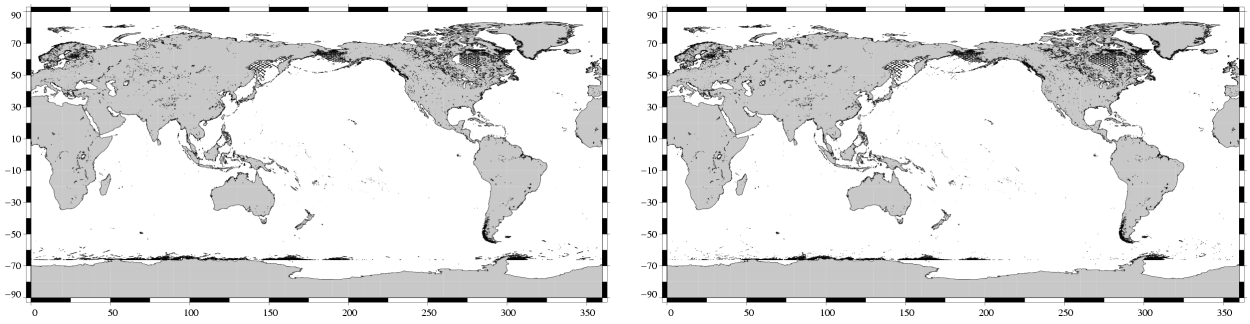

Figure 9: *Map of edited measurements by ice flag criterion on cycle 185 (left) and map of measurements, which would be edited when using ice flag criterion of type ERS on cycle 185 (right).*

3.2.5 Flagging quality criteria: Rain flag

The rain flag is not used for data selection since it was tuned on GDRs version "a". It is thus recommended not to be used by users. The percentage of rain edited measurements is plotted in figure 10 over cycles 140 to 176 (covering one year). It shows that measurements are especially edited near coasts, but also in the equatorial zone and open ocean. The rain flag seems to be to strict, using it would lead to editing 5.5% of additional measurements.

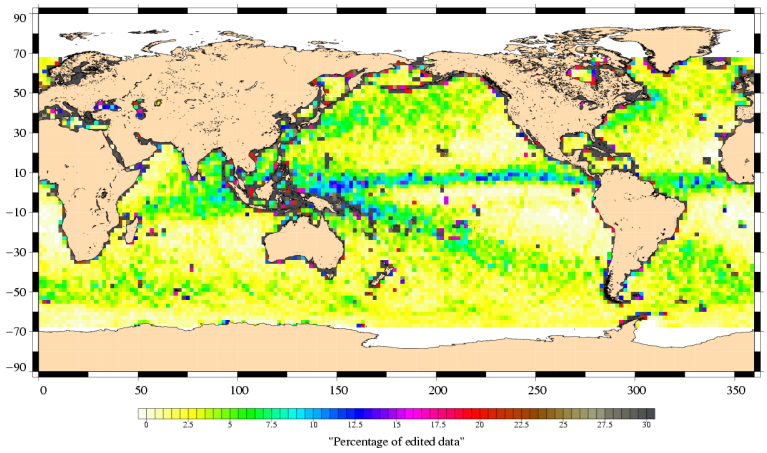

Figure 10: *Map of percentage of edited measurements by rain flag criterion over an one-year period (cycles 140 to 176)*

3.2.6 Threshold criteria: Global

Instrumental parameters have also been analyzed from comparison with thresholds, after having selected only ocean/lake measurements and applied flagging quality criteria (ice flag). Notice that no measurements are edited by the following corrections : dry troposphere correction, inverted barometer correction, equilibrium tide, earth and pole tide.

The percentage of measurements edited using each criterion has been monitored on a cycle per cycle basis (figure 11). The mean percentage of edited measurements is about 2.9%. An annual cycle is visible due to the seasonal sea ice coverage in the northern hemisphere. Indeed most of northern hemisphere coasts are without ice during northern hemisphere summer. Consequently some of these coastal measurements are edited by the thresholds criteria in summer instead of the ice flag in winter. This seasonal effect visible in the statistics is not balanced by the southern hemisphere coasts due to the shore distribution between both hemispheres.
Notice that for some cycles, especially cycles 69 and 179, the percentage of edited measurements is higher than usual. This is mostly due to the radiometer wet troposphere correction, see section 3.2.11.

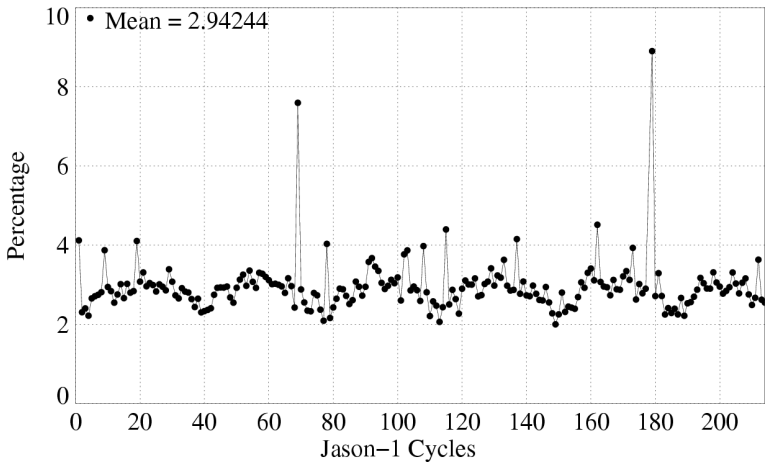

Figure 11: *Cycle per cycle percentage of edited measurements by threshold criteria*

3.2.7 Threshold criteria: 20-Hz measurements number

The percentage of edited measurements because of a too low number of 20-Hz measurements is represented on left side of figure 12. No trend neither any anomaly has been detected, except for cycle 212. Indeed during this cycle, about half of a pass had all altimetry parameters set at default values, due to off-pointing of the satellite, avoiding the retrieval of the altimetry parameters.

The map of measurements edited by 20-Hz measurements number criterion is plotted on right side of figure 12 and shows correlation with heavy rain and wet areas. Indeed the waveforms are distorted by rain cells, which mades them often unexploitable for SSH calculation. In consequence edited measurements due to several altimetric criteria are often correlated with wet areas.

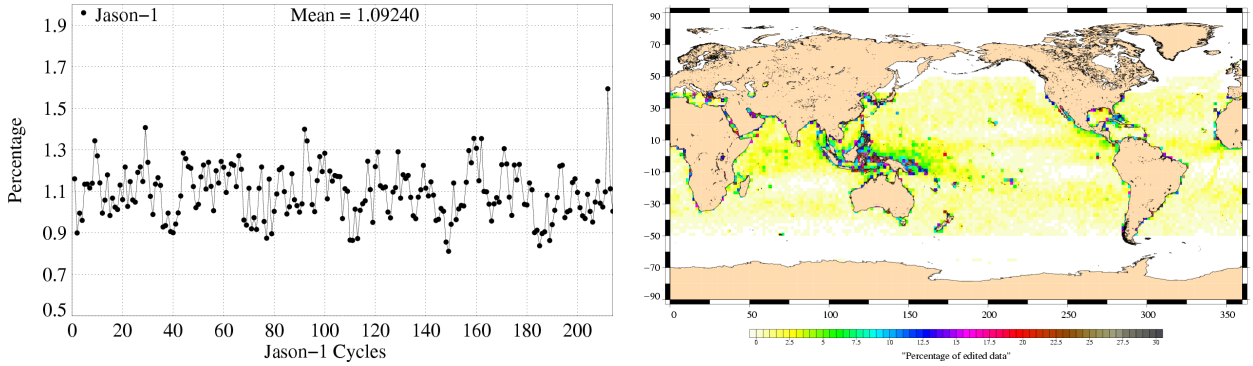

Figure 12: *Cycle per cycle percentage of edited measurements by 20-Hz measurements number criterion (left). Right: Map of percentage of edited measurements by 20-Hz measurements number criterion over an one-year period (cycles 140 to 176).*

3.2.8 Threshold criteria: 20-Hz measurements standard deviation

The percentage of edited measurements due to 20-Hz measurements standard deviation criterion is shown in figure 13. The annual signal observed (left) is linked to the seasonal variability associated to the ice coverage. After removing the annual signal (figure 13 right), there is no trend visible.

Figure 14 shows a map of measurements edited by the 20-Hz measurements standard deviation criterion. As in section 3.2.7, edited measurements are correlated with wet areas.

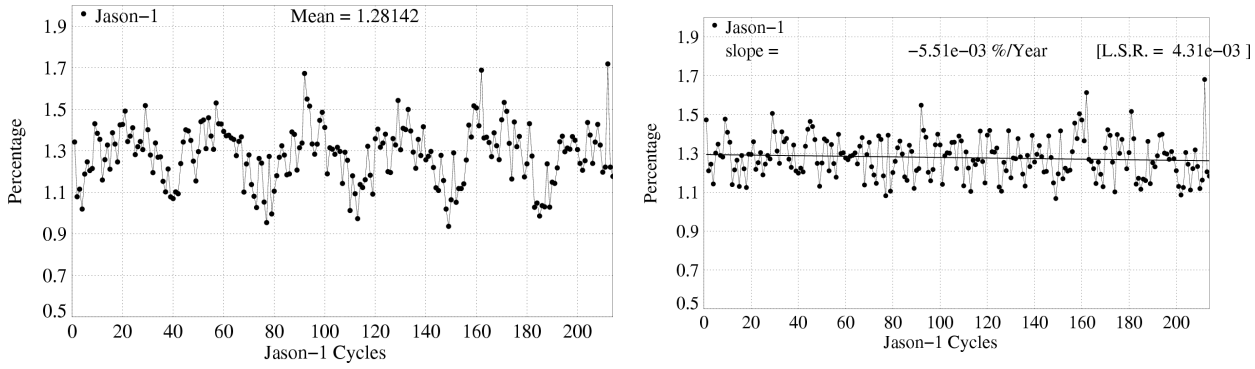

Figure 13: *Cycle per cycle percentage of edited measurements by 20-Hz measurements standard deviation criterion (left); after removing annual signal (right).*

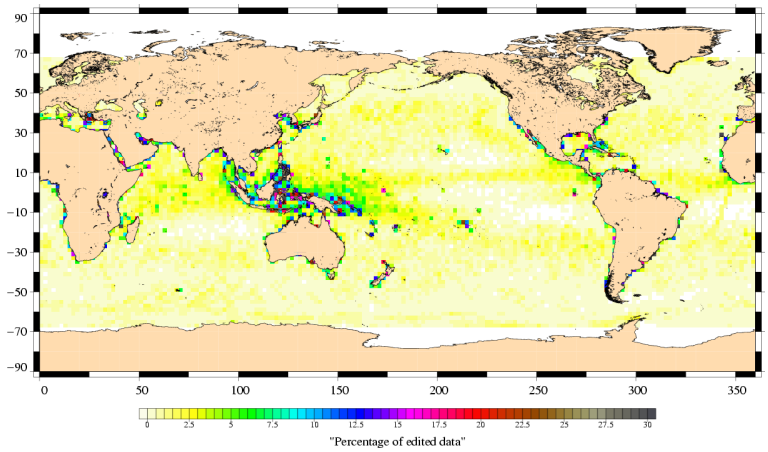

Figure 14: *Map of percentage of edited measurements by 20-Hz measurements standard deviation criterion over an one-year period (cycles 140 to 176).*

3.2.9 Threshold criteria: Significant wave height

The percentage of edited measurements due to significant wave height criterion is represented in figure 15. It is about 0.55%. No drift has been detected over the Jason-1 period. The peak visible for cycle 212 is due to a portion of a pass at default values. Figure 15 (right part) shows that measurements edited by SWH criterion are especially found near coasts in the equatorial regions.

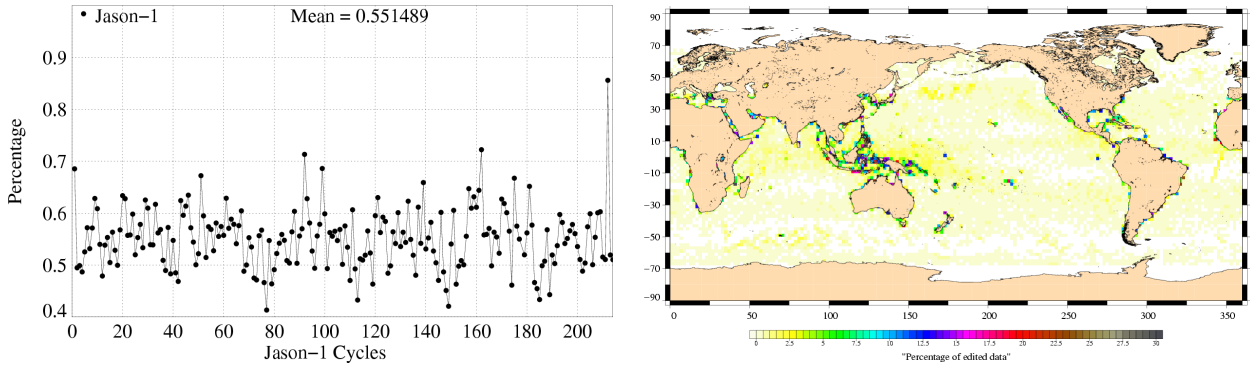

Figure 15: *Cycle per cycle percentage of edited measurements by SWH criterion (left). Right: Map of percentage of edited measurements by SWH criterion over an one-year period (cycles 140 to 176).*

3.2.10 Backscatter coefficient

The percentage of edited measurements due to backscatter coefficient criterion is represented in figure 16. It is about 0.51% and shows no drift. The peak visible for cycle 212 is due to a portion of a pass at default values. The right part of figure 16 shows that measurements edited by backscatter coefficient criterion are especially found near coasts in the equatorial regions.

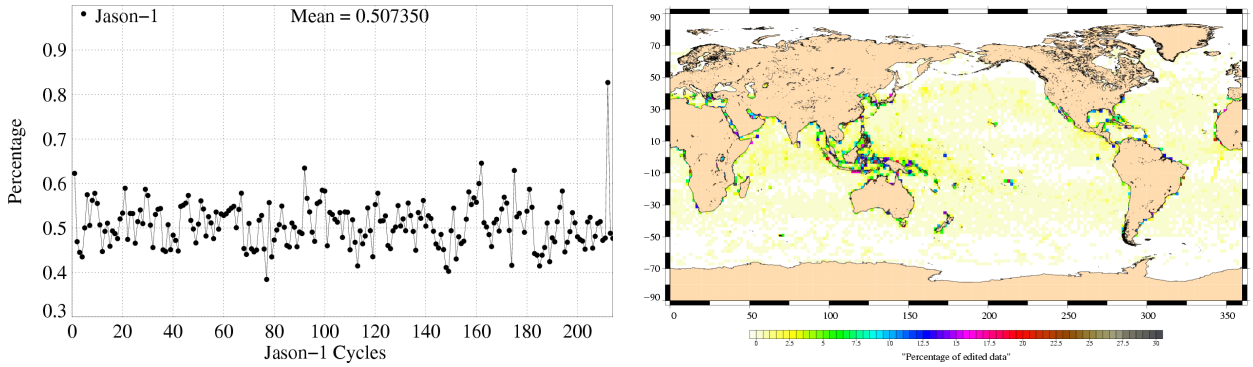

Figure 16: *Cycle per cycle percentage of edited measurements by Sigma0 criterion (left). Right: Map of percentage of edited measurements by Sigma0 criterion over an one-year period (cycles 140 to 176).*

3.2.11 Radiometer wet troposphere correction

The percentage of edited measurements due to radiometer wet troposphere correction criterion is represented in figure 17. It is about 0.15%. When removing cycles which experienced problems, percentage of edited measurements drops to 0.07%. The figure shows irregular oscillations which are not correlated to annual cycle. At the end of the shown period, percentage of edited measurements decreases (due to a decrease of default values). This might be related to use of new CMA version 9.0 (since cycle 198). The map 17 shows that only few measurements are edited by radiometer wet troposphere correction criterion.

Notice that for some cycles the percentage of edited measurements is higher than usual. This is often linked to the Jason safe hold mode on some of these cycles (69, 78, 137, and 179): the radiometer has been set on 2 hours later than the altimeter. As a result, the radiometer wet troposphere correction has been set to default value during this period and these measurements have been edited.
For cycle 1 radiometer wet troposphere correction is missing for passes, which were absent in GDR "a" product version. Concerning cycles 8 and 19, radiometer wet troposphere correction is missing for a portion of a pass, for which it was present in GDR "a" product version.

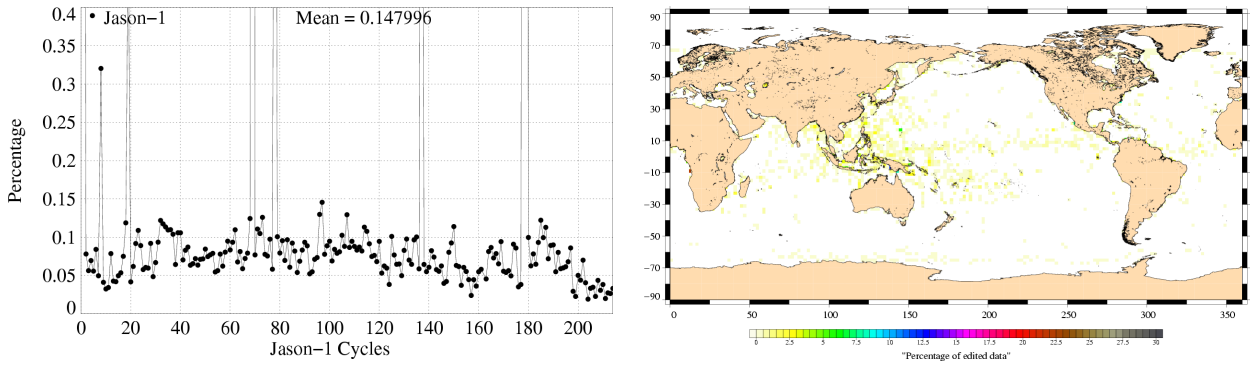

Figure 17: *Cycle per cycle percentage of edited measurements by radiometer wet troposphere criterion (left). Map of percentage of edited measurements by radiometer wet troposphere criterion over an one-year period (cycles 140 to 176).*

3.2.12 Dual frequency ionosphere correction

The percentage of edited measurements due to dual frequency ionosphere correction criterion is represented in figure 18. It is about 1.08% and shows no drift. The map 18 shows that measurements edited by dual frequency ionosphere correction are mostly found in equatorial regions. Two passes are visible, they belong to cycle 173 which experienced an altimeter SEU.
Notice that for cycles 9, 91, 102, 103, 108, 115, 133, 173, 181, 198, and 212 the percentage of edited measurements is higher than usual. This is almost always linked to an altimeter SEU (C band) occurred on these cycles. The dual frequency ionosphere correction has been set to default value during this period and these measurements have been edited. Only the peak for cycle 212 is not due to an altimeter SEU (see section 3.2.7).

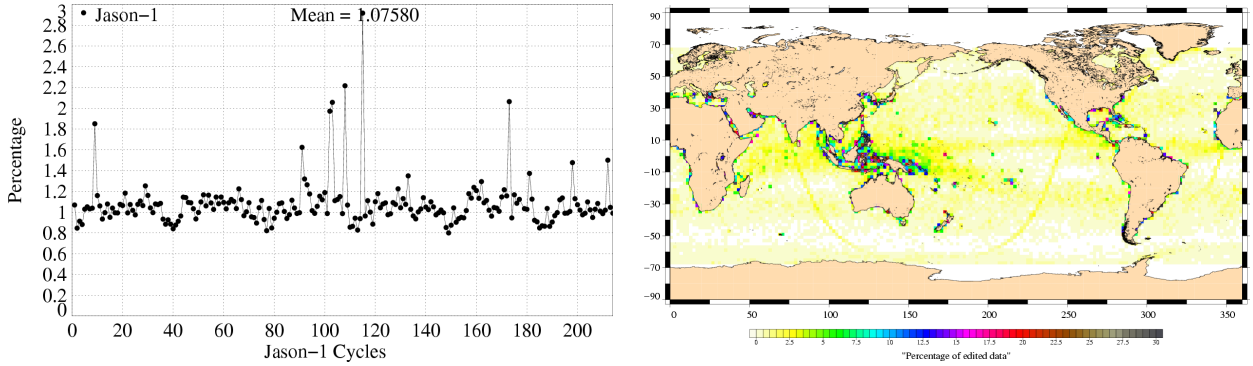

Figure 18: *Cycle per cycle percentage of edited measurements by dual frequency ionosphere criterion (left). Map of percentage of edited measurements by dual frequency ionosphere criterion over an one-year period (cycles 140 to 176).*

3.2.13 Square off-nadir angle

The percentage of edited measurements due to square off-nadir angle criterion is represented in figure 19. It is about 0.48% and shows no drift. The peak in cycle 212 is due to very high mispointing caused by low star tracker availability and gyro wheels behavior. This even avoided retrieval of altimetric parameters for a portion of a pass. The map 19 shows that edited measurements are mostly found in coastal regions.

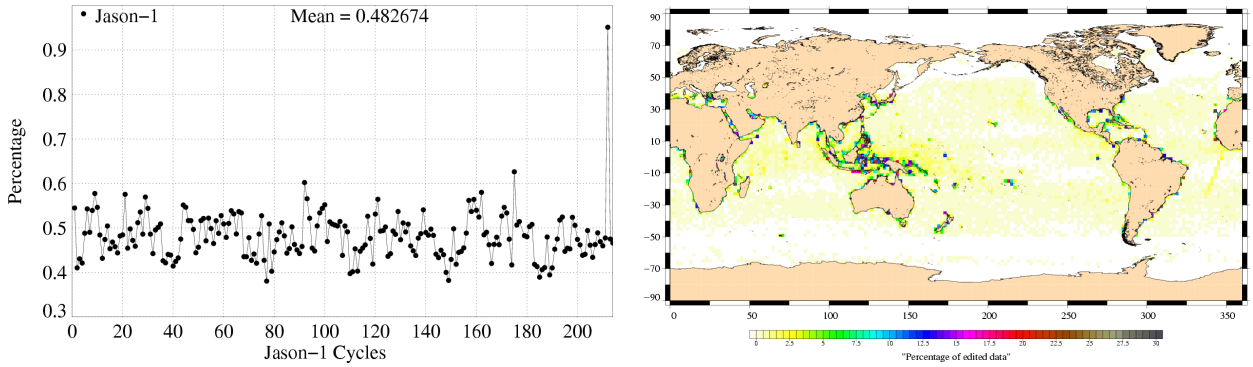

Figure 19: *Cycle per cycle percentage of edited measurements by square off-nadir angle criterion (left). Right: Map of percentage of edited measurements by square off-nadir angle criterion over an one-year period (cycles 140 to 176).*

3.2.14 Sea state bias correction

The percentage of edited measurements due to sea state bias correction criterion is represented in figure 20. The percentage of edited measurements is about 0.91% and shows no drift. There is an annual cycle visible, which is highly correlated to the percentage of edited measurements by wind speed criterion, as sea state bias is computed with significant wave height and wind speed.

The map 20 shows that edited measurements are mostly found in equatorial regions near coasts.

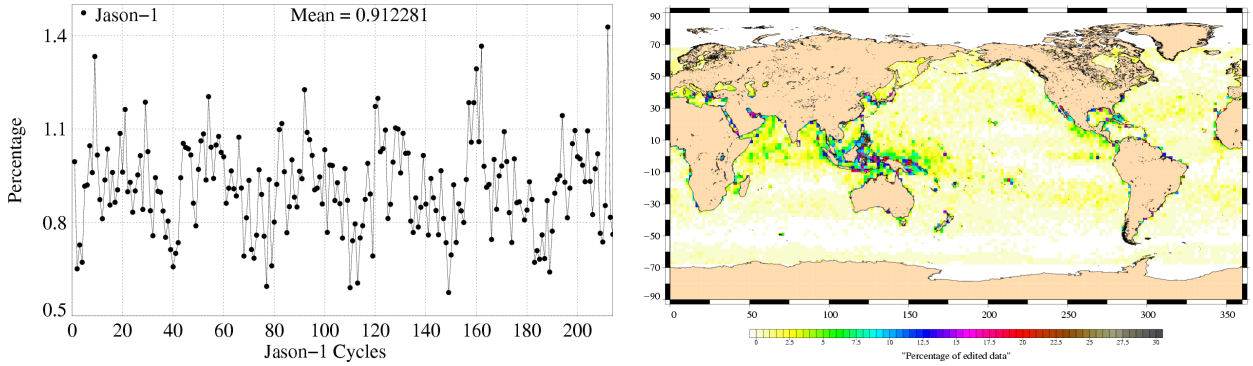

Figure 20: *Cycle per cycle percentage of edited measurements by sea state bias criterion (left). Right: Map of percentage of edited measurements by sea state bias criterion over an one-year period (cycles 140 to 176).*

3.2.15 Altimeter wind speed

The percentage of edited measurements due to altimeter wind speed criterion is represented in figure 21. It is about 0.91% and shows no drift. The measurements are edited, because they have default values. This is the case when sigma0 itself is at default value, or when it shows very high values (higher than 25 dB), which occur during sigma bloom and also over sea ice. The annual cycle is probably due to sea ice, which was not detected by the ice flag.

The map 21 showing percentage of measurements edited by altimeter wind speed criterion is highly correlated with the map 20.

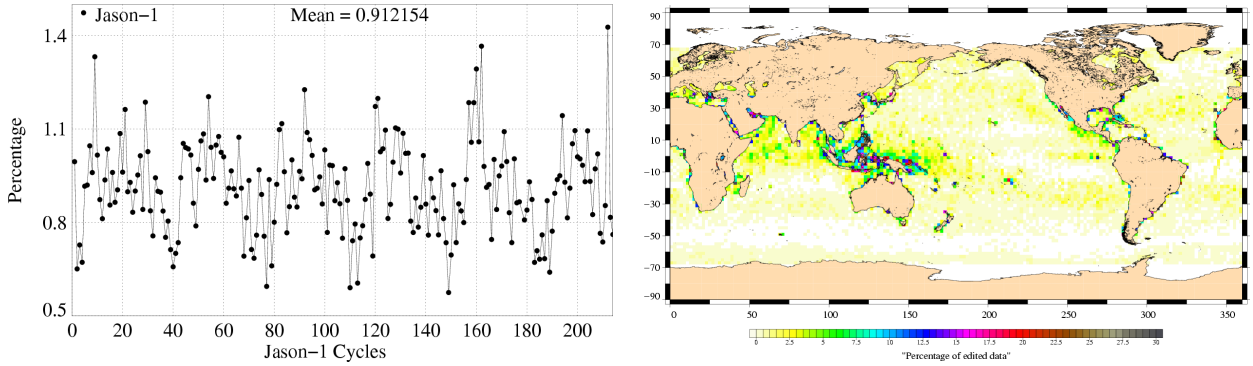

Figure 21: *Cycle per cycle percentage of edited measurements by altimeter wind speed criterion (left). Right: Map of percentage of edited measurements by altimeter wind speed criterion over an one-year period (cycles 140 to 176).*

3.2.16 Ocean tide correction

The percentage of edited measurements due to ocean tide correction criterion is represented in figure 22. It is about 0.04% and shows no drift. The ocean tide correction is a model output, there should therefore be no edited measurements. Indeed there are no measurements edited in open ocean areas, but only very few near coasts or in lakes or rivers (see map 22). These measurements are mostly at default values.

Some of these lakes are in high latitudes and therefore periodically covered by ice. This explains the annual signal visible in figure 22.

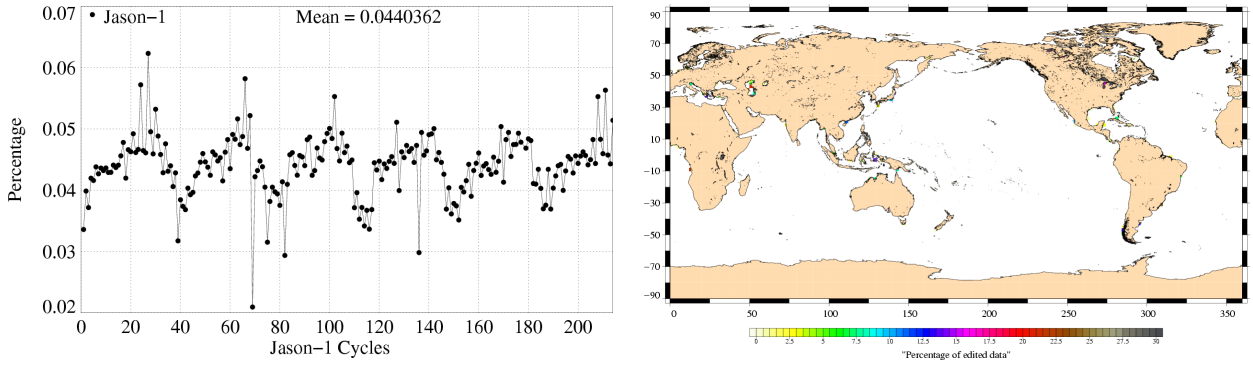

Figure 22: *Cycle per cycle percentage of edited measurements by ocean tide criterion (left). Right: Map of percentage of edited measurements by ocean tide criterion over an one-year period (cycles 140 to 176).*

3.2.17 Sea surface height

The percentage of edited measurements due to sea surface height criterion is represented in figure 23. It is about 0.75% and shows no drift. There is however an annual signal visible. For the peak in cycle 212 see section 3.2.13.

The measurements edited by sea surface height criterion are mostly found near coasts in equatorial regions (see map 23)

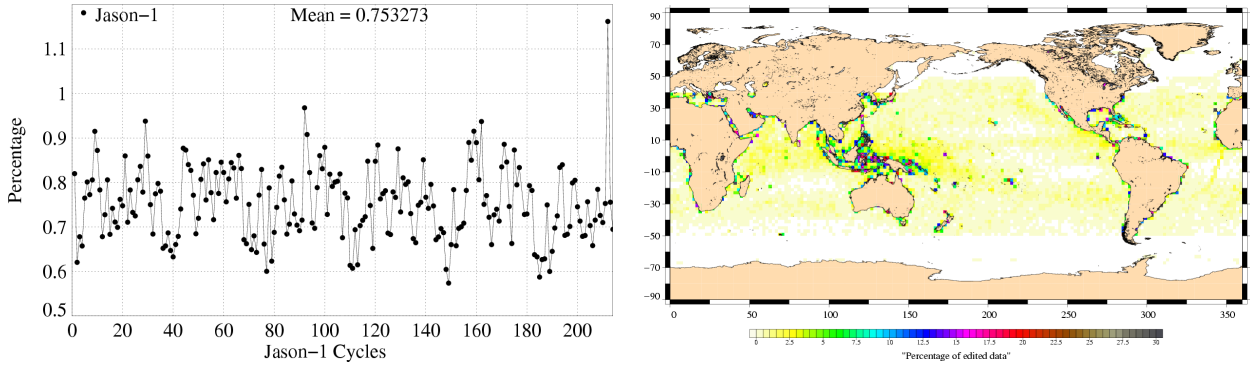

Figure 23: *Cycle per cycle percentage of edited measurements by sea surface height criterion (left). Right: Map of percentage of edited measurements by sea surface height criterion over an one-year period (cycles 140 to 176).*

3.2.18 Sea level anomaly

The percentage of edited measurements due to sea level anomaly criterion is represented in figure 24. It is about 1.39% and shows no drift. The graph is quite similar to the one in figure 11 (showing the percentage of measurements edited by all the threshold criteria), as the SLA clip contains many of the parameters used for editing.
Whereas the map in figure 24 allows us to plot the measurements edited due to sea level anomaly out of thresholds (after applying all other threshold criteria). These are only very few measurements.

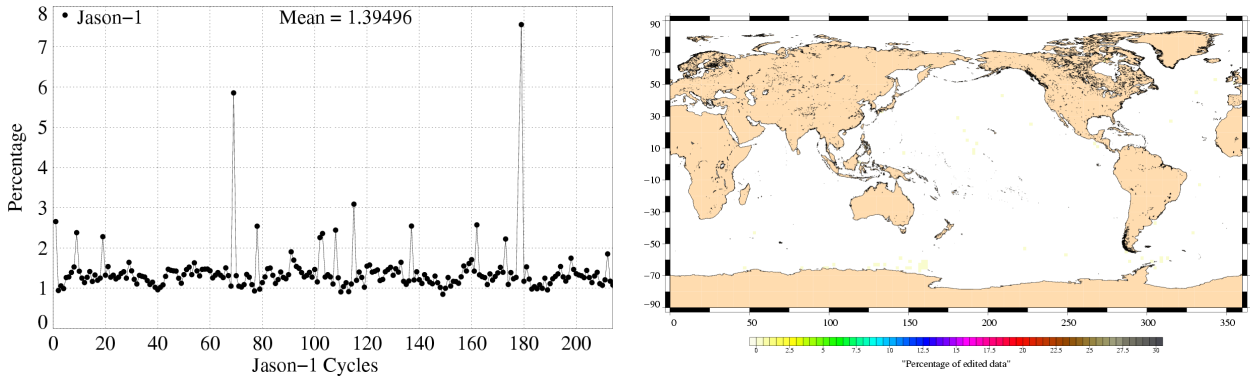

Figure 24: *Cycle per cycle percentage of edited measurements by sea level anomaly criterion (left). Right: Map of percentage of edited measurements by sea level anomaly criterion (after applying all other threshold criteria) over an one-year period (cycles 140 to 176).*

4 Monitoring of altimeter and radiometer parameters

4.1 Methodology

Both mean and standard deviation of the main parameters of Jason-1 have been monitored since the beginning of the mission. Moreover, a comparison with T/P parameters has been performed: it allows us to monitor the bias between the parameters of the 2 missions. The comparison is done till the end of scientific mission of T/P, which occurred during Jason-1 cycle 138. Two different methods have been used to compute the bias:

- During the verification phase, Jason-1 and T/P ground tracks are on the same ground track and are spaced out about 1 minute apart. The mean of the T/P Jason-1 differences can be computed using a point by point repeat track analysis.
- From cycle Jason-1 22 (Cycle T/P 365), the 15th of August 2002, a maneuver sequence was conducted over 30 days to move T/P to the new Tandem Mission orbit : Furtheron T/P was located one half the TP/Jason-1 track spacing to the West of Jason-1. Geographical variations are then too strong to directly compare Jason-1 and T/P parameters on a point by point basis. Therefore cycle per cycle differences have been carried out to monitor Jason-1 and T/P differences, but data gaps on both satellites have been taken into account.

4.2 20 Hz Measurements

The monitoring of the number and the standard deviation of 20 Hz elementary range measurements used to derive 1 Hz data is presented here. These two parameters are computed during the altimeter ground processing. Before a regression is performed to derive the 1 Hz range from 20 Hz data, a MQE criterion is used to select valid 20 Hz measurements. This first step of selection thus consists in verifying that the 20 Hz waveforms can be effectively approximated by a Brown echo model (Brown, 1977 [9]) (Thibaut et al. 2002 [64]). Through an iterative regression process, elementary ranges too far from the regression line are discarded until convergence is reached. Thus, monitoring the number of 20 Hz range measurements and the standard deviation computed among them is likely to reveal changes at instrumental level.

4.2.1 20 Hz measurements number in Ku-Band and C-Band

Figure 25 shows the cycle per cycle mean of 20-Hz measurements number in Ku-Band (on the left) and C-Band (on the right). Apart from a very weak seasonal signal, no trend neither any anomaly has been detected.

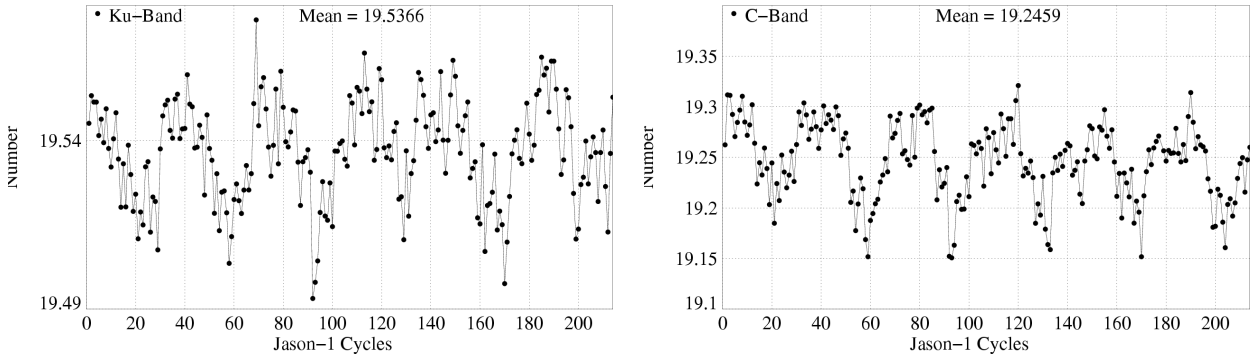

Figure 25: *Cycle per cycle mean of 20-Hz measurements number in Ku-Band (left) and C-Band (right)*

4.2.2 20 Hz measurements standard deviation in Ku-Band and C-Band

Figure 26 shows the cycle per cycle standard deviation of the 20 Hz measurements in Ku-Band (on the left) and C-Band (on the right). Apart from a weak seasonal signal, no trend neither anomaly has been detected. Values of C-Band standard deviation of the 20 Hz measurements are higher than those of Ku-Band, as integration is done over less waveforms leading to an noise increase.

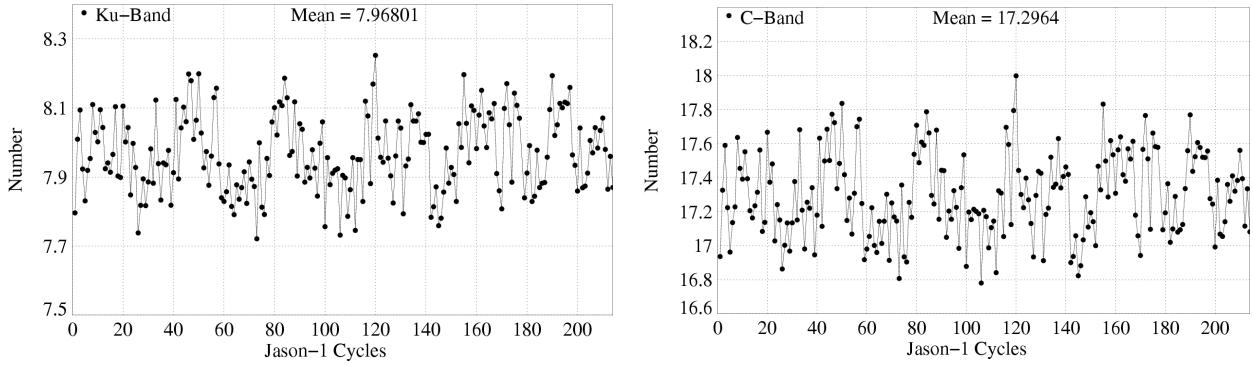

Figure 26: *Cycle per cycle mean of 20-Hz measurements standard deviation in Ku-Band (left) and C-Band (right)*

4.3 Off-Nadir Angle from waveforms

The off-nadir angle is estimated from the waveform shape during the altimeter processing. The square of the off-nadir angle, averaged in a one-cycle basis, has been plotted in figure 27. The mean values are slightly positive. This mean value is not significant in terms of actual platform mispointing. In fact squared attitude is what is retrieved from waveforms, not attitude. During the first half of the mission off-nadir angles are low and quite stable, except for cycle 69 related to a platform safehold mode. During the second half of the mission (since approximately cycle 100), off-nadir angle has very strong values. There are periods where the combination of low Beta angles and Sun glint or Moon in FOV significantly reduce the tracking performance of both star trackers, especially during fixed-yaw. These periods when the off-nadir angle is larger than the 0.2 degree specification, which can introduce errors in the altimeter parameters if not taken into account in the ground processing (Vincent et al., 2003), made an improvement of the retracking algorithm necessary. The improvements available in the GDR version "b" (section 2.3) of the ground retracking algorithm lead to correct estimations of altimeter parameters for mispointing angle errors up to 0.8 deg. (Amarouche et al. 2004 [7]).

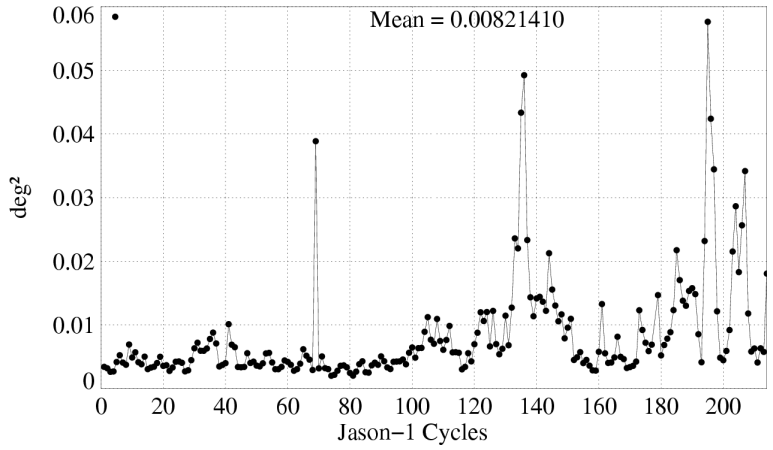

Figure 27: *Cycle mean of the square of the off-nadir angle deduced from waveforms (deg^2)*

4.4 Significant wave height

4.4.1 Ku-band SWH

Jason-1 and T/P Ku SWH are compared in terms of global statistics in figure 28: cycle means and standard deviations of both missions are presented in a cycle basis, as well as mean differences between T/P and Jason-1. Global variations of the SWH statistics are the same on the two missions. A weak annual signal is visible. Jason-1 SWH shows a very small drift of 5 mm/yr. The (TOPEX - Jason-1) SWH bias is about 8.2 cm. This value remains almost steady at the 1 cm level throughout the Jason-1 mission (showing only a weak drift of 1.2 mm/yr), even if some variability is observed for particular cycles. The estimation of the (Poseidon-1 - Poseidon-2) SWH difference is about 15.0 cm for Poseidon cycle 18 not plotted here.
The standard deviation of Ku-band SWH shows an annual signal for both Jason-1 and T/P data.

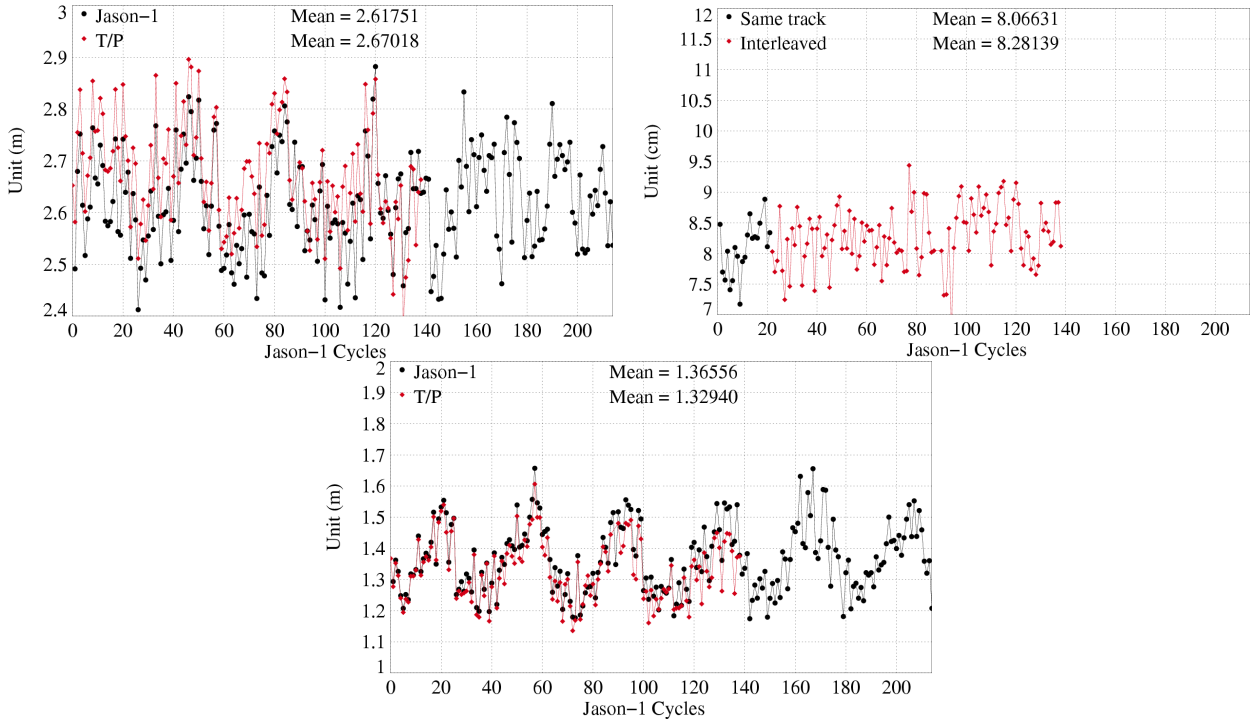

Figure 28: *Cycle per cycle mean (left), T/P−Jason mean differences (right), and standard deviation (bottom) of Ku-band SWH*

4.4.2 C-band SWH

Figure 29 shows global statistics of Jason-1 and T/P C-band SWH. The cycle per cycle mean of both missions shows a small annual signal (figure 29 top left). Jason-1 and T/P values are quite similar. After removing annual signal, Jason-1 data show a very small drift of 4.8 mm/yr. The (TOPEX - Jason-1) C-band SWH mean bias is about 10 cm (figure 29 top right). There is a drift of -4 mm/yr visible. Standard deviation of C-band SWH are quite similar on both missions showing an annual signal.

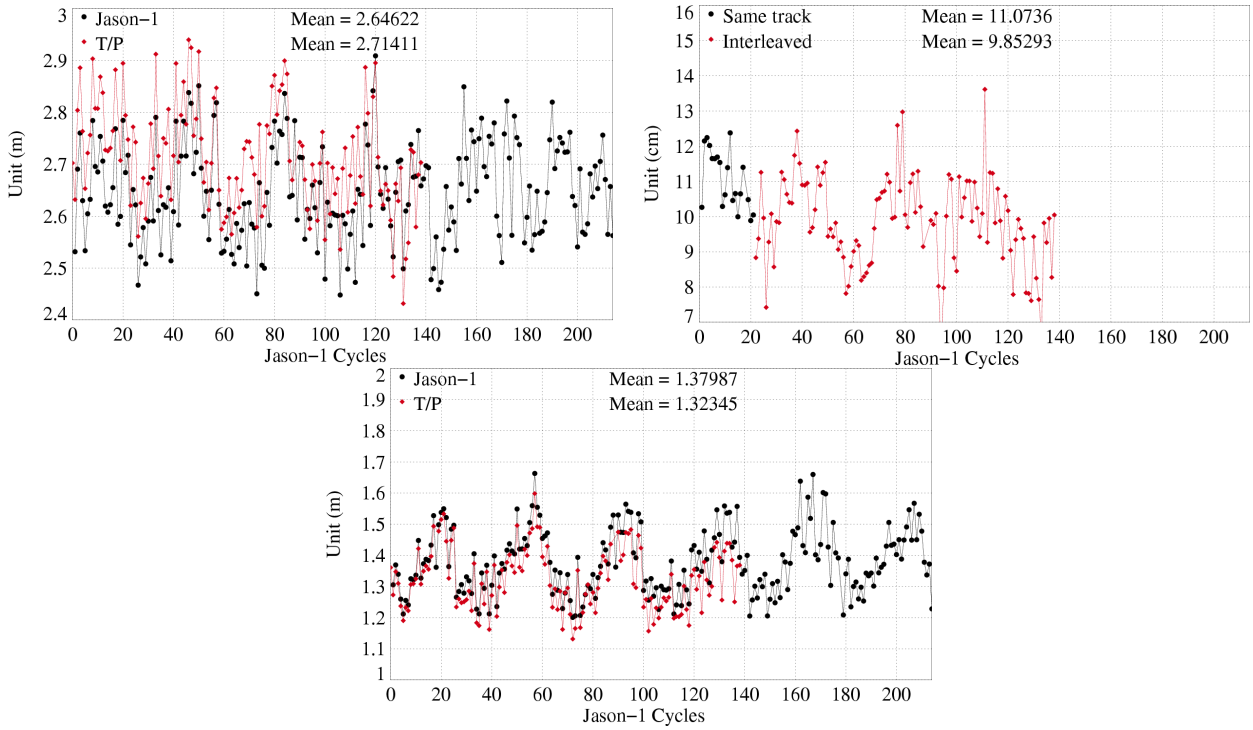

Figure 29: *Cycle per cycle mean (left), T/P−Jason mean differences (right), and standard deviation (bottom) of C-band SWH*

4.5 Backscatter coefficient

4.5.1 Ku-band Sigma0

The cycle per cycle mean (figure 30: top panel on the left) for Jason-1 (black curve) Ku-band sigma0 is coherent with the TOPEX mean (red curve). In order to compare both parameters and keep a significant dynamic scale, TOPEX Ku-Sigma0 is biased by a 2.26 dB value to align TOPEX with the Jason-1 uncalibrated Sigma0. The bias between the two corrections (figure 30: top panel on the right) is quite stable about -2.5 dB. A small trend close to -0.02 dB/yr has been detected for Jason-1 and is analyzed thanks to altimeter wind comparisons in the next section.
Besides, the absolute bias is higher than usual from T/P cycle 433 to 437 (J1 cycles 90 to 94) by 0.1 dB : this is due to the TOPEX Sigma0. Indeed, the satellite attitude was impacted by a pitch wheel event linked to the T/P safe-hold mode occurred on cycle T/P 430 (see electronic communication : T/P Daily Status (26/07/2004)). This anomaly has probably biased the TOPEX sigma0 during this period. Jason-1 and T/P curves on bottom panel, showing the standard deviation differences, are very similar .

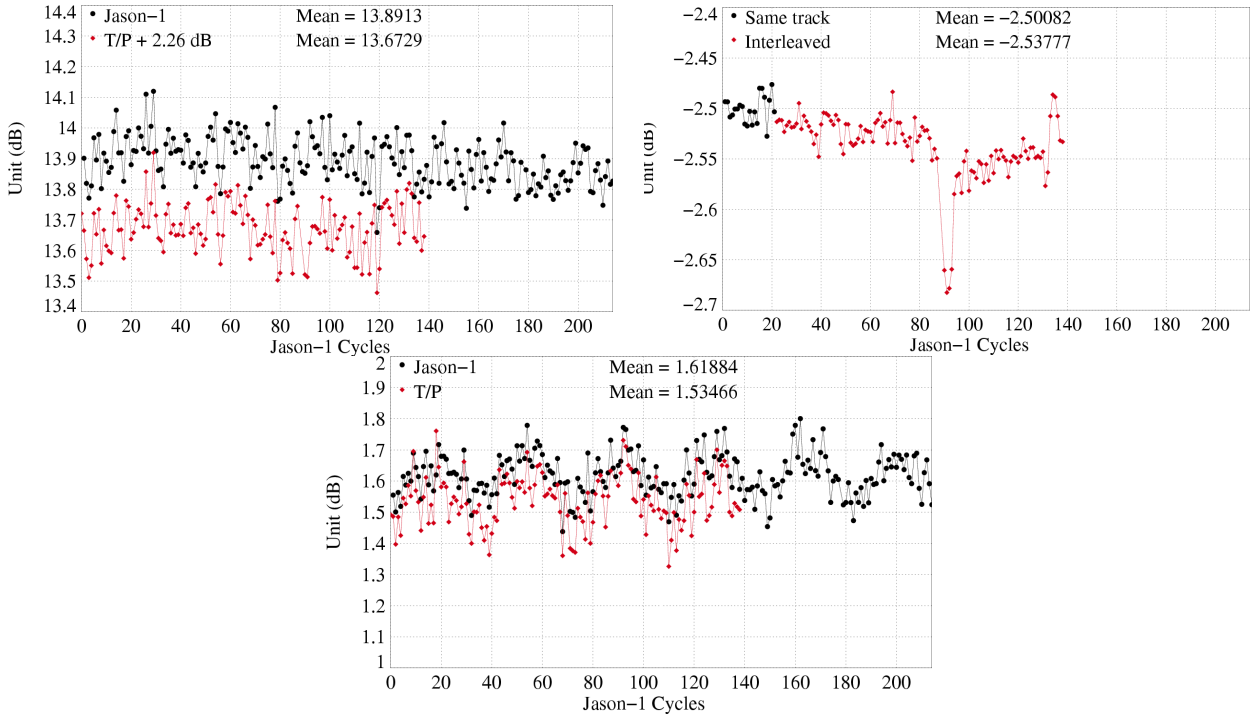

Figure 30: *Cycle per cycle mean (left), T/P−Jason mean differences (right), and standard deviation (bottom) of Ku-band SIGMA0*

4.5.2 Origin of Ku-band Sigma0 drift

As detected in last section, Jason-1 sigma0 decreases by -0.02 dB/yr. Even though this figure is weak, it impacts the MSL evolution by 0.1 mm/yr through the sea state bias correction. This drift can be due to

instrumental anomaly (instrument ageing for instance), or due to a natural geophysical evolution. In order to determine the origin of this drift, the different sigma0 trends derived from Jason-1, T/P and Envisat have been plotted (on left side of figure 31). A similar drift is detected for the 2 first satellites after removing last T/P cycles where some instrumental problems impact the T/P sigma0 evolution. However the Envisat curve highlights no significant evolution. Then, to complete this first analyze, a second comparison has been performed using wind speed provided by altimeters and ECMWF model (figure 31). Indeed, the Jason-1 wind speed trend (close to 5 $cm.s^{-1}/yr$) is directly derived from Jason-1 sigma0 drift (-0.02 dB/yr). The ECMWF curve shows a very good agreement with the Jason-1 wind with a slope close to 6 $cm.s^{-1}/yr$. Besides, ECMWF model does not assimilate Jason-1 or TOPEX data, therefore it is an independent data source. Finally, the sigma0 drift is probably linked to a natural geophysical evolution. It might be explained with the global warming. But in this case, the Envisat sigma0 stagnation would display an abnormal behavior. These conclusions have to be thoroughly analyzed.

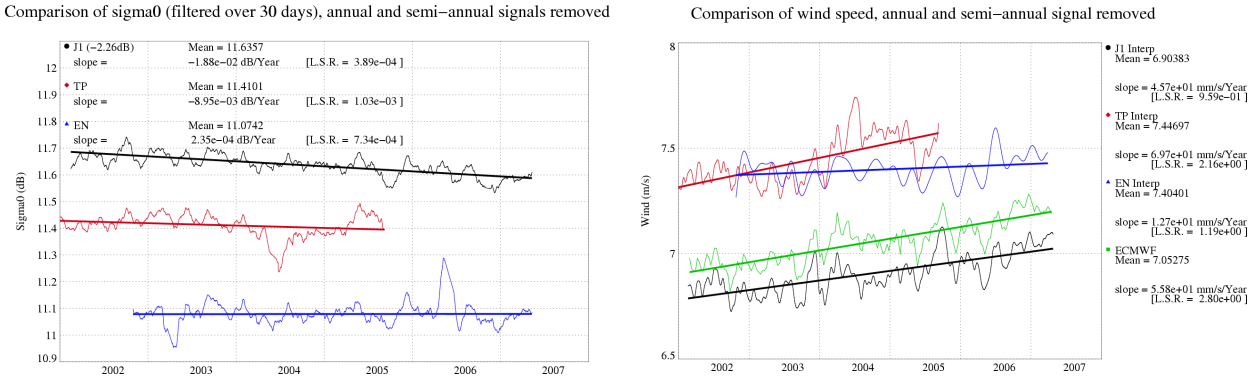

Figure 31: *Global slopes of daily sigma0 mean (filtered over 30 days) measured by Jason-1, Topex/Poseidon and Envisat altimeter (left). Global slopes of different wind speed sources (Jason-1, T/P, Envisat, ECMWF model) over the Jason-1 period. Time series were filtered over 30 days.*

4.5.3 C-band Sigma0

The cycle per cycle mean (figure 32: top panel on the left) for Jason-1 (black curve) Ku-band sigma0 is coherent with the TOPEX mean (red curve). The bias between the two corrections (figure 32: top panel on the right) decreases from -0.6 dB to -0.8 dB. This is due to the T/P C-band Sigma0 (Ablain et al. 2004 [3]). Notice that, the Jason C-Sigma0 is biased by a -0.26 dB value to align it on TOPEX in the science processing software. Standard deviation of C-band sigma0 (figure 32: bottom) has similar values for both missions and shows an annual signal.

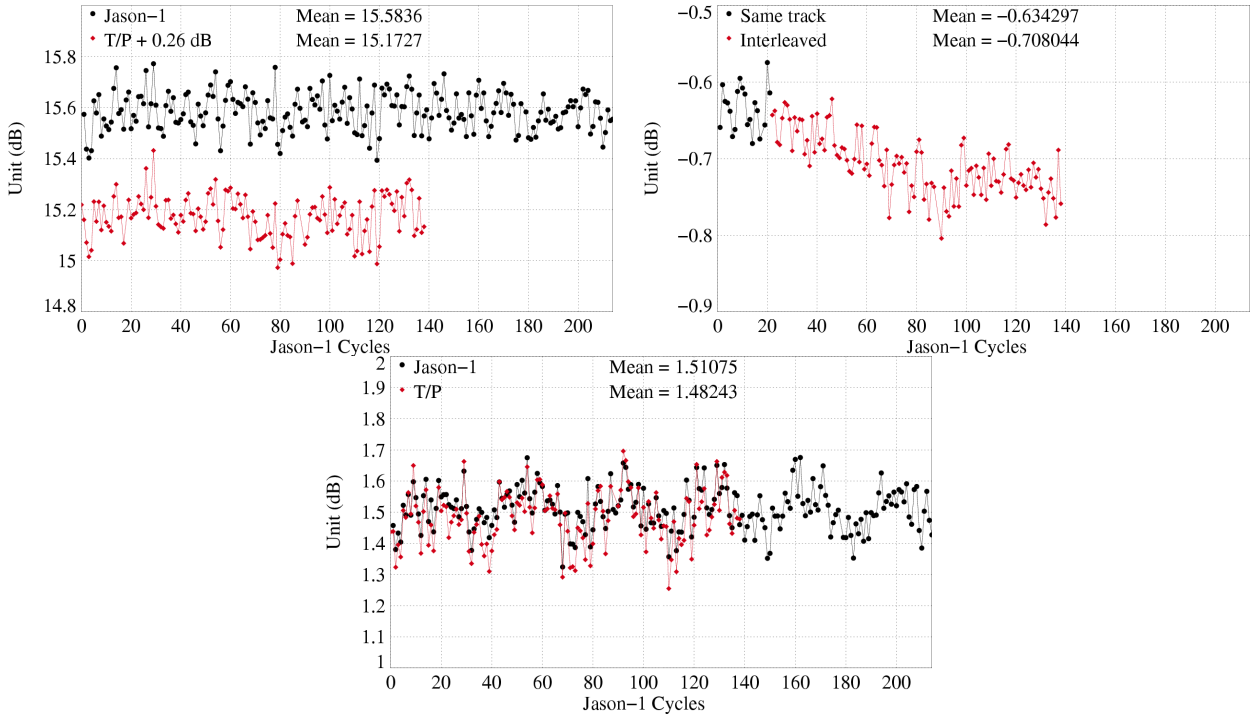

Figure 32: *Cycle per cycle mean (left), T/P−Jason mean differences (right), and standard deviation (bottom) of C-band SIGMA0*

4.6 Dual-frequency ionosphere correction

The dual frequency ionosphere corrections derived from the TOPEX and Jason-1 altimeters have been monitored and compared in the same way (figure 33). The mean difference between TOPEX and Jason-1 estimates is about 0 mm, with cycle to cycle variations lower than 2 mm. There is nevertheless a small drift of 0.03 cm/yr visible. Both corrections are very similar and vary according to the solar activity. Notice that, as for TOPEX (Le Traon et al. 1994 [42]), it is recommended to filter the Jason-1 dual frequency ionosphere correction before using it as a SSH geophysical correction (Chambers et al. 2002 [14]). A low-pass filter has thus been used to remove the noise of the correction in all SSH results presented in the following sections.

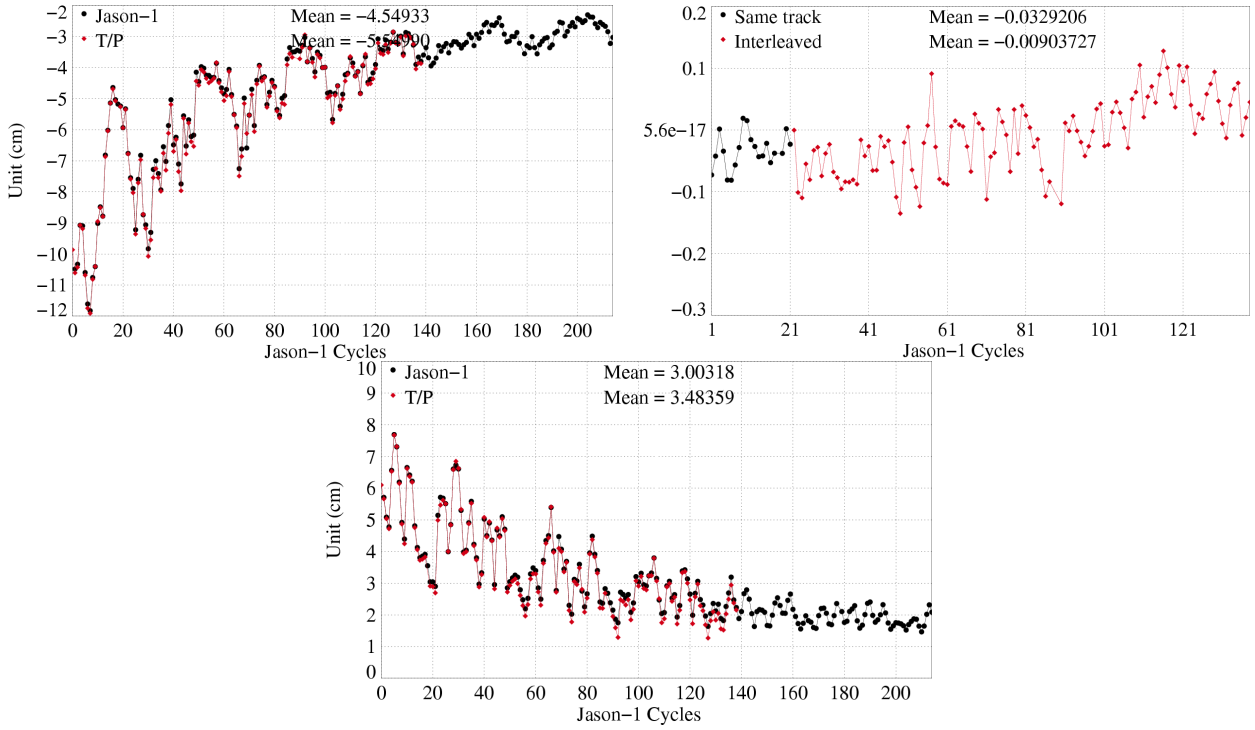

Figure 33: *Cycle per cycle mean (left), T/P−Jason mean differences (right), and standard deviation (bottom) of dual frequency ionosphere correction*

Figure 34 shows differences between Jason-1 dual-frequency ionosphere correction and DORIS ionosphere correction. In fact, mean differences have been computed according to several local time intervals of 4 hours and afterwards averages for each year have been computed.
Differences between Jason-1 and DORIS ionosphere corrections are quite high (especially for local hours of 10 a.m. to 6 p.m., reaching 1.5 cm of difference) during the beginning of the Jason-1 mission. This is probably correlated with the higher solar activity in the beginning of the mission (during 2002). In the following, solar activity (and therefore difference between Jason-1 and DORIS ionosphere) decreases.

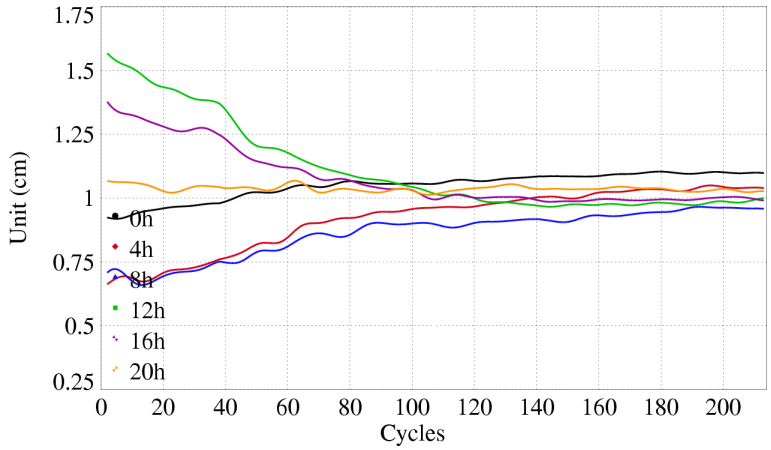

Figure 34: *Difference between DORIS and Jason-1 ionospheric correction in function of local time*

4.7 JMR Wet troposphere correction

4.7.1 Comparison with the ECMWF model

The JMR correction provided in the GDR "a" contained several anomalies already described in the previous Jason-1 annual report. These anomalies were brought out using a comparison with the ECMWF model which is stable in term of bias through the Jason-1 mission (except for the first cycle : (see http://www.ecmwf.int/products/data/operational_system/evolution/evolution_2003.html). The daily mean of radiometer and ECMWF model wet troposphere correction differences using GDR "a" have been plotted on the left of figure 35 (red curve) which highlighted these following anomalies :

- A drift of about 5 mm from cycle 27 to cycle 32 due to instrumental changes (see Obligis et al.,2004 [48])
- A jump of 9 mm at cycle 69 linked to a platform incident
- 60-day signals of an amplitude of almost 5 mm due to yaw mode transitions

The JMR correction provided in the GDR "b" is meant to correct for this problems. As for the GDR "a" correction, the radiometer and ECMWF model wet troposphere correction differences using this new correction have been plotted in the same figure 35 (black curve). This figure show that the new JMR correction allows us to correct partially the previous anomalies:

- The first anomaly between cycle 27 and 32 is softened, but still visible.
- The jump of 9 mm observed at cycle 69 is very well corrected.
- The 60 day signals have been reduced over the GDR "a" period, but they are still present showing a strong amplitude (5 to 7 mm) after 2006.

ECMWF model is continually improved. This is visible on the standard deviation of wet troposphere correction difference (between radiometer and ECMWF model) which is shown the right of figure 35. In

the beginning of 2003 standard deviation decreases from 1.7 cm to 1.4 cm. This corresponds to a model evolution. In the following, it continues to decrease.

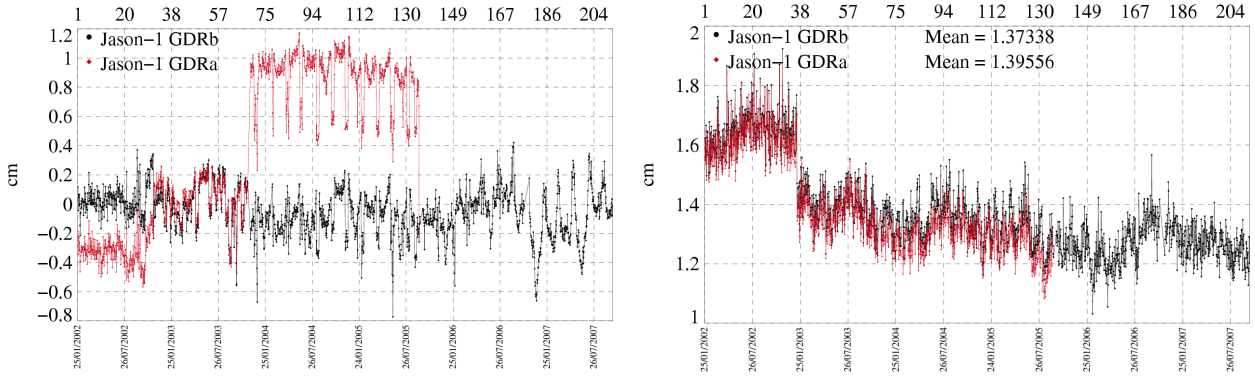

Figure 35: *Daily mean (left) and standard deviation (right) of radiometer and ECMWF model wet troposphere correction differences for Jason-1 using radiometer correction of GDR version "a" (red) and GDR version "b" (black).*

4.7.2 Comparison with others missions using the ECMWF model

Figure 36 shows the difference of radiometer and ECMWF model wet troposphere correction for different missions. For Jason-1, the monitoring of the mean of the wet troposphere difference shows, that it is noisier than for the other missions. This is probably due to the signals generated by the yaw mode transitions. The standard deviation of the wet troposphere correction difference (figure 36, left) is for Jason-1 the smallest among the different missions. But this does not mean that the JMR is better than the other radiometers. Indeed, if the JMR correction is too smooth, it will be more consistent with the model (which is itself quite smooth).

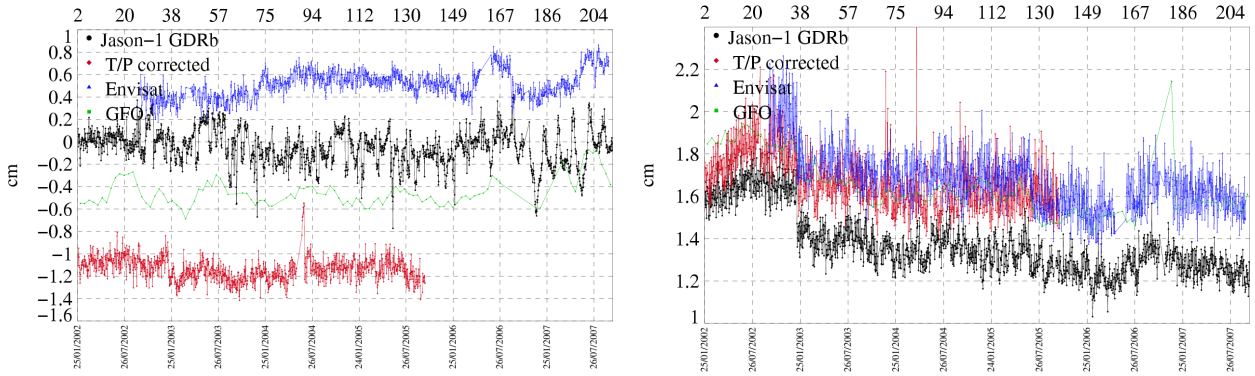

Figure 36: *Comparison of daily mean (left) and standard deviation (right) of radiometer and ECMWF model wet troposphere correction differences between several altimeter missions: Jason-1 (black), Envisat (blue), Topex/Poseidon (red) and GFO (green).*

4.7.3 Impact for the Mean Sea Level

It should now be possible to use the new radiometer wet troposphere correction available in GDR version "b" to compute the mean sea level, instead of the model correction, which might change (jump of several mm in January 2002). The local and global slopes of the radiometer and model (wet troposphere) differences are shown on figure 37, in order to show which error will be committed when using either one or the other wet tropospheric correction. Using the radiometer correction to estimate the global slope of the mean sea level, comes to increase the slope of the MSL by 0.2 mm/yr (it was 2.2 mm/yr with the model corrections). The cartography of the local slopes shows differences reaching locally 5 mm/yr. This is quite high, since the observed maximum of the local slopes of the Jason-1 MSL are 10 mm/yr. This shows that the wet troposphere correction remains a big budget error to compute the global and local MSL trends.

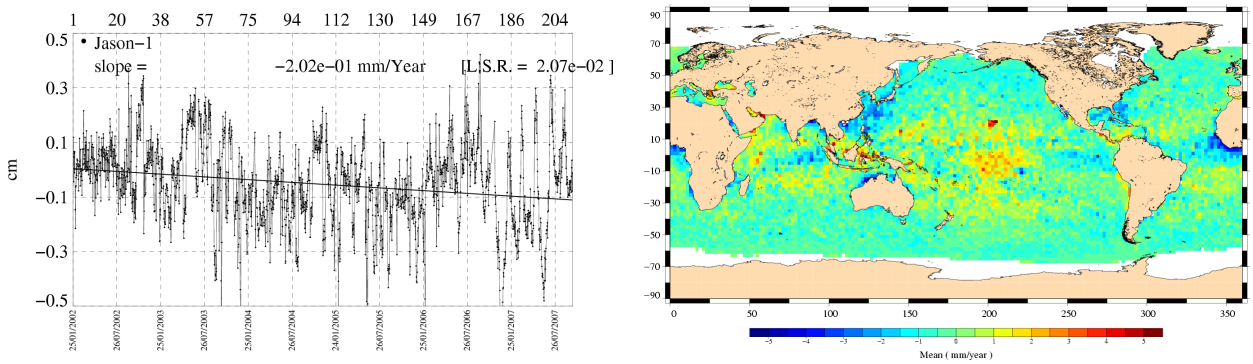

Figure 37: *Local and global slopes of the difference between radiometer and model wet troposphere for Jason-1.*

5 Crossover analysis

Crossover differences are systematically analyzed to estimate data quality and the Sea Surface Height (SSH) performances. Furthermore, T/P crossover performances (as long as they were available) have been monitored in order to compare both performances. SSH crossover differences are computed on a one cycle basis, with a maximum time lag of 10 days, in order to reduce the impact of ocean variability which is a source of error in the performance estimation. The main SSH calculation for Jason-1 and T/P are defined below. For TOPEX, Jason-1 standards have been used for the tidal and atmospheric corrections.

$$SSH = Orbit - Altimeter\ Range - \sum_{i=1}^{n} Correction_i$$

with $Jason-1\ Orbit = POE\ CNES\ orbit$ and

$$\begin{aligned}
\sum_{i=1}^{n} Correction_i \;=\; & Dry\ troposphere\ correction : new\ S1\ and S2\ atmospheric\ tides\ applied \\
+\; & Combined\ atmospheric\ correction :\ MOG2D\ and\ inverse\ barometer \\
+\; & Radiometer\ wet\ troposphere\ correction \\
+\; & Filtered\ dual\ frequency\ ionospheric\ correction \\
+\; & Non\ parametric\ sea\ state\ bias\ correction \\
+\; & Geocentric\ ocean\ tide\ height,\ GOT\ 2000 :\ S1\ atmospheric\ tide\ is\ applied \\
+\; & Solid\ earth\ tide\ height \\
+\; & Geocentric\ pole\ tide\ height
\end{aligned}$$

Note that for TOPEX data, a non-parametric sea state bias has been updated over TOPEX B period according to the collinear method (Gaspard et al., October 2002, [32]). For Poseidon-1 data, non-parametric SSB is not yet available.

5.1 Mean crossover differences

The mean of crossover differences represents the average of SSH differences between ascending and descending passes. It should not be significantly different from zero. The map of the Jason-1 crossover differences averaged over the whole period of available GDR (cycle 1 to 214) has been plotted in figure 38 (on the left). It is quite homogeneous. Substantial improvements in orbit calculation were made by the use of new gravity models (based on GRACE), see [5] and [6]. A small bias between northern and southern hemisphere is observable.

The cycle mean of Jason-1 and T/P SSH crossover differences is plotted for the whole Jason-1 period in figure 38 (right). Slightly larger variations are observed for Jason-1 than for TOPEX in the first cycles. However, some correlation between the two curves can be deduced from this figure. That shows that consistent signals impact the two systems. Jason-1 SSH differences at crossovers show a slope of about 0.5 mm/yr. This is originated in different behavior of SLA slopes when separating in ascending and descending passes (see section 6.2.1).

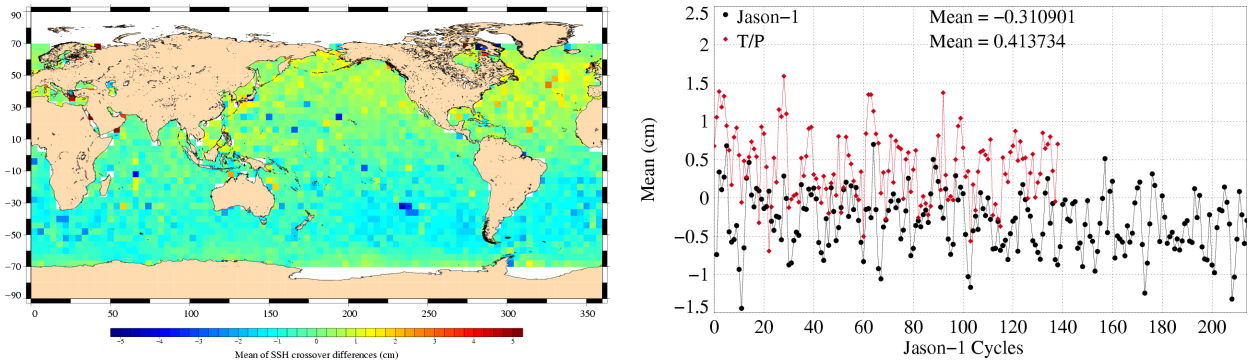

Figure 38: *Map of mean crossovers for Jason cycle 1 to 214(GDR version "b", left) and cycle per cycle mean crossovers (right)*

5.2 Standard deviation of crossover differences

The cycle per cycle standard deviation of crossover differences are plotted in figure 39 (on the left) according to different crossover selections. 3 selections are applied:

- Black curve: no selection is applied. The mean value is 6.47 cm. It shows an annual signal linked to the sea ice variations in the Northern Hemisphere.
- Red curve: shallow waters have been removed (bathy<-1000m). The previous annual signal has been removed by this selection even though it remains a signal probably due to seasonal ocean variations.
- Blue curve: the last selection allows monitoring the Jason-1 system performance. Indeed, areas with shallow waters (1000 m), of high ocean variability (> 20 cm) and of high latitudes (> |50| degrees) have been removed. The standard deviation then provides reliable estimates of the altimeter system performances. In that case, no trend is observed in the standard deviation of Jason-1 SSH crossovers: good performances are obtained, with a standard deviation value of about 5.2 cm all along the mission.

The map of standard deviation of crossover differences overall the Jason-1 period, in figure 39 (on the right) shows usual results with high variability areas linked to ocean variability.

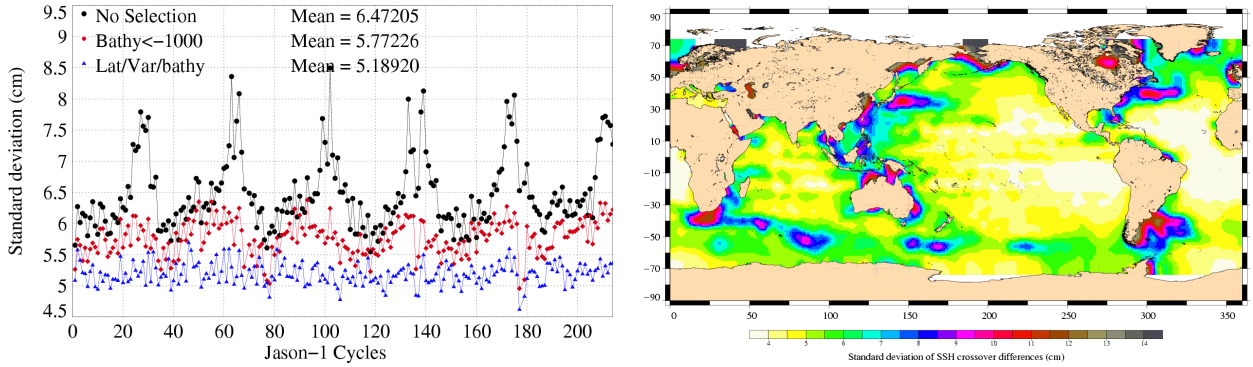

Figure 39: *Cycle per cycle standard deviation crossovers with different selections and map of Jason-1 standard deviation crossovers*

5.3 Comparison of Jason-1 and T/P at crossovers

When comparing performances relative to another mission, much care has to be taken in order to cancel out the contributions of ocean variability and geophysical corrections. Such a comparison between Jason-1 and T/P results has been performed. Apart from homogeneity in geophysical corrections for the two missions, additional processing care has been taken in order to get the most meaningful comparison figures as possible: only open ocean data are selected, away from areas with large ocean variability or with seasonal coverage by sea ice. Furthermore, to account for missing measurements on both missions - in particular due to tape recorder problems on T/P - data are only considered from common datasets. Finally, the SSH computation at crossovers is performed with exactly the same interpolation procedure using cubic spline functions. In order to keep the full 1 Hz high frequency content of the two missions, the spline functions are forced to go through the exact values of the points used in the interpolation, without any smoothing.

In order to distinguish between the effects of long wavelength signals such as orbit errors and the effects of short wavelengths such as instrumental noise, an along-track filtering procedure is used before crossovers are computed. A low-pass filter (Hamming, 1977 [34]) with a cut-off wavelength of 50 km is applied to both Jason-1 and T/P (SSH - MSS) differences. In this case, the CLS01 MSS global model is used. The low frequency signal is directly the output of the filtering routine, while the high frequency signal is derived from the difference between the original signal and the low frequency signal. Then the standard deviation of crossover differences is computed for both satellites on three different datasets: for all wavelengths, for wavelengths larger than 50 km and for wavelengths shorter than 50 km.

The results are presented in figure 40 (bottom). Please note, that the shown results were done using Jason-1 GDRs version "a". It is planned to update the presented study with GDRs version "b" in the future. The overall standard deviation is higher for Jason-1 than for TOPEX. However, the 1 Hz high frequency content is not the same, due to different altimeter ground processing. At the opposite of TOPEX, Jason-1 data are processed by a ground retracking algorithm which makes altimeter measurements more decorrelated (Zanife et al. 2003 [74]). Therefore, TOPEX data are then smoother than Jason-1 data: the 1 Hz high frequency content is lower for TOPEX. The respective contribution of low and high frequencies in Jason-1 and TOPEX crossover residuals is displayed in figure 40.

Figure 40 on the top right shows that short wavelengths contribute a lot in the difference between Jason-1 and TOPEX. While a value of 3 cm is obtained for Jason-1, less than 2.5 cm is observed on TOPEX when wavelengths shorter than 50 km are only considered. Note that for T/P cycle 361 (Jason-1 cycle 18), the Poseidon-1 altimeter was switched on and leads to comparable results relative to Jason-1. Still in figure 40 on the right, another interesting feature is observed from T/P cycles 366 to 369 (Jason-1 cycles 22 to 25): the T/P standard deviation increases and then remains higher than at the beginning of the series. During this period, the T/P satellite was moved away from its original ground track (presently the Jason-1 ground track). Since the along-track filtering is performed on (SSH - MSS) differences, (SSH - MSS) differences between ascending and descending passes are computed instead of SSH differences. Thus errors of the global MSS model away from the initial nominal T/P ground track impact the T/P results after the orbit is moved. Since the crossover location is the same on the two passes - ascending and descending -, higher variance reveals the signature of MSS slope errors in the crossing directions, away from the nominal track used to compute the MSS.

The contribution of wavelengths higher than 50 km is analyzed in figure 40 on the left. Larger differences between Jason-1 and TOPEX are observed before Jason-1 cycle 8. Then Jason-1 and T/P curves are

very similar, even if TOPEX figures are slightly lower than Jason ones. Orbit errors are probably responsible for Jason-1 degraded results on early cycles. It is worth recalling that when producing the GDR ("a") dataset, improvements have been brought to the Jason-1 POE orbit calculation, in particular to manage maneuvers. Because these orbits were recomputed from cycle 9 only, higher variance is obtained for the 8 first Jason-1 cycles.

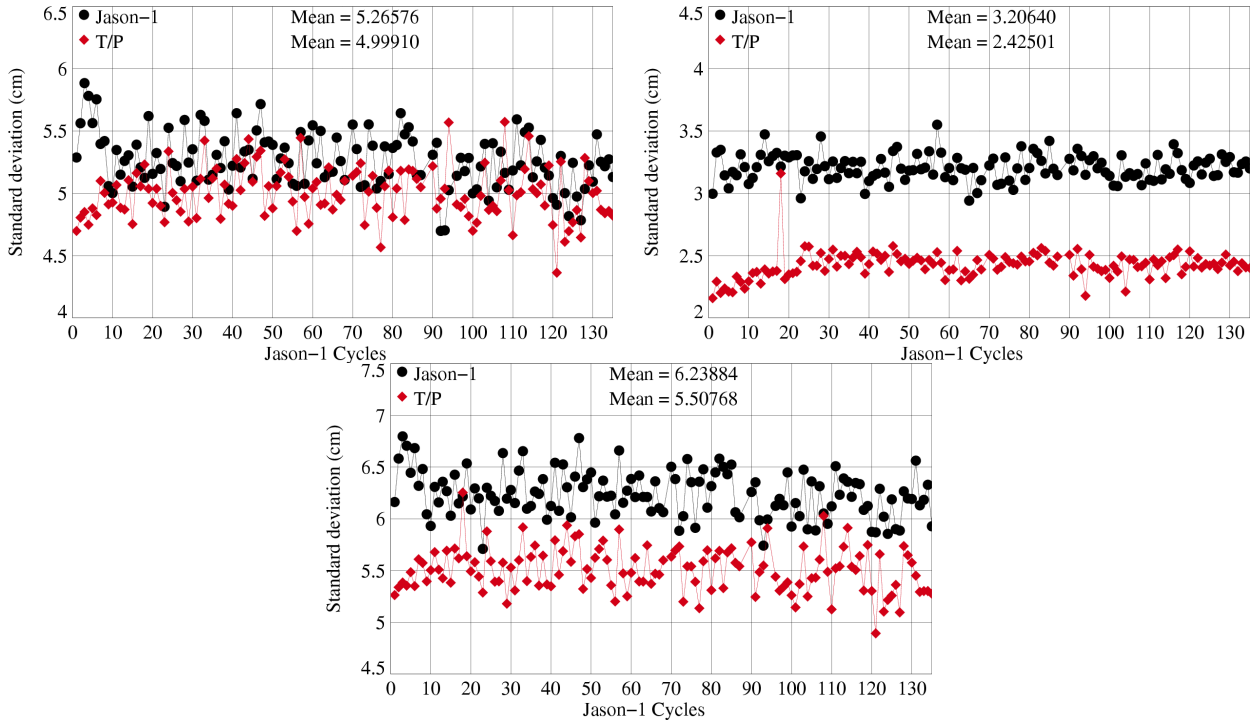

Figure 40: *Cycle per cycle standard deviation crossovers for long wave length content (left), short wave length content (right) and total content (bottom)*

6 Along-track analysis

This analysis is used to compute Sea Level Anomalies (SLA) variability and thus to estimate data quality; it is used to determine the SSH bias between Jason-1 and T/P and the trend in the Mean Sea Level (MSL).

6.1 Along-track performances

6.1.1 Along-track performances before along-track filtering

Along track analyzes are also used to assess the altimeter system performances, by computing Sea Level Anomalies (SLA). The SLA variance gives an estimate of the errors of the system, even though the ocean variability fully contributes in this case. As in the crossover analysis (see in section 5.3), the same type of comparison between Jason-1 and T/P has been performed computing the variance of SLA relative to the CLS01 MSS. This allows global and direct calculations.
The SLA standard deviation is plotted in figure 41 for Jason-1 (GDRs version "b") and T/P. It exhibits similar and good performances for both satellites. However, during the verification phase, the variability is slightly higher for Jason-1 but from cycle 26 onward the performances are very similar. A significant signal is observed from cycle 25 to 35. It is due to the 2002-2003 "El Niño" (McPhaden, 2003, [49]).

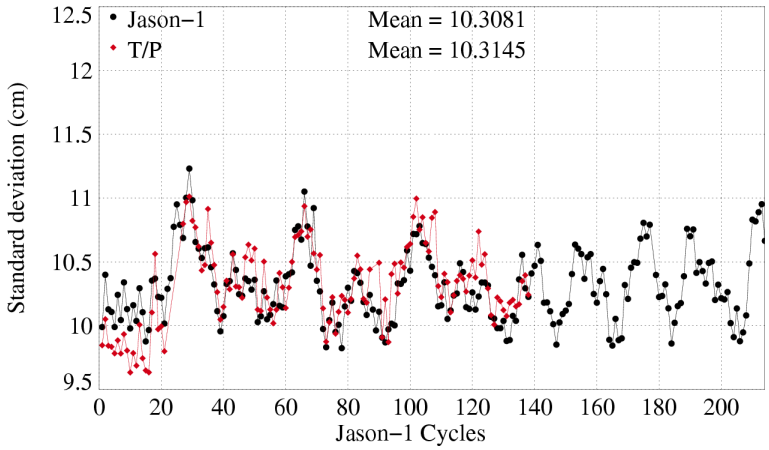

Figure 41: *Cycle per cycle SLA standard deviation*

6.1.2 Along-track performances after along-track filtering

Prior filtering of (SSH - MSS) differences has been applied to produce estimations of the variance (standard deviation) of Jason-1 and T/P SLA according to the selected wavelengths. SLA are computed relative to a global MSS model because the data can be processed in the same way before and after the T/P ground track moves. Moreover, like in the crossover analysis case, measurements are carefully extracted from common datasets and identical processing is applied to both missions.

Figure 42 shows the standard deviation of Jason-1 (GDRs version "a") and T/P SLA differences after along-track filtering, in order to investigate different ranges of wavelengths: less than 50 km, between 50 and 500 km, and more than 500 km. Since geophysical corrections are the same for the two satellites, the first wavelength interval is expected to mostly represent differences in high frequency content, while the last should mainly evidence orbit error differences. Like in the crossover analysis, the Jason-1 high frequency content is higher than the TOPEX one. As already explained, the difference mainly comes from different altimeter ground processing. Poseidon cycle 361 (Jason-1 cycle 18) is evidenced on the curve, with a standard deviation estimation very close to those of Jason-1. For Wavelengths between 50 and 500 km (figure 42 on the right), the standard deviation curves obtained for Jason-1 and T/P are indistinguishable when the two satellites are flying on the same ground track. The signature of MSS errors appears in both figures 42 on the right and bottom after the T/P ground track changes. The long wavelength content showed in figure 42 on the left principally differs between the two satellites in the beginning of the Jason-1 mission. Until Jason-1 cycle 8, larger orbit errors are present on Jason-1 data because these cycles have not been reprocessed, as explained previously. However the difference seems to continue to around cycle 15, contrary to what was observed in the crossover analysis. Higher orbit errors on these Jason-1 particular cycles might be one explanation of this higher variability relative to the MSS. After the first cycles, even slightly larger, the Jason-1 results are much closer to the T/P ones. It is planned to update this analysis with the Jason-1 GDRs in version "b".

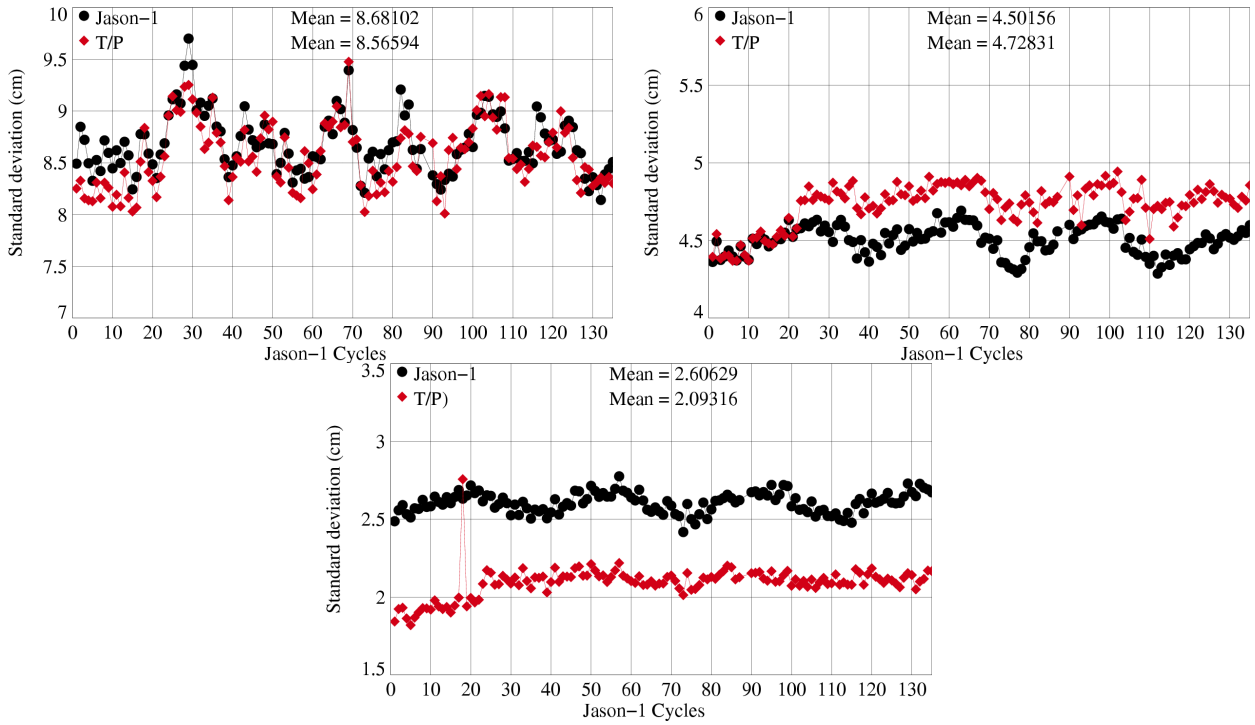

Figure 42: *Cycle per cycle SLA standard deviation for long wavelength content (left), medium wave length content (right) and short wavelength content (bottom)*

6.2 Jason-1 Mean sea level

6.2.1 Sea surface height estimation

Estimation of the mean sea level trend is important for climate change studies. MSL estimation from Jason-1 and T/P are plotted in figure 43 (on the left), after reduction of the relative bias between the two time series.
Several error sources can influence MSL evolution (see section 7.6), one of them is the choice of wet troposphere correction. On the one hand ECMWF model wet troposphere correction might be influenced be model evolutions, on the other hand radiometer wet troposphere correction is influenced by yaw mode transitions (see section 4.7.1). Therefore MSL calculated with radiometer correction (black curve) and with model correction (blue curve) are shown in figure 43. Note that a shift of 1 cm was introduced in order to distinguish the two curves. The results are obtained after area weighting (Dorandeu and Le Traon 1999 [20]). The figure shows good agreement between the two missions and demonstrates that the Jason-1 mission ensures continuous precise MSL monitoring as it was done for more than a decade by the T/P mission. On both missions, seasonal signals are observed, because the inverse barometer correction has been applied in the SSH computation (Dorandeu and Le Traon 1999 [20]). Moreover, 60-day signals are also detected on Jason-1 and T/P series, with nearly the same amplitude. A source of error could be from the largest tidal constituents at twice-daily periods which alias at periods near 60 days for Jason-1 and T/P (Marshall et al. 1995 [45]). Orbit errors in T/P altimeter series used to compute the tide solutions could also have contaminated these models (Luthcke et al. 2003 [44]). Using JMR or model wet troposphere correction has only a slight impact on the slope of about 0.1 mm/year.

On the right of figure 43, annual, semi-annual, and 60-days signals have been adjusted. This allows to decrease the adjustment formal error for both satellites. The global MSL slope is lower for Jason-1 (2.44 mm/yr) than for T/P (2.67 mm/yr), but for Jason-1, the shown time period is more than two years longer than for T/P. Also, the MSL slope of Jason-1 shows a flattening in the end of 2006 and during 2007. Calibration with In-situ data (see section 7.5.1 and more detailed in annual reports [69] and [70]) show no drift of altimetric MSL. Therefore this flattening might be due to the "La Niña" currently active (see section 6.3).

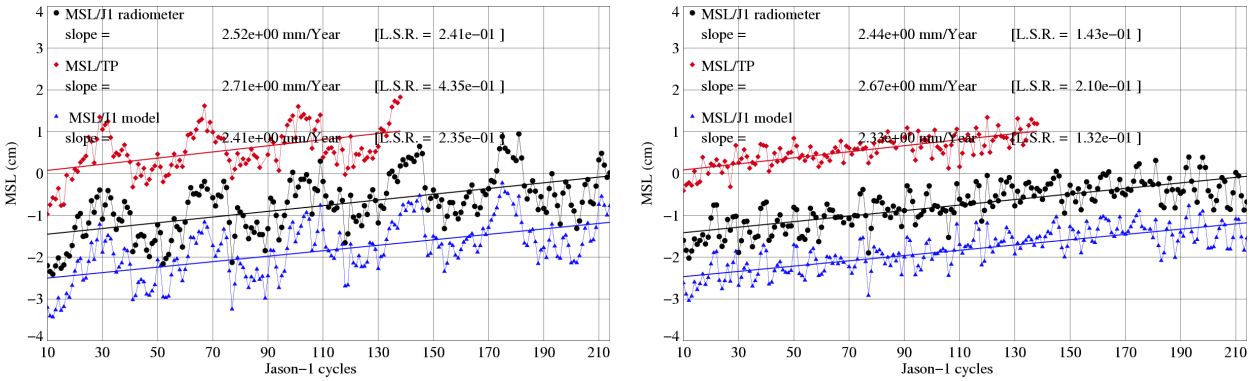

Figure 43: *Jason-1 and T/P mean sea level (on the left) with annual, semi-annual and 60-days adjustment (on the right)*

The shown MSL trends were computed using as well ascending and descending passes, but when com-

puting Jason-1 MSL slope separately for ascending and descending passes, differences are noticed. Figure 44 shows SLA slopes using Jason-1 GDRs (with ECMWF model wet troposphere correction) and T/P MGDRs. SLA slopes are calculated like in section 7.
Jason-1 SLA slopes are quite different:

- 1.95 mm/yr using descending passes
- 2.74 mm/yr using ascending passes

This represents a difference of almost 1 mm/yr. For Envisat data, difference of SLA slope between ascending and descending passes is even greater as shown in [29]. SLA slopes using T/P data are far more homogeneous when separating ascending and descending passes.

- 3.26 mm/yr using descending passes
- 3.11 mm/yr using ascending passes

There is no explanation up to now, for this behavior of Jason-1 data. Since ascending and descending passes cover the same geographical regions, there is no reason why SLA slope should rise differently. A study using several orbit solutions showed, that use of different orbits has an impact on difference of SLA slope noticed between ascending and descending passes. Nevertheless the difference between SLA using ascending or descending passes, is especially visible for 2007, unfortunately none of the studied orbits (except for orbit in the GDR product) was available for 2007. As soon as they will be available, this study will be updated.

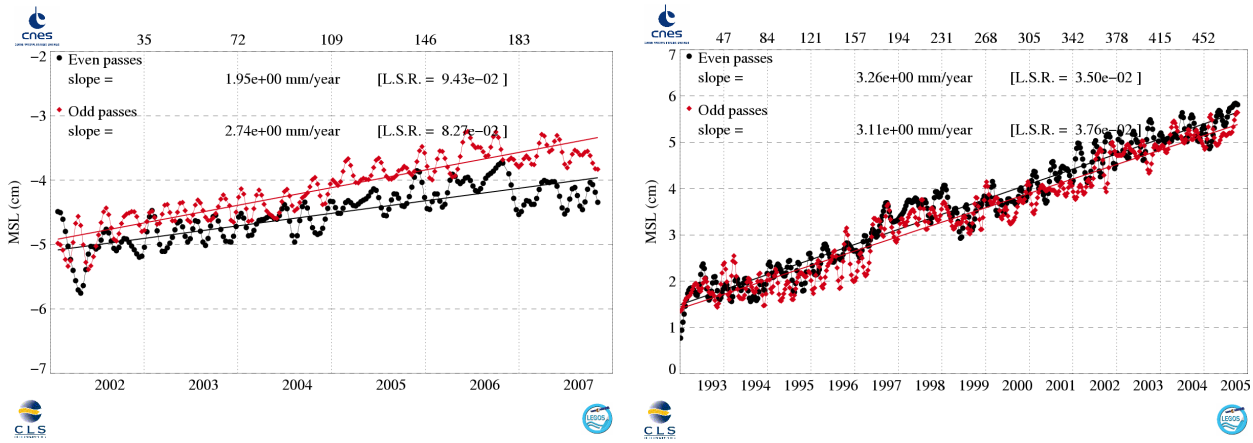

Figure 44: *J1 (left) and T/P (right) SLA slopes using only ascending (odd) or descending (even) passes.*

6.2.2 SSH bias between Jason-1 and T/P

6.2.2.1 Temporal evolution of SSH bias between Jason-1 and T/P

The ECMWF wet troposphere correction is also used in figure 45 which represents the temporal evolution of the SSH bias between T/P and Jason-1. This prevents from errors due to radiometer biases, as the model correction is the same for the two missions. The impact of all geophysical corrections and the particular effect of the SSB correction are also investigated in the figure. Among all geophysical corrections, the greater impact on the T/P to Jason-1 SSH bias estimation is produced by the SSB correction, since results differ by more than 1 cm when applying or not this correction. This is already a great improvement, since difference was 6 cm when using Jason-1 GDRs version "a". Notice that present results have been obtained using a dedicated TOPEX Side B SSB estimation (S. Labroue et al. 2002), since TOPEX side A and side B SSB models are different (e.g. Chambers et al. 2003). Apart from higher variability for Jason-1 cycle 18 (Poseidon-1 was switched on for T/P cycle 361), the T/P to Jason-1 SSH bias nearly remains constant through the Jason-1 mission period.

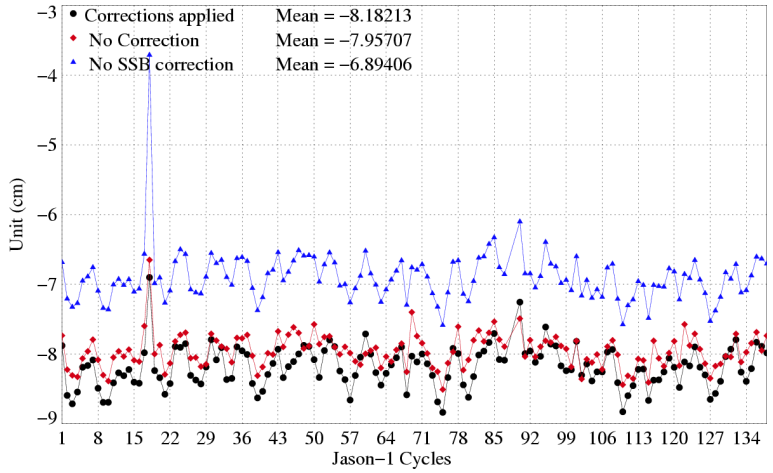

Figure 45: *Cycle per cycle mean of (T/P−Jason-1) SSH differences*

6.2.2.2 Spatial distribution of SSH bias between Jason-1 and T/P

Jason-1 and T/P have not been on the same track from cycle 21 onward. Consequently, the SSH differences can not be obtained directly as a result of the ocean variability. Thus, the map of the SSH differences between Jason-1 and T/P is obtained at the Jason-T/P crossovers in figure 46. The figure was generated using Jason-1 GDR version "b" (cycle 1 to 138) with the new orbit based on EIGEN-CG03C gravity field, whereas T/P still contains an orbit based on JGM3 gravity field. Large structures of negative and positive differences up to an amplitude of 2 cm are visible. These are due to residual orbit errors on T/P mission. Use of an orbit based on GRACE gravity model for T/P strongly reduces these differences, as visible on figure 47. The data of both missions are much more homogeneous, when looking at global maps. Indeed, when separating ascending and descending passes during computing T/P - Jason-1 SLA differences, large hemispheric biases appear (see figure 48)

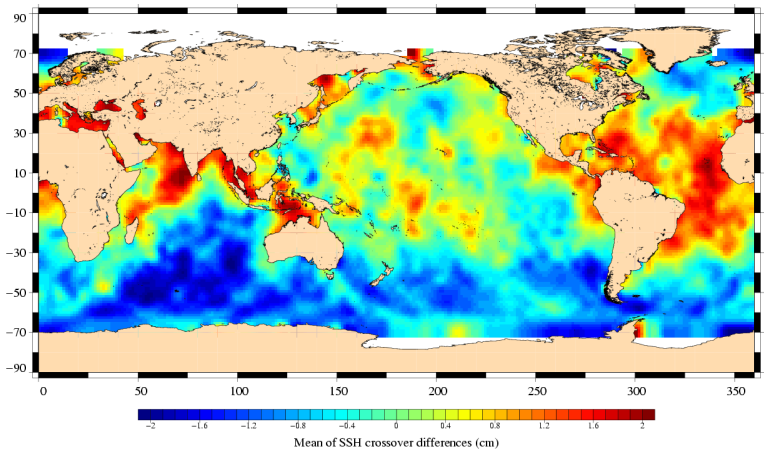

Figure 46: *Map of (T/P−Jason-1) SSH differences for Jason-1 GDR version "b" period.*

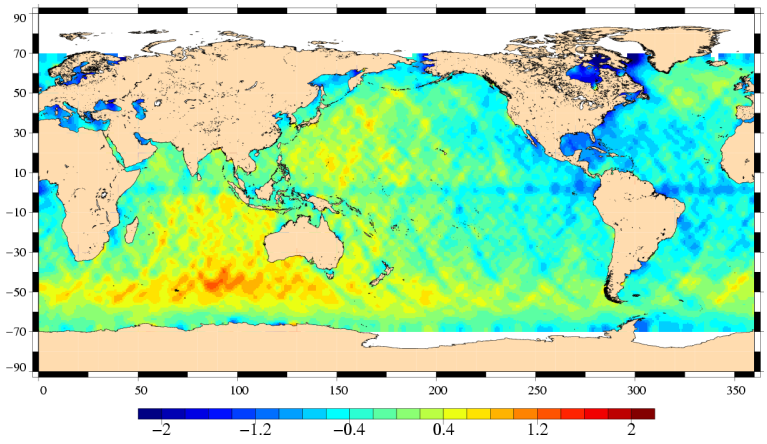

Figure 47: *Map of (T/P−Jason-1) SSH differences for Jason-1 cycles 1 - 21, using orbit based on GRACE gravity model for T/P.*

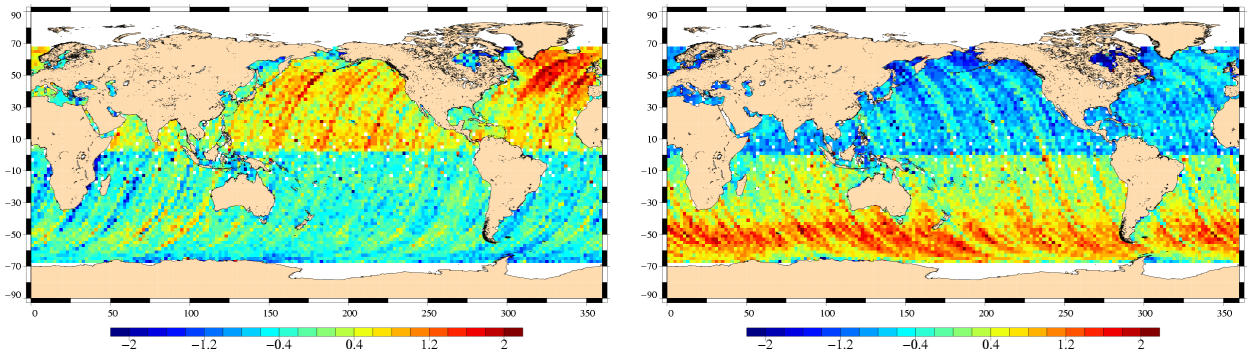

Figure 48: *Map of (T/P−Jason-1) SSH differences separating ascending and descending passes for cycles 1 - 21, using orbit based on GRACE gravity model for T/P.*

6.2.2.3 Hemispheric SSH bias between Jason-1 and T/P

In order to further investigate hemispheric (T/P−Jason-1) SSH biases, its temporal evolution is presented in figure 49. It shows hemispheric differences between T/P and Jason-1, when separating northern and southern hemisphere. From the northern hemisphere to the southern hemisphere the (T/P−Jason-1) SSH bias estimates can thus differ by up to 2 cm. These hemispheric differences seem consistent from one cycle to another. These differences are mainly due to the orbit. The use of GDRs version "b" has already considerably lowered the difference between northern and southern hemisphere during cycles 50 to 70. Using orbits with ITRF 2005 reference system for both Jason-1 and T/P will probably further reduce these hemispheric differences.

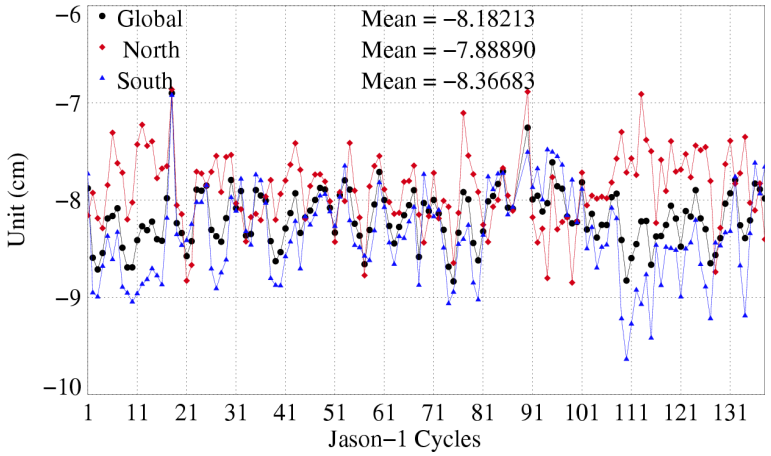

Figure 49: *Cycle per cycle mean of (T/P−Jason-1) SSH differences by hemisphere*

6.3 Sea level seasonal variations

From Sea Level Anomalies computed relative to the Mean Sea Surface CLS 2001 (Hernandez et al, 2001), the surface topography seasonal variations have been mapped in figure 50 for the overall Jason-1 data set. Major oceanic signals are showed clearly by these maps: it allow us to assess the data quality for oceanographic applications. The most important changes are observed in the equatorial band with the development of an El Niño in 2002-2003. The event peaked in the fourth quarter of 2002, and declined early in 2003. Conditions indicate an event of moderate intensity that is significantly weaker than the strong 1997-1998 El Niño (McPhaden,2003, [49]).
End of 2007, an La Niña event is visible in Eastern Pacific on figure 55. It will probably last till the first quarter of 2008 (see [68]).

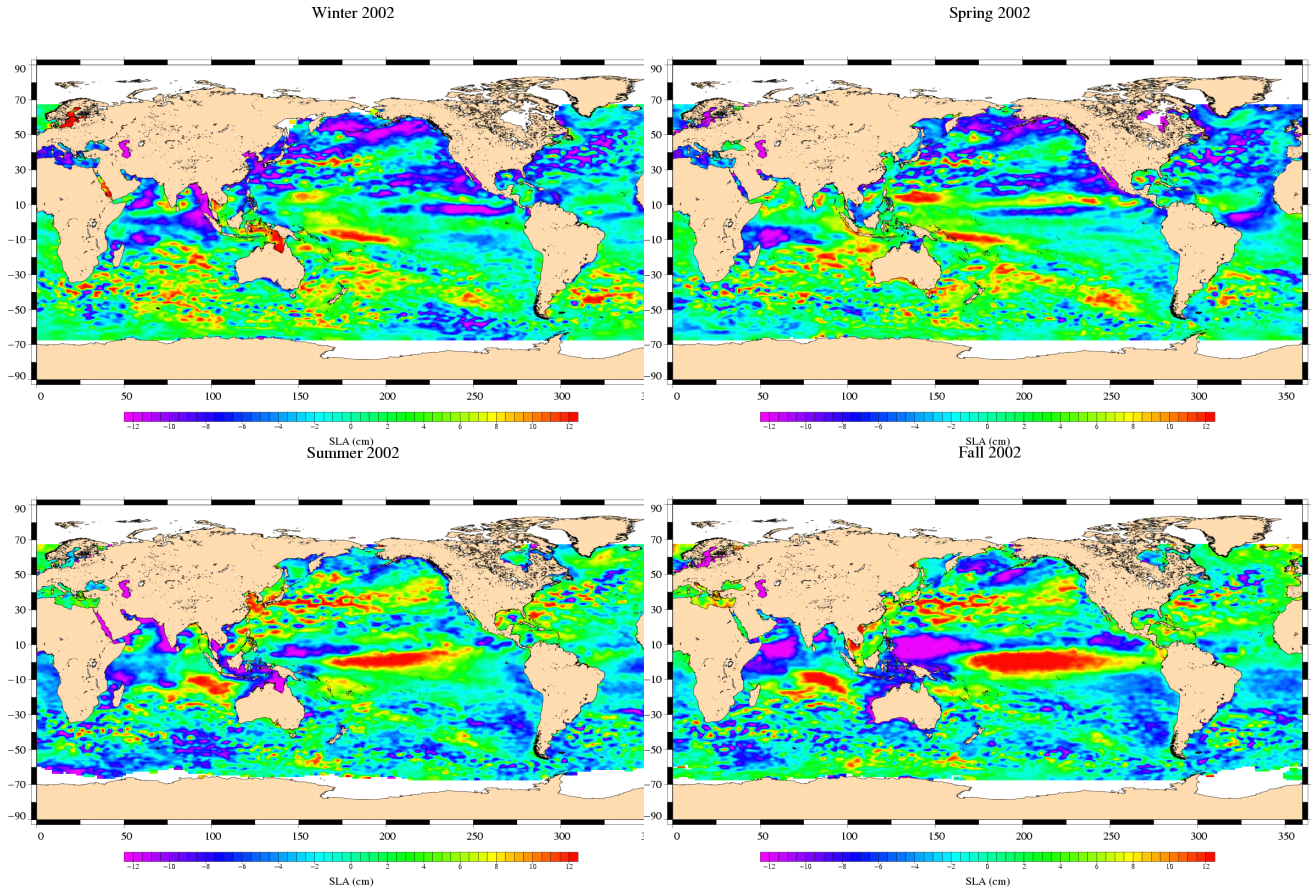

Figure 50: *Seasonal variations of Jason SLA (cm) for year 2002 relative to a MSS CLS 2001*

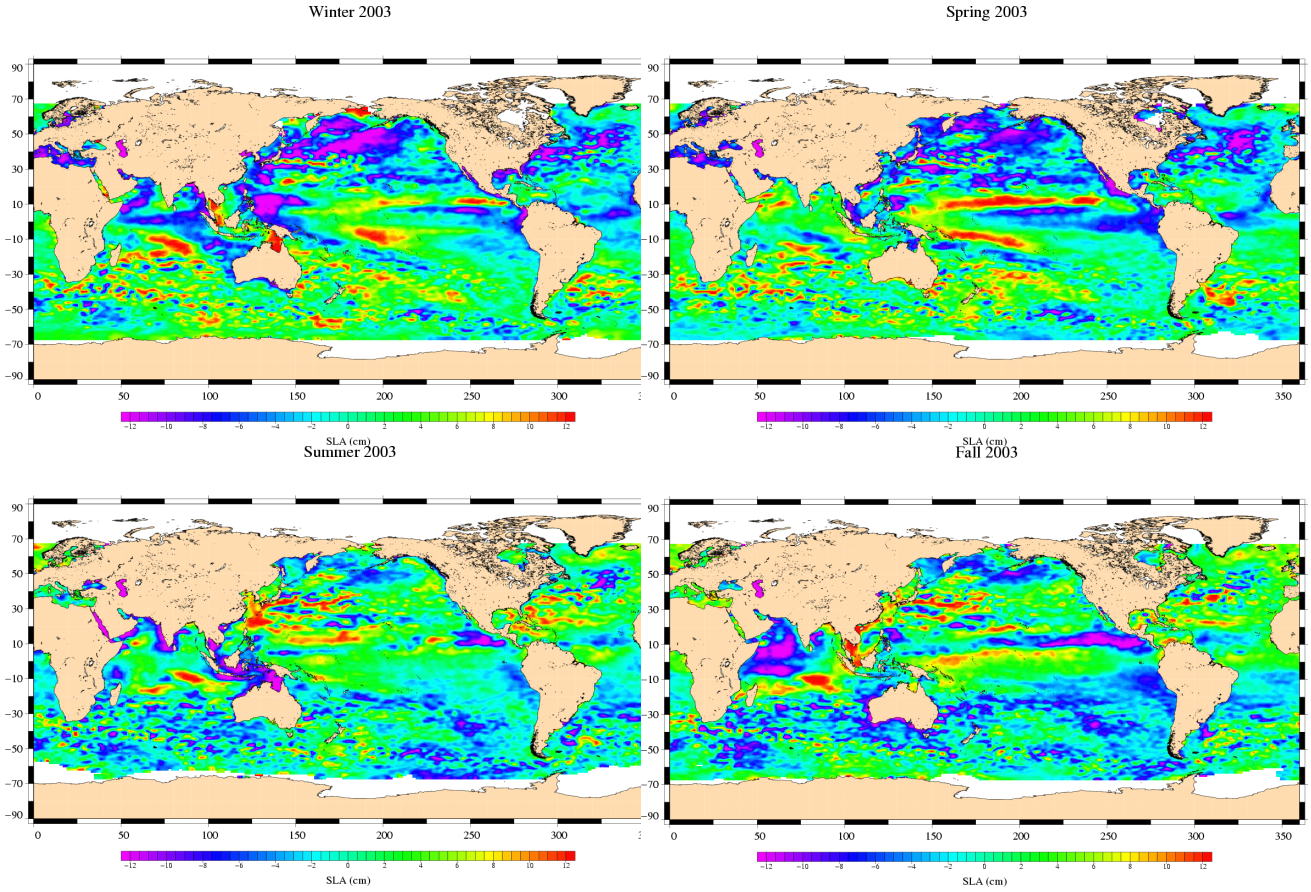

Figure 51: *Seasonal variations of Jason SLA (cm) for year 2003 relative to a MSS CLS 2001*

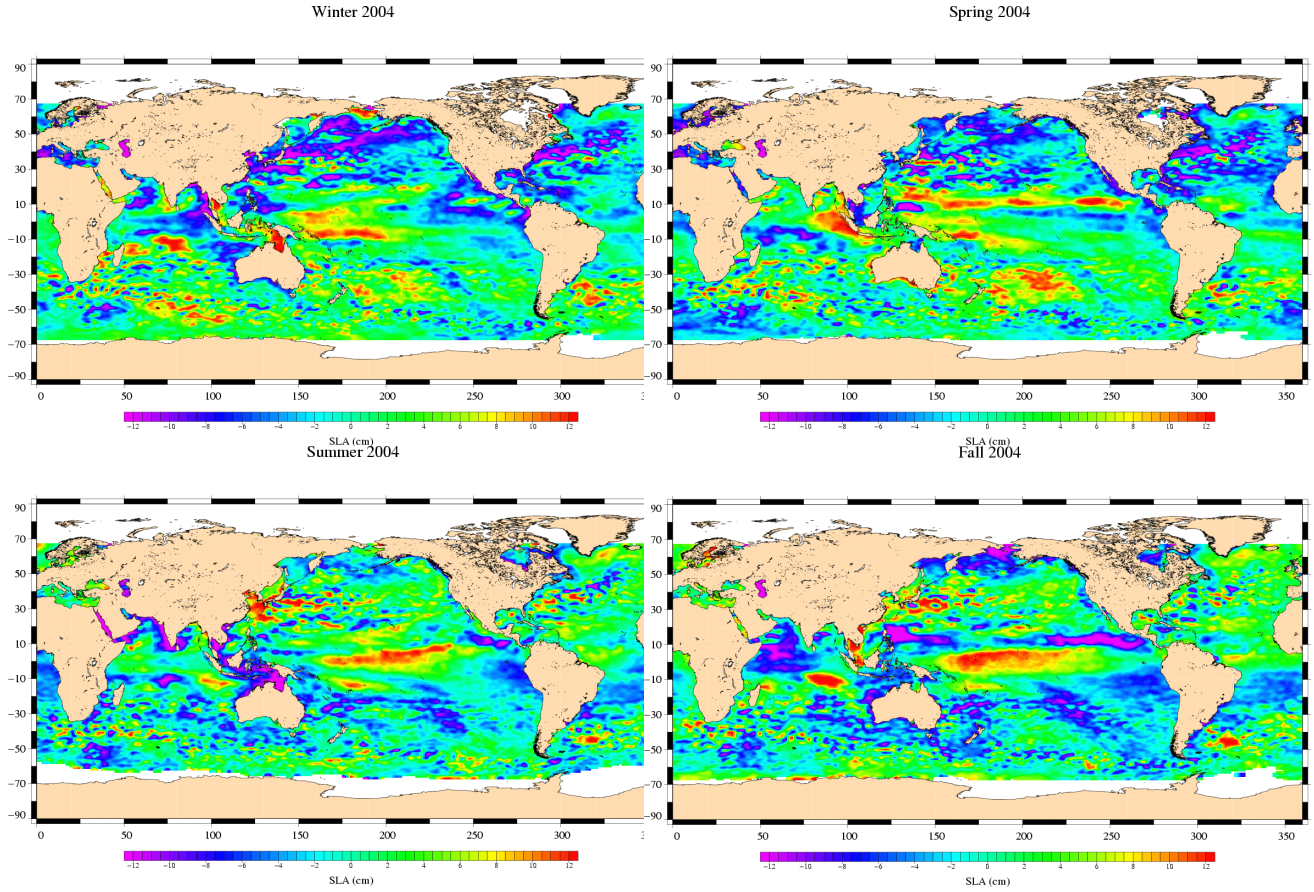

Figure 52: *Seasonal variations of Jason SLA (cm) for year 2004 relative to a MSS CLS 2001*

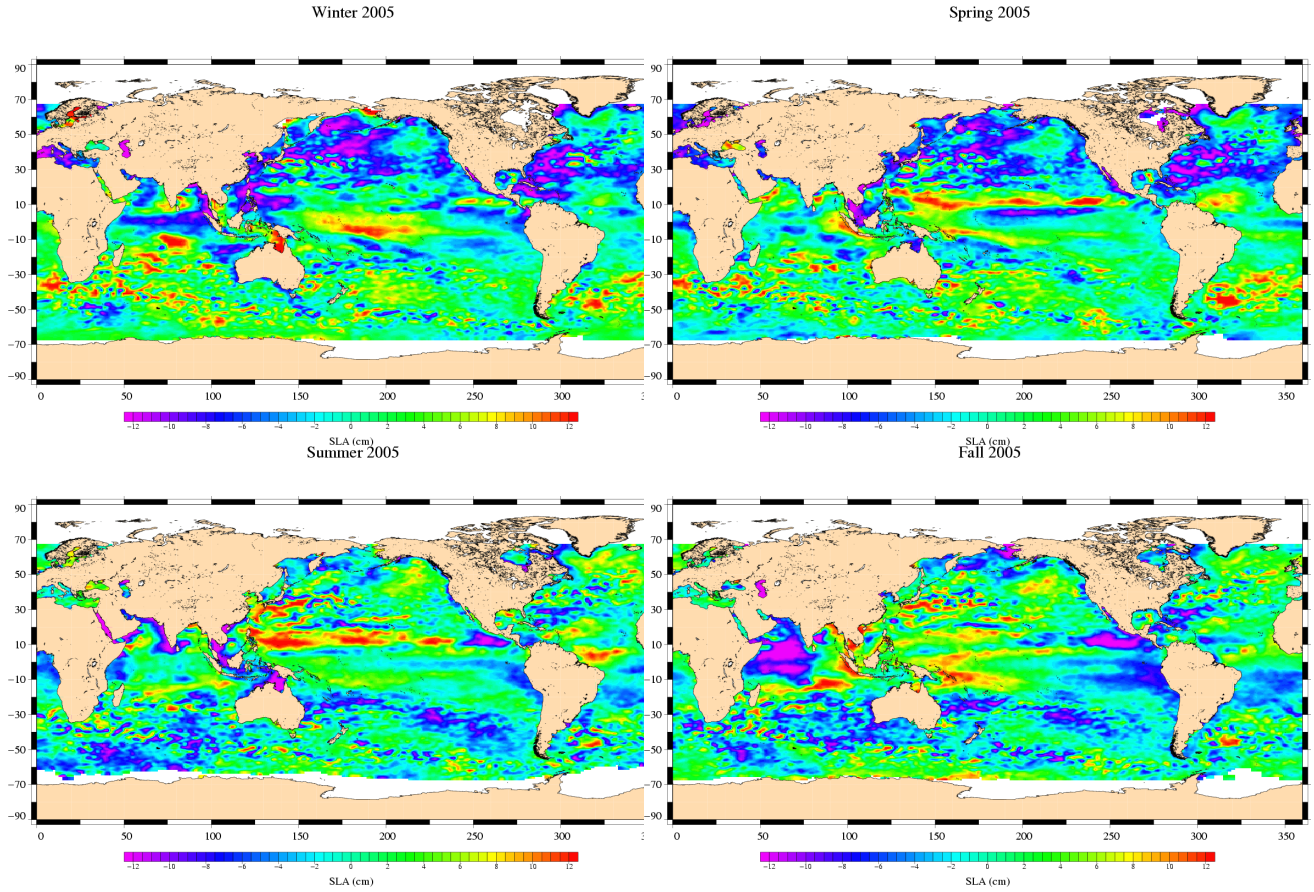

Figure 53: *Seasonal variations of Jason SLA (cm) for year 2005 relative to a MSS CLS 2001*

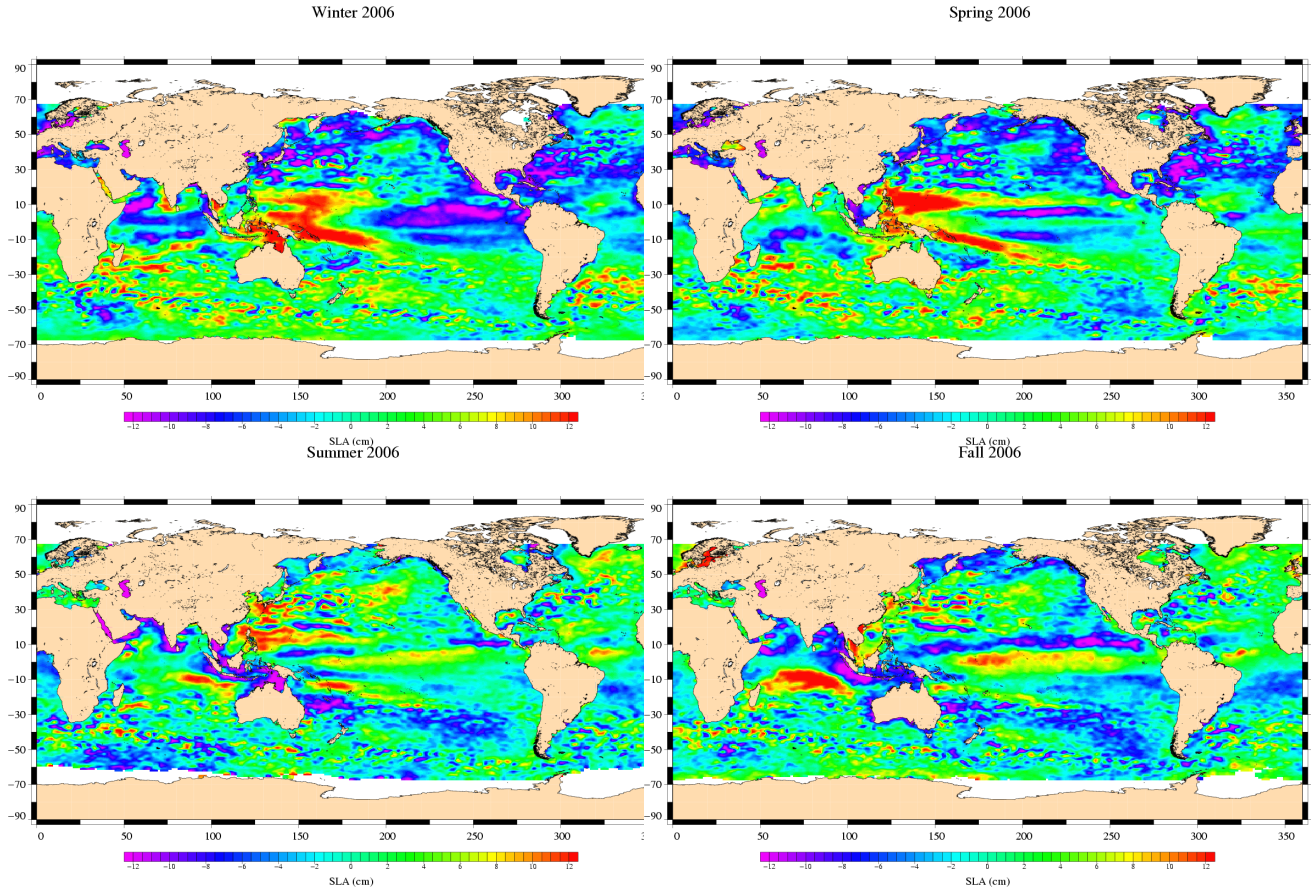

Figure 54: *Seasonal variations of Jason SLA (cm) for year 2006 relative to a MSS CLS 2001*

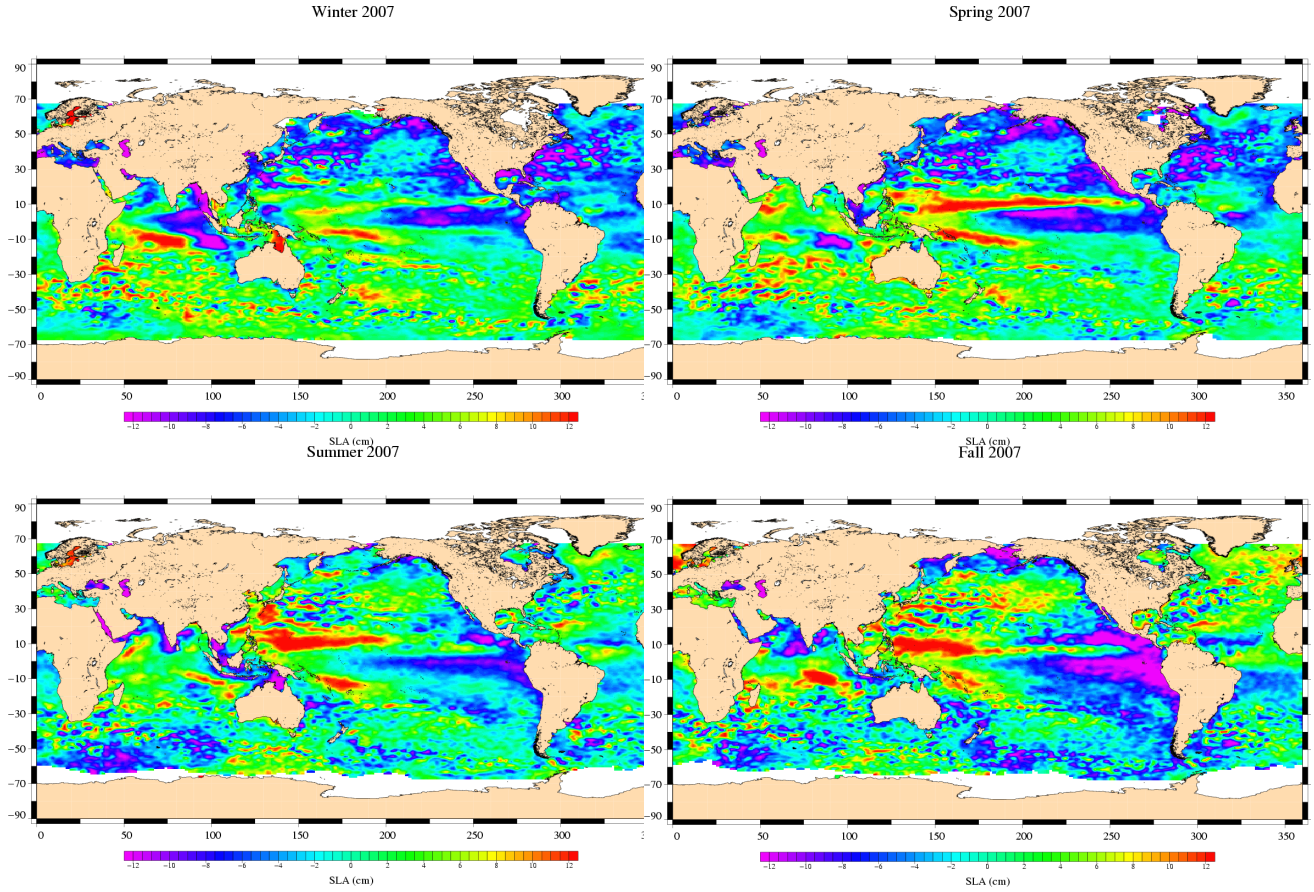

Figure 55: *Seasonal variations of Jason SLA (cm) for year 2007 relative to a MSS CLS 2001*

7 Global and regional Mean Sea Level (MSL) trends

7.1 Overview

Long-term MSL change is a variable of considerable interest in the studies of global climate change. Thus, a lot of works have been performed on the one hand to survey the mean sea level trends and on the other hand to assess the consistency between the MSL derived from all the operational altimeter missions. Besides, external data source have been used to assess the altimetric MSL evolution. The in-situ data provided by tide gauges and temperature/salinity (T/S) profiles have been used to compare the MSL. The main results derived from these works are summarized here (the complete analysis are available in the annual reports [69] and [70]). In addition, the Reynolds SST have been also monitored over the global ocean to analyze the MSL trend.

7.2 SSH applied for the MSL calculation

The SSH formula used to compute the MSL is defined for all the satellites as below :

$$SSH = Orbit - Altimeter\ Range - \sum_{i=1}^{n} Correction_i$$

with :

$$\begin{aligned}
\sum_{i=1}^{n} Correction_i \;=\; & Dry\ troposhere\ correction\ new\ S1\ and S2\ atmospheric\ tides\ applied \\
+\; & Combined\ atmospheric\ correction :\ MOG2D\ and\ inverse\ barometer \\
+\; & Wet\ troposhere\ correction\ (radiometer\ or\ ECMWF\ model) \\
+\; & Filtered\ dual\ frequency\ ionospheric\ correction \\
+\; & Non\ parametric\ sea\ state\ bias\ correction \\
+\; & Geocentric\ ocean\ tide\ height,\ GOT\ 2000 :\ S1\ atmospheric\ tide\ is\ applied \\
+\; & Solid\ earth\ tide\ height \\
+\; & Geocentric\ pole\ tide\ height
\end{aligned}$$

The SSH formula has been modified or updated for each satellite in order to calculate the best MSL. Especially, stability problems of the radiometer wet troposphere correction have been taken into account :

- For Jason-1 : the radiometer wet troposphere correction is used even though 60-days signals are still detected since 2006.
- For Envisat : the ECMWF model wet troposphere correction is used to remove the effects of abnormal changes or trends observed on the radiometer wet troposphere correction, the USO correction has been applied (drift and anomaly (see Envisat yearly report [29])

- For T/P : the radiometer wet troposphere correction drift has been corrected with Scharroo's correction (Scharroo R., 2004 [61]), the relative bias between TOPEX and Poseidon and between TOPEX A and TOPEX B has been taken into account, the drift between the TOPEX and DORIS ionosphere corrections has been corrected for on Poseidon cycles.
- For Geosat Follow-On: the ECMWF model wet troposphere correction is used, the GIM model has been used for the ionospheric correction.

7.3 Analyze of the MSL trend

7.3.1 Global MSL trend derived from Jason-1 and T/P data

The global MSL trend derived from satellite altimetry - TOPEX/Poseidon and Jason-1 - is now used as the reference for climate studies. A SSH bias of 7.5 cm has been applied on Jason-1 data to link both MSL series. This bias has been calculated using the verification phase where Jason-1 and T/P were on the same orbit. This allows us to compute accurately the SSH bias. This MSL plotted on figure 56 highlights a global trend close to 3.07 mm/yr when the post glacial rebound is not taken into account. The adjustment formal error is low (lower than 0.03 mm/yr) showing a linear evolution of the MSL. However, the MSL rise is lower and very weak since 2006. During this period, only Jason-1 measurements are present, thus the comparisons with T/P MSL is not possible to confirm this behavior. But the comparisons with other satellites and in-situ data as described further, do not evidence an abnormal drift on Jason-1 measurements. Besides, a very strong "La Niña" phenomena is on going (since 2007), and might explain this MSL trend change. In this case, the MSL should increase as soon as "La Niña" will be finished, probably in second part of 2008.

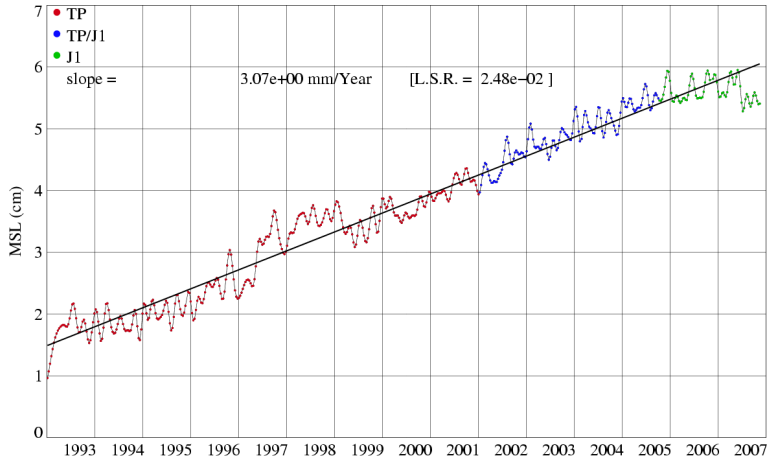

Figure 56: *Global MSL trend derived from Jason-1 and T/P data*

7.3.2 Regional MSL trends derived from AVISO merged products

The AVISO merged products are used to compute the regional MSL trends. Indeed, thanks to the high resolution of their grids (0.5 degrees), the MSL regional trends can be also calculated with a good resolution. This allows to very well displayed the variability of regional slopes as plotted on map 57. The local slopes

range between ±10mm/yr with large structure in the main oceans, especially in Pacific Ocean. This kind of map bring a lot of information about the regional MSL evolution, which have to be analyzed in details. For instance, the Gulf Stream current displayed a strong negative slope. This behavior might be related with a decrease of the current intensity linked with the climate warming.

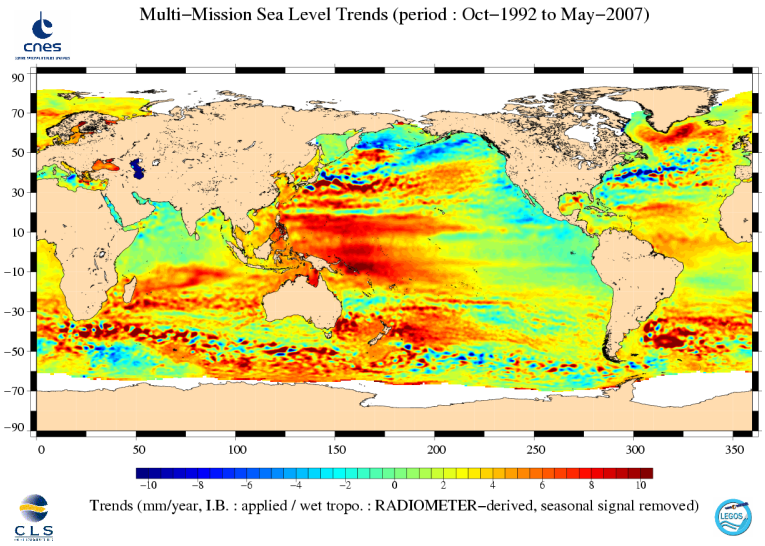

Figure 57: *Regional MSL trends derived from AVISO merged products*

7.4 Multi-mission comparisons of global MSL trends

The MSL has been monitored for each satellite altimeter over global ocean in order to assess the global MSL trend and also to detect any anomalies or any drifts on each MSL series. These different MSL have been plotted in figure 58, after removing annual and semi-annual signals, and filtering out signals lower than 60 days. The T/P and Jason-1 slopes since the beginning of Jason-1 period are very close within 0.2 mm/yr. Even though GFO slope is smaller by 0.7 mm/year over the Jason-1 period, it indicates a similar trend. Finally, only Envisat MSL shows a trend quite different with a global slope close to 1 mm/yr. The estimation of the Envisat MSL seems impacted by an unexpected behavior on the early years partly linked with a potential drift of USO correction. This item is described in detail in the Envisat annual report [29].

7.5 External data comparisons

7.5.1 Tidal gauges and T/S profiles

In order to assess the global MSL trend, comparisons to independent in-situ datasets are of great interest. Two methods have been developed in the frame of in-situ Cal/val and thoroughly described in annual reports ([69] and [70]). First, TOPEX/Poseidon and Jason-1 altimetric data have been compared with tide gauge measurements thanks to a dedicated method which aims at detecting potential drifts in sea surface heights (SSH). The tide gauge network processed is the GLOSS/CLIVAR "fast" sea level database, formerly known as the WOCE network. Secondly, an innovating method with similar objectives has been developed using thousands of free-drifting profiling floats of the ARGO network. Altimetric data have thus been compared

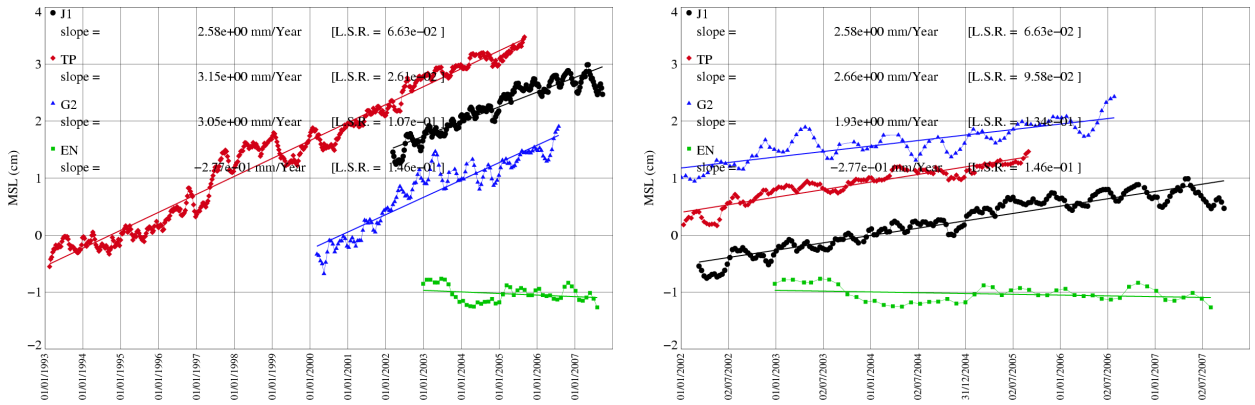

Figure 58: *Multi-mission MSL over global ocean since the beginning of T/P mission on the left and the beginning of Jason-1 mission on the right after removing annual, semi-annual and 60-day signals.*

to sea level heights computed from these in-situ temperature/salinity profiles. Both methods complement each other since the first one using tide gauges only concerns coastal areas while the second one using T/S profiles is well widespread to get an assessment of the MSL in the open ocean.
From these comparison methods, SSH bias monitorings have been computed and bring out a drift lower than 0.5 mm/year (see figure 59) whatever in-situ data used. This trend results both from the error on datasets and the intrinsic error of the method, partly linked to the colocation of the altimetric and in-situ measurements in space and time. Finally, this study provides an upper bound of the error of the global MSL trend. This error will keep on refining in the future using new in-situ datasets, especially for the T/S profile method.

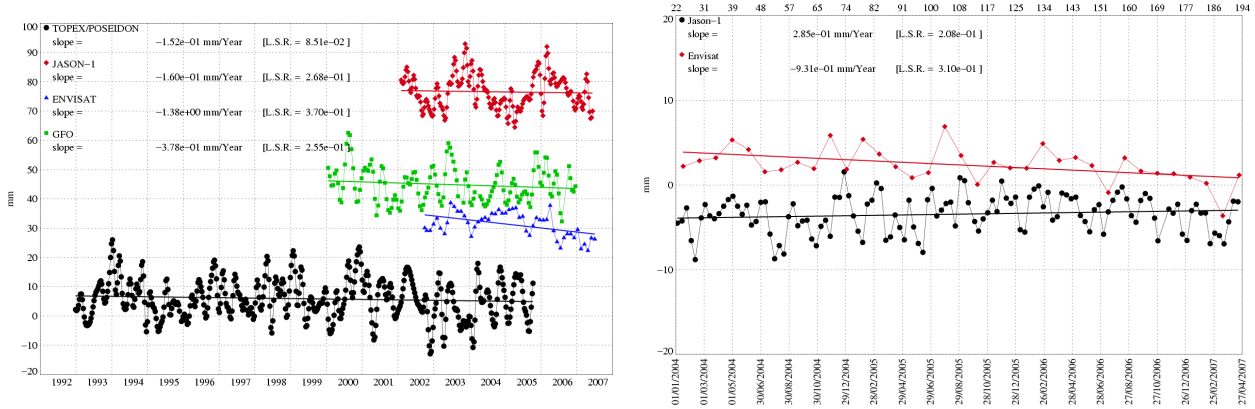

Figure 59: *Altimetric MSL drifts using tide gauges measurements (left) and T/S profiles (right)*

7.5.2 Reynolds's SST

The Reynold's SST has been monitored over the 15 year period from 1993 to 2007 along the T/P and Jason-1 tracks. It is compared with the reference MSL in figure 60, after removing annual signal, semi-annual signal, and signals lower than 60 days. In order to compare the dynamic of the MSL and SST increases, the SST scale has been adjusted on the MSL scale so that the SST trend and the MSL trend are

visually the same. The mean SST rises by about 0.013 degree/yr with a dynamic stronger than the MSL. In particular, the signature of "El Niño" is more visible. Besides, the SST curve is relatively flat for 4 or 5 years. It even seems to decrease in 2007, which might be the signature of "La Niña".

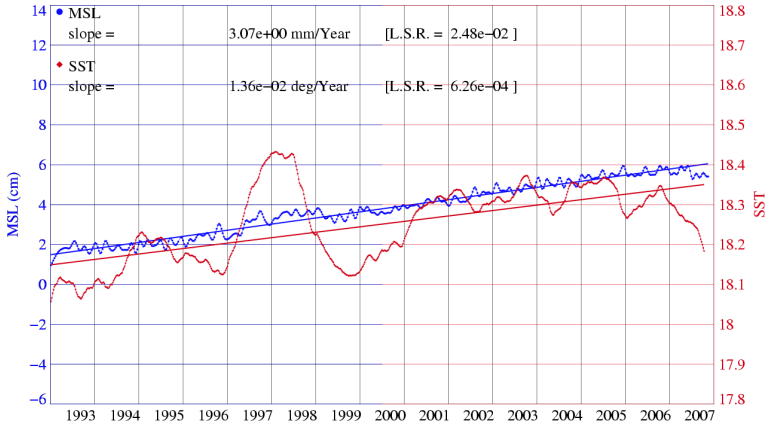

Figure 60: *Comparison of MSL and SST trend over global ocean for the T/P period*

7.6 Estimation of global MSL error

As described previously, the MSL derived from satellite altimetry (TOPEX/Poseidon and Jason-1) is now used as the reference for climate studies : a global rate of 3.1 mm/yr is obtained over the 15 year period from 1993 to 2007 when the post glacial rebound is not taken into account. Besides, the regional sea level trends bring out an inhomogeneous repartition of the ocean elevation with local MSL slopes ranging from +/- 10 mm/year. The different errors which can impact the global and regional MSL trends have been estimated and analyzed. The potential drifts detected in the orbit models and in the geophysical corrections - as wet troposphere and atmospheric corrections - are the main sources of error impacting the MSL trends. The use of different orbit solutions provided by JPL, CNES and GSFC allowed to estimate the MSL slope uncertainty, highlighting a north/south hemispheric effect on the regional MSL slope close to ± 2 mm/yr. Especially, using ITRF2005 in new orbits solutions has an hemispheric impact as displayed in figure 61. Concerning the geophysical corrections, a similar method is applied using different meteorological models (NCEP, ECMWF, ERA40). It brings out a global MSL slope error close to 0.3 mm/year. In particular for the radiometer wet troposphere correction, the comparison with the ECMWF model using different altimetric missions highlights an uncertainty close to 0.2 mm/yr for the global Jason-1 MSL trend as plotted in figure 62. Other sources of slope discrepancies have been identified and estimated: the error due to the Sea Surface Height (SSH) bias at the connection point between Jason-1 and TOPEX/Poseidon MSL series, but also between Side-A and Side-B TOPEX altimeters. The SSH bias is indeed associated with an error leading directly to an error on the MSL trend calculation.
Finally, the combination of all errors will provide an error estimate of global and regional MSL trends. Taking into account the covariance of each error through an inverse method will allow to calculate a more realistic overall error budget.

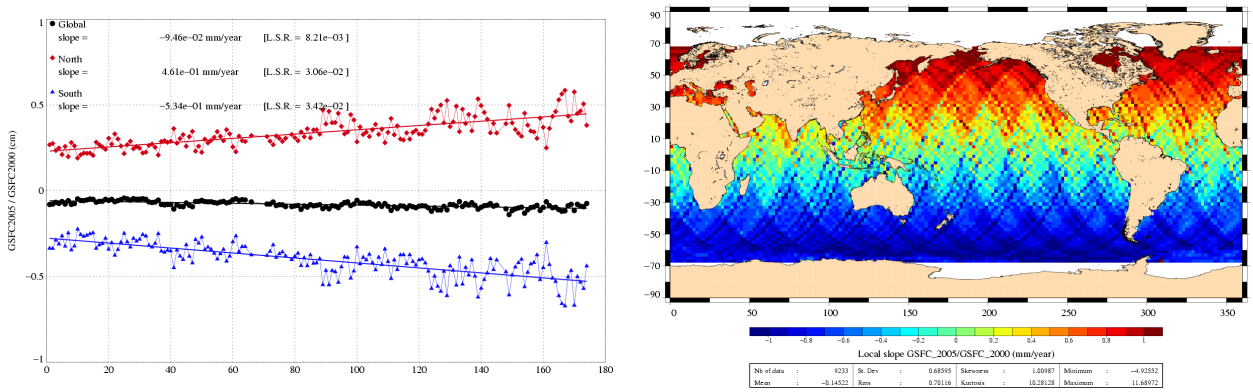

Figure 61: *Impact on Jason-1 MSL trends of using GFSC orbit with ITRF2005 instead of ITRF2000*

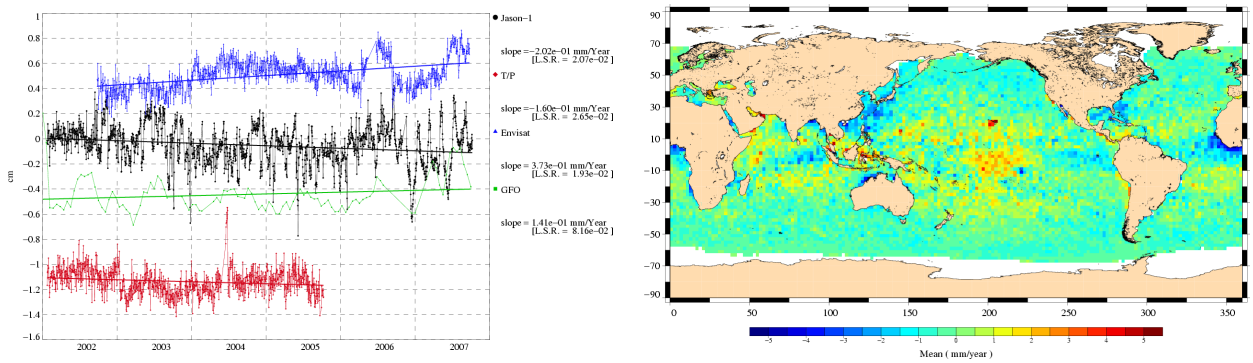

Figure 62: *Impact on Jason-1 MSL trends of using wet tropospheric corrections derived from ECWMF model instead of radiometer*

8 Conclusion

Since the beginning of the Jason-1 mission and until the end of the T/P mission in October 2005, T/P and Jason-1 overflew the ocean over 2 parallel passes except the 21 first cycles, when there were on the same pass. Thanks to this long flight configuration, performances comparisons between both missions have been performed with success during 4 years, proving that the major objective of the Jason-1 mission to continue the T/P high precision has been reached. Almost six years of Jason-1 data are now available. The good quality of Jason-1 data has been shown in this report : the main altimeter parameters are stable and have the same behaviors as T/P ones, the crossover and along-track performances remain very good.

Moreover, the new GDR release (version "b") allowed us to impove significantly the Jason-1 data in comparison with the former GDR version. The new geophysical corrections (as DAC high frequency correction), the new orbit (using Grace data) and new retracking (MLE-4) are the main sources of improvement. Thanks to these improvements, the SSH correlated geographical biases have been reduced and the SSH performances are significantly better. However some problems are remaining and will be taken into account in a future GDR release. First, the radiometer wet troposphere correction provided in the GDRs "b" allows us to correct partially the anomalies observed in the GDR "a" especially for the 60-day signal linked to the yaw maneuvers. Secondly, the orbit improvement highlighted a time tag shift of about 0.3 ms in the new GDR Jason-1. The impact of this anomaly is an SSH ascending/descending bias of about 0.5 cm.

The Jason-1 GDR reprocessing in version "b" was finished mid-2007, Jason-1 data are now available in a homogeneous series. It is also planned to make an other GDR release probably in 2008. The major evolutions will be a new precise orbit based on new Grace data and new ITRF model, better ECMWF meteo fields, new geophysical corrections, new SSB correction. Besides it is planned to re-process T/P M-GDRs data with similar algorithms. Then, performances and comparisons will be carried out again using these new data in order to assess the GDRs reprocessing and to assess the consistency between Jason-1 and T/P sea surface height.

9 References

References

[1] Ablain, M., J. Dorandeu, Y. Faugère, F. Mertz, B. Soussi, F. Mercier, P. Vincent, and N. Picot. 2003a. SSALTO/CALVAL Jason-1 data quality assessment and Jason-1 / TOPEX cross-calibration using GDRs. *Paper presented at the Jason-1 and TOPEX/Poseidon Science Working Team Meeting, Arles (France), November.*

[2] Ablain, M., J. Dorandeu, Y. Faugere, F. Mertz, 2004. Jason-1 Validation and Cross-calibration activities Contract No 731/CNES/00/8435/00. Available at: http://www.jason.oceanobs.com/documents/calval/validation_report/j1/annual_report_j1_2004.pdf

[3] Ablain, M. and J. Dorandeu, 2005. TOPEX/Poseidon validation activities, 13 years of T/P data (GDR-Ms), Available at: http://www.jason.oceanobs.com/documents/calval/validation_report/tp/annual_report_tp_2005.pdf

[4] Ablain, M., S. Philipps, P. Thibaut, J. Dorandeu, and N. Picot 2007. Jason-1 GDR Quality Assessment Report. Cycle 211. SALP-RP-P2-EX-21072-CLS211, November. http://www.jason.oceanobs.com/html/calval/validation_report/j1/j1_calval_bulletin_211_uk.html

[5] Ablain, M., S. Philipps, S. Labroue, J. Dorandeu, and N. Picot, 2007. SSALTO CALVAL Consistency assessment between Jason-1 and TOPEX. poster presented at OSTST meeting, Hobart, Australia, 12-15 march 2007. Available at: http://www.jason.oceanobs.com/documents/swt/posters2007/ablain_J1TP.pdf

[6] Ablain, M., S. Philipps, J. Dorandeu, and N. Picot, 2007. SSALTO CALVAL Performance assessment Jason-1 data. Poster presented at OSTST meeting, Hobart, Australia, 12-15 march 2007. Available at: http://www.jason.oceanobs.com/documents/swt/posters2007/ablain_J1.pdf

[7] Amarouche, L., P. Thibaut, O.Z. Zanife, P. Vincent, and N. Steunou. 2004. Improving the Jason-1 Ground Retracking to Better Account or Attitude Effects. *Mar. Geod.***27 (1-2): 171-197.**

[8] Arnault, S., N. Chouaib, D. Diverres, S. Jaquin, and O. Coze, 2004. Comparison of TOPEX/Poseidon and JASON Altimetry with ARAMIS In Situ Observations in the Tropical Atlantic Ocean. *Mar. Geod.***27 (1-2): 15-30.**

[9] Brown G.S., "The average impulse response of a rough surface and its application", IEEE Transactions on Antenna and Propagation, Vol. AP 25, N1, pp. 67-74, Jan. 1977.

[10] Callahan, Phil. electronic communication (retrk-gdr-data-rec-r10.062.pdf) send to OSTST on 13 February 2006.

[11] Carayon, G., N. Steunou, J. L. Courrière, and P. Thibaut. 2003. Poseidon 2 radar altimeter design and results of in flight performances. *Mar. Geod.***26(3-4): 159-165.**

[12] Carrère, L., and F. Lyard, Modeling the barotropic response of the global ocean to atmospheric wind and pressure forcing - comparisons with observations. 2003. Geophys. Res. Lett., 30(6), 1275, doi:10.1029/2002GL016473.

[13] Chambers, D. P., S. A. Hayes, J. C. Ries, and T. J. Urban. 2003. New TOPEX sea state bias models and their effect on global mean sea level. J. Geophys. Res. 108(C10): 3305.

[14] Chambers, D., P., J. Ries, T. Urban, and S. Hayes. 2002. Results of global intercomparison between TOPEX and Jason measurements and models. Paper presented at the Jason-1 and TOPEX/Poseidon Science Working Team Meeting, Biarritz (France), 10-12 June.

[15] Chambers, D. P. and B. D. Tapley, 1998: Reduction of Geoid Gradient Error in Ocean Variability from Satellite Altimetry. *Mar. Geod.*, **21, 25-39.**

[16] Choy, K, J. C. Ries, and B. D Tapley, 2004. Jason-1 Precision Orbit Determination by Combining SLR and DORIS with GPS Tracking Data. *Mar. Geod.***27(1-2): 319-331.**

[17] Desai, S. D., and B. J. Haines, 2004. Monitoring Measurements from the Jason-1 Microwave Radiometer and Independent Validation with GPS. *Mar. Geod.***27(1-2): 221-240.**

[18] Dibarbour, G., Bruit Jason et Analyse spectrale, March 2001, CLS.ED/NT

[19] Dorandeu, J., M. H. De Launay, F. Mertz and J. Stum, 2001. AVISO/CALVAL yearly report. 8 years of TOPEX/Poseidon data (M-GDRs).

[20] Dorandeu, J. and P.Y. Le Traon, 1999: Effects of Global Atmospheric Pressure Variations on Mean Sea Level Changes from TOPEX/Poseidon. *J. Atmos. Technol.,***16, 1279-1283.**

[21] Dorandeu, J, M. Ablain, Y . Faugere, B. Soussi, and J . Stum. 2002a. Global statistical assessment of Jason-1 data and Jason-1/TOPEX/Poseiodn Cross-calibration. Paper presented at the Jason-1 and TOPEX/Poseidon Science Working Team Meeting, Biarritz (France), **10-12 June.**

[22] Dorandeu, J., P. Thibaut, O. Z. Zanife, Y. Faugère, G. Dibarboure, N. Steunou, and P. Vincent. 2002b. Poseidon-1, Poseidon-2 and TOPEX noise analysis. Paper presented at the Jason-1 and TOPEX/Poseidon Science Working Team Meeting, New-Orleans (USA), **October.**

[23] Dorandeu., J., M. Ablain, P. Y. Le Traon, 2003a. Reducing Cross-track Geoid Gradient Errors around TOPEX/Poseidon and Jason-1 Nominal Tracks. Application to Calculation of Sea Level Anomalies. *J. Atmos. Oceanic Technol.,***20, 1826-1838.**

[24] Dorandeu, J., Y. Faugère, and F. Mertz. 2003b. ENVISAT data quality: Particular investigations. Proposal for ENVISAT GDR evolutions. Paper presented at the ENVISAT Ra-2 & MWR Quality Working Group meeting. **October.**

[25] Dorandeu.,J., M. Ablain, Y. Faugère, F. Mertz, 2004 : Jason-1 global statistical evaluation and performance assessment. Calibration and cross-calibration results. *Mar. Geod.***This issue.**

[26] Y.Faugere, J.Dorandeu, F.Lefevre, N.Picot and P.Femenias, 2005: Envisat ocean altimetry performance assessment and cross-calibration. Submitted in the special issue of SENSOR 'Satellite Altimetry: New Sensors and New Applications'

[27] Y.Faugere and J.Dorandeu, 2004: Nouvel algorithme de détection des glaces de mer pour Jason-1. SALP-PR-MA-EA-21235-CLS.

[28] Faugere Y., Estimation du bruit de mesure sur jason-1, December 2002, CLS.ED/NT.

[29] Y.Faugere, N.Granier, and A.Ollivier, 2007: Envisat validation activities. 2007 yearly report, Available at: http://www.jason.oceanobs.com/documents/calval/validation_report/en/annual_report_en_2007.pdf

[30] Förste, C., F. Flechtner, R. Schmidt, U. Meyer, R. Stubenvoll, F. Barthelmes, R. König, K.-H. Neumayer, M. Rothacher, C. Reigber, R. Biancale, S. Bruinsma, J.-M. Lemoine, and J.C. Raimondo. A New Heigh Resolution Global Gravity Field Model Derived From Combination of GRACE and CHAMP Mission and Altimetry/ Gravimetry Surface Gravity Data. *Poster presented at EGU General Assembly 2005, Vienna, Austria, 24-29 April 2005.*

[31] Fu, L. L., 2002. Minutes of the Joint Jason-1 and TOPEX/Poseidon Science Working Team Meeting, Oct. 21-23, JPL Tech. Report. JPL D-25506, edited by L. Fu, USA.

[32] Gaspar, P., S. Labroue, F. Ogor, G. Lafitte, L. Marchal and M. Rafanel, 2002: Improving non parametric estimates of the sea state bias in radar altimeter measurements of sea level. *J. Atmos. Oceanic Technol.,***19, 1690-1707.**

[33] Haines, B., Y. Bar-Sever, W. Bertiger, S. Desai, P. Willis, 2004: One-Centimeter Orbit Determination for Jason-1: New GPS-Based Strategies. *Mar. Geod.***27(1-2): 299-318.**

[34] Hamming, R. W., 1977. Digital Filter. Prentice-Hall Signal Processing Series, edited by A. V. Oppenheim Prentice-Hall, Englewood Cliffs, N. J.

[35] Hernandez, F. and P. Schaeffer, 2000: Altimetric Mean Sea Surfaces and Gravity Anomaly maps intercomparisons AVI-NT-011-5242-CLS, 48 pp. CLS Ramonville St Agne.

[36] Hirose N., Fukumori I., Zlotnicki V., Ponte R. M. 2001: High-frequency barotropic response to atmospheric disturbances : sensitivity to forcing, topography, and friction, J. Geophys. Res. 106(C12), 30987-30996.

[37] Keihm, S. J., V. Zlotnicki, and C. S. Ruf. 2000. TOPEX Microwave Radiometer performance evaluation, 1992-1998, *IEEE Trans. Geosci. Rem. Sens.,***38(3): 1379-1386.**

[38] Labroue, S. and P. Gaspar, 2002: Comparison of non parametric estimates of the TOPEX A, TOPEX B and JASON 1 sea state bias. Paper presented at the Jason 1 and TOPEX/Poseidon SWT meeting, New-Orleans, 21-12 October.

[39] Labroue, S. P. Gaspar, J. Dorandeu, O.Z. Zanifé, P. Vincent, and D. Choquet. 2004. Non Parametric Estimates of the Sea State Bias for Jason 1 Radar Altimeter. *Mar. Geod.***This issue.**

[40] Labroue, S., Ph. Gaspar, J. Dorandeu, O.Z. Zanife. Latest Results on Jason-1 Sea State Bias with the Non-Parametric Technique. *Talk presented at OSTST meeting, Venice, Italy, 16-18 March 2006.*

[41] Lemoine, F. G., S. B. Luthcke, N. P. Zelinsky, D. S. Chinn, T. A. Williams, C. M. Cox, and B. D. Beckley. 2003. An Evaluation of Recent gravity Models Wrt to Altimeter Satellite Missions.*Paper presented at the Jason-1 and TOPEX/Poseidon Science Working Team Meeting,***Arles (France), November.**

[42] Le Traon, P.-Y., J. Stum, J. Dorandeu, P. Gaspar, and P. Vincent, 1994: Global statistical analysis of TOPEX and POSEIDON data. *J. Geophys. Res.,***99, 24619-24631.**

[43] Le Traon, P. Y., and G. Dibarboure, 2004. An Illustration of the Contribution of the TOPEX/Poseidon-Jason-1 Tandem Mission to Mesoscale Variability Studies. *Mar. Geod.***27(1-2) 3-13.**

[44] Luthcke. S. B., N. P. Zelinsky, D. D. Rowlands, F. G. Lemoine, and T. A. Williams. 2003. The 1-Centimeter Orbit: jason-1 Precision Orbit Determination Using GPS, SLR, DORIS, and Altimeter Data. *Mar. Geod.***26(3-4): 399-421.**

[45] Marshall, J. A., N. P. Zelinsky, S. B. Luthcke, K. E., Rachlin, and R. G. Williamson. 1995. The temporal and spatial characterustics of TOPEX/Poseidon radial orbit error. *J. Geophys. Res.* **100(C2):25331-25352.**

[46] Martini A., 2003: Envisat RA-2 Range instrumental correction : USO clock period variation and associated auxiliary file, Technical Note ENVI-GSEG-EOPG-TN-03-0009 Available at http://earth.esa.int/pcs/envisat/ra2/articles/USO_clock_corr_aux_file.pdfhttp://earth.esa.int/pcs/envisat/ra2/auxdata/

[47] Ménard, Y. 2003. Minutes of the Joint TOPEX/Poseidon and Jason-1 Science Working Team Meeting. CNES-SALP-CR-MA-EA-15190-CN.

[48] Obligis, E, N. Tran, and L. Eymard, 2004. An assessment of Jason-1 microwave radiometer measurements and products. *Mar. Geod.***27(1-2) 255-277.**

[49] Phaden Mc.J., April2003 : Evolution of the 2002-03 El Niño, *UCLA Tropical Meteorology and Climate Newsletter,***No57**.

[50] Philipps, S. and M. Ablain,September 2007 : SALP - BC 60453-6-04: Retraitement des GDRs Jason-1 en version 'B' pour les cycles 022 à 127, SALP/BC60453-6-04.

[51] Picot, N., K. Case, S. Desai and P. Vincent, 2003. AVISO and PODAAC User Handbook. IGDR and GDR Jason Products, SMM-MU-M5-OP-13184-CN (AVISO), JPL D-21352 (PODAAC).

[52] Provost., C. Arnault, N. Chouaib, A. Kartavtseff, L. Bunge, and E. Sultan, 2004. TOPEX/Poseidon and Jason Equatorial Sea Surface Slope Anomaly in the Atlantic in 2002: Comparison with Wind and Current Measurements at 23W. *Mar. Geod.***27(1-2) 31-45.**

[53] Quartly, G. D., 2004. Sea State and Rain: A Second Take on Dual-Frequency Altimetry. Mar. Geod. 27(1-2) 133-152

[54] Queffeulou, P. 2004. Long Term Validation of Wave Height Measurements from Altimeters. *Mar. Geod.***This issue.**

[55] Ray, R. (1999). A Global Ocean Tide Model From TOPEX/Poseidon Altimetry/ GOT99.2 - NASA/TM-1999-209478. Greenbelt, MD, Goddard Space Flight Center/NASA: 58

[56] Ray, R. D., and B. D. Beckley, 2003. Simultaneaous Ocean Wave Measurements by the Jason and Topex Satellites, with Buoy and Model Comparisons *Mar. Geod.***26(3-4): 367-382.**

[57] Ray, R. D. 2003. Benefits of the joint T/P−Jason mission for improving knowledge of coastal tides. Paper presented at the Jason-1 and TOPEX/Poseidon Science Working Team Meeting, Arles (France), November.

[58] Ray, R.D. and R.M. Ponte, Barometric tides from ECMWF operational analyses. *Annales G*, **99, 24995-25008**, 1994.

[59] Ruf C., S. Brown, S. Keihm and A. Kitiyakara, 2002a. JASON Microwave Radiometer : On Orbit Calibration, Validation and Performance, *Paper presented at the Jason-1 and TOPEX/Poseidon Science Working Team Meeting, New-Orleans (USA),***21-23 October.**

[60] Ruf. C. S., 2002b. TMR Drift - Correction to 18 GHz Brightness Temperatures, Revisited. Report to TOPEX Project, June.

[61] Scharroo R., J. L. Lillibridge, and W. H. F. Smith, Cross-Calibration and Long-term Monitoring of the Microwave Radiometers of ERS, TOPEX, GFO, Jason-1, and Envisat, **Marine Geodesy, 27:279-297**, 2004.

[62] Tapley, B.D., M.M. Watkins, J.C. Ries, G.W. Davis, R.J. Eanes, S.R. Poole, H.J. Rim, B.E. Schultz, C.K. Shum, R.S. Nerem, F.J. Lerch, J.A. Marshall, S.M. Klosko, N.K. Pavlis, and R.G. Williamson, 1996. The Joint Gravity Model 3. *J. Geophys. Res.***101(B12): 28029-28049.**

[63] Tierney, C., J. Wahr, et al. 2000. Short-period oceanic circulation: implications for satellite altimetry. Geophysical Research Letters 27(9): 1255-1258

[64] Thibaut, P. O.Z. Zanifé, J.P. Dumont, J. Dorandeu, N. Picot, and P. Vincent, 2002. Data editing : The MQE criterion. Paper presented at the Jason-1 and TOPEX/Poseidon Science Working Team Meeting, New-Orleans (USA), 21-23 October.

[65] Thibaut, P. L. Amarouche, O.Z. Zanife, N. Steunou, P. Vincent, and P. Raizonville. 2004. Jason-1 altimeter ground processing look-up tables. *Mar. Geod.***This issue.**

[66] Tournadre, J. 2002. Validation of the rain flag. Paper presented at the Jason-1 and TOPEX/Poseidon Science Working Team Meeting, Biarritz (France), 10-12 June.

[67] Tran, N., D. W. Hancock III, G.S. Hayne. 2002. "Assessment of the cycle-per-cycle noise level of the GEOSAT Follow-On, TOPEX and POSEIDON." *J. Atmos. Oceanic Technol.,***19(12): 2095-2117.**

[68] World Meteorological Organization. 2007. El Niño/ La Niña Update (31 October 2007). Available at http://www.wmo.ch/pages/prog/wcp/wcasp/documents/El_Nino_Oct07_Eng.pdf.

[69] Valladeau, G., M. Ablain, and Fabien Lefevre. Validation activities between altimetric data and tide gauges measurements. SALP-NT-MA-P2-21449-CLS, CLS.DOS/NT/07-166.

[70] Valladeau, G., and M. Ablain. Activités de calibration/validation entre les données altimétriques et les mesures in-situ issues de profils T/S sur les missions altimétriques TOPEX/Poseidon, Jason-1, Envisat et Geosat Follow-On. SALP-NT-MA-P2-21449-CLS, CLS.DOS/NT/07-250.

[71] Vincent, P., S. D. Desai, J. Dorandeu, M. Ablain, B. Soussi, P. S. Callahan, and B. J. Haines 2003a. Jason-1 Geophysical Performance Evaluation. *Mar. Geod.***26(3-4): 167-186.**

[72] Vincent, P., S. Desai, J. Dorandeu, M. Ablain, B. Soussi, Y. Faugère, B. Haines, N. Picot, K. Case, A. Badea, 2003b. Summary about Data Production and Quality. Paper presented at the Jason-1 and TOPEX/Poseidon Science Working Team Meeting, Arles (France), November

[73] Vincent, P., J.P. Dumont, N. Steunou, O.Z. Zanife, P. Thibaut, and J. Dorandeu. 2003c. Jason-1 I/GDR science processing: ground retracking improvements. Paper presented at the European Geophysical Society meeting, Nice, April.

[74] Zanife, O. Z., P. Vincent, L. Amarouche, J. P. Dumont, P. Thibaut, and S. Labroue, 2003. Comparison of the Ku-band range noise level and the relative sea-state bias of the Jason-1, TOPEX and Poseidon-1 radar altimeters. *Mar. Geod.***26(3-4): 201-238.**

10 Annex

This annex contains posters presented at OSTST meeting in 2007, as well as a study concerning high frequency content of Envisat and Jason-1 data. The latter was taken from Envisat annual report 2007 ([29]).

10.1 Poster presented at OSTST meeting 2007

(A) SSALTO CALVAL Performance assessment Jason-1 data

Michaël ABLAIN (michael.ablain@cls.fr), Sabine PHILIPPS, José DORANDEU - CLS

Nicolas PICOT - CNES

Introduction

Since the beginning of the mission, Jason-1 data have been analyzed and monitored in order to assess the quality and the performances of Jason-1 GDR products for oceanographic applications. This work routinely performed at CLS under contract with the CNES, includes careful monitoring of all altimeter and radiometer parameters, performance assessment, geophysical evaluation and cross-calibration with T/P measurements. This poster is basically concerned with the more relevant results, and specific studies linked to these activities.

Context

Jason-1 data (GDR: geophysical data record) were processed until current cycle 185. From cycle 136 onwards, current GDRs are processed in version 'B'. The main evolutions in the GDR 'B' were the implementation of a new retracking algorithm[1] (order 2 MLE-4), a new precise orbit[2] based on a GRACE gravity model and new geophysical corrections (tidal models, MOG2D, Sea State Bias). A reprocessing of the GDR in version 'B' was done last year from cycle 1 to 21 and 128 to 135. In order to provide an homogeneous data set in version 'B', a GDR reprocessing in version 'B' is on-going from cycle 22 to 127.

A) SSH performances

SSH performances is monitored in order to assess the global system performances since the beginning of the Jason-1 mission. GDR used to provide these statistics are in version 'A' from cycle 1 to 135 and in version 'B' from cycle 136 onwards. Even if T/P mission is finished since November 2005, SSH T/P performances are superimposed to compare both missions.

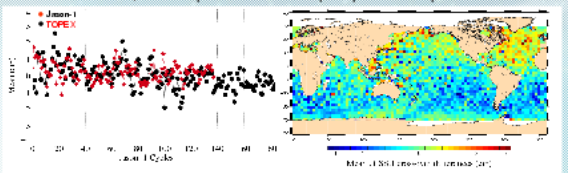

Figure 1 : Mean differences [cm] of SSH at crossover : cyclic monitoring (left) and map (right, only GDR 'B' cycles)

The cyclic mean differences of SSH crossover (figure 1 left) is stable and similar with T/P ones. The map of mean differences shows weak signal (< 2 cm). However an hemispheric bias is detected thanks to the very good quality of new orbits (see "Reprocessing in version B").

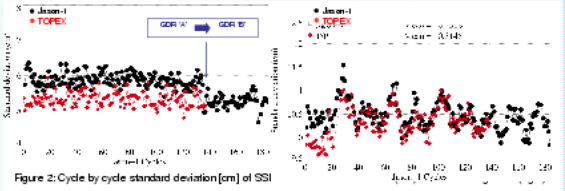

Figure 2 : Cycle by cycle standard deviation [cm] of SSH

The cyclic standard deviation of SSH differences at crossover and along-track (figure 2) is stable and similar to T/P ones. However different ground processing between T/P and Jason-1 explain the slightly lower statistics for T/P. After applying similar retracking algorithms for both missions (RGDR T/P, Calahan 2007), same SSH high frequency content is obtained (see Faugere poster or presentation - retracking splinter).

B) Reprocessing in version 'B'

Last year (in 2006), GDRs were reprocessed in version 'B' from cycle 1 to 21 and 128 to 135. The reprocessing of all GDRs is on-going (from cycle 22 to 127). The quality of the reprocessed GDR 'B' is monitored cycle by cycle, and compared with the former GDR 'A'. Here are presented the SSH performances at crossovers.

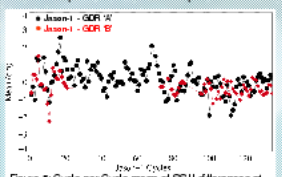

Figure 5 : Cycle per Cycle mean of SSH differences at crossover

The crossover mean is more stable with the GDR 'B' (figure 5) especially for the first cycles thanks to the new orbit. With new orbit quality, small signals can now be detected such as an hemispheric bias at crossovers (figure 1 right) using GDR 'B' data. A time shift of 0.173 ms has been added in the GDR 'B' L1-B processing. The sign of this correction has been checked and not explains the observed hemispheric bias even if the pseudo time-tag bias estimated is about -0.3 ms.

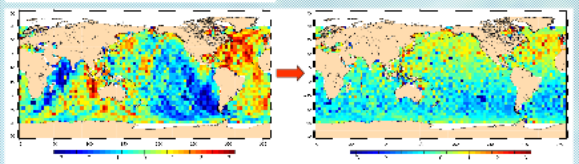

Figure 6 : Mean of SSH crossover differences when using GDR 'A' data on the left and GDR 'B' on the right (cm²)

The crossover standard deviation using geographical selections (bathy < -1000m, |latitude| < 50° and ocean variability < 20 cm) decreases from 6.1 cm to 5.2 cm with the GDR 'B' (figure 7) : MOG2D HF correction, new orbit and MLE-4 retracking are the main sources of improvement.

Finally, the use of GDR 'B' data allows us to decrease significantly the variance at crossover in comparisons with the GDR 'A' (figure 8): the variance has dropped by 35% (3.9 cm rms).

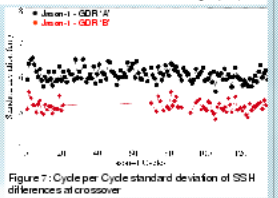

Figure 7 : Cycle per Cycle standard deviation of SSH differences at crossover

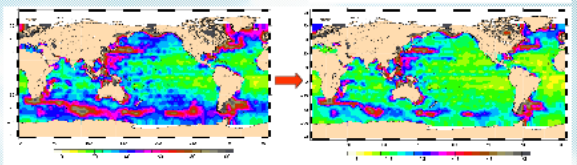

Figure 8 : SSH crossover variance when using GDR 'A' data on the left and GDR 'B' on the right (cm²)

C) Radiometer wet troposphere correction

The JMR correction provided in the GDR 'A' (red curve in figure 3 top) contains several anomalies when looking at JMR-ECMWF model differences: a drift of 5 mm between cycles 27 to 32, a jump of 9 mm at cycle 69, and 60 days signals of almost 5 mm amplitude due to yaw mode transitions.

PODDAC provides a JMR correction[3] (same as in GDR 'B') for whole Jason-1 mission (black curve). It corrects partly the anomalies: the jump at cycle 69 is very well corrected, but the drift is still visible as well as yaw mode transitions (especially in the end).

Figure 3 bottom shows daily mean differences of radiometer and ECMWF model wet troposphere corrections for different missions. Daily mean values for Jason-1 are noisier than those for the other missions. This apparent noise is linked to signals generated by yaw mode transitions.

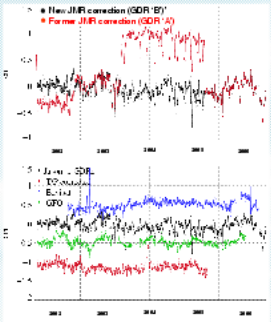

Figure 3 : Daily mean differences between radiometer and ECMWF model wet troposphere correction for Jason-1 (top) and in comparison to other missions (bottom).

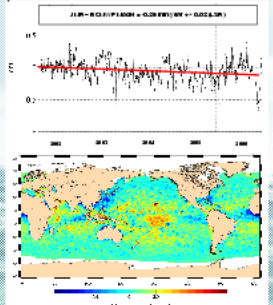

Figure 4 : Global (top) and local (bottom) slope estimation of the difference between radiometer and model wet troposphere correction.

New JMR correction could now be used in MSL calculation instead of ECMWF model whose stability is not warranty (a jump of ECMWF model is observed for the first Jason-1 cycle). But the analyze of the slope between both corrections leads to an increase of 0.26 mm/year for the estimation of the global MSL (see Figure 4 top) and the local slopes can reach 5 mm/year (see figure 4 bottom). Considering that the JMR correction is not completely well tuned, the use of the ECMWF model is probably preferable for the MSL estimation.

Finally this analyze shows that the wet troposphere correction is an important item in the error budget of the Jason-1 MSL.

D) Mean sea level (MSL)

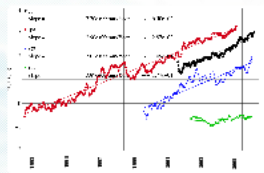

Figure 9 : MSL over global ocean seen by different missions after removing of annual, semi-annual and 60-day signals.

T/P and Jason-1 MSL have to be fitted together since T/P mission is finished (November 2005). This is possible applying homogeneous corrections and the J1/TP SSH bias. The T/P+Jason-1 MSL shows a slope of 2.8 mm/year (figure 10). However some discrepancies exist between both missions: TMR correction is used for T/P instead of the ECMWF model for Jason-1, T/P and Jason-1 orbits are not homogeneous over the whole period. Other corrections could impact the MSL as for example the ECMWF pressure fields in the T/P data. Studies on going are shared between GOHS/LEGOS and CLS to estimate a more realistic error budget of the MSL due to these differences.

Peculiar attention is paid for the MSL slope estimation which is a sensitive subject. The Jason-1 MSL is calculated using the wet troposphere ECMWF model (see section C) showing a MSL elevation of 3.3 mm/year (figure 9). T/P and GFO MSL slopes are very similar with respectively 2.9 and 3.0 mm/year. Only Envisat MSL shows an inconsistency probably due to ground processing anomalies: USO drifts, ... (for more details see Faugere poster - Calval splinter)

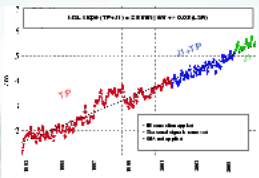

Figure 10 : MSL over global ocean seen T/P + Jason-1 after linking up both missions.

Complete MSL results are available at (http://www.aviso-oceanobs.com/msl), see also dedicated AVISO MSL poster.

References: 1: Amarouche, L., P. Thibaut, O.Z. Zanife, J.-P. Dumont, P. Vincent and N. Steunou, 2004: Improving the Jason-1 Ground Retracking to Better Account for Attitude Effects. Marine Geodesy, Vol. 27, pp. 171-197.

2: Choi, K.-R., J.C. Ries, and B.D. Tapley, 2004: Jason-1 Precision Orbit Determination by Combining SLR and DORIS with GPS Tracking Data. Marine Geodesy, Vol 27, pp. 315-331.

3: Desai, S.: JMR replacement product available at ftp://podaac.jpl.nasa.gov/sea_surface_height/jason/jmr_replacement

Figure 63: *Poster presented at OSTST meeting, Hobart 2007*

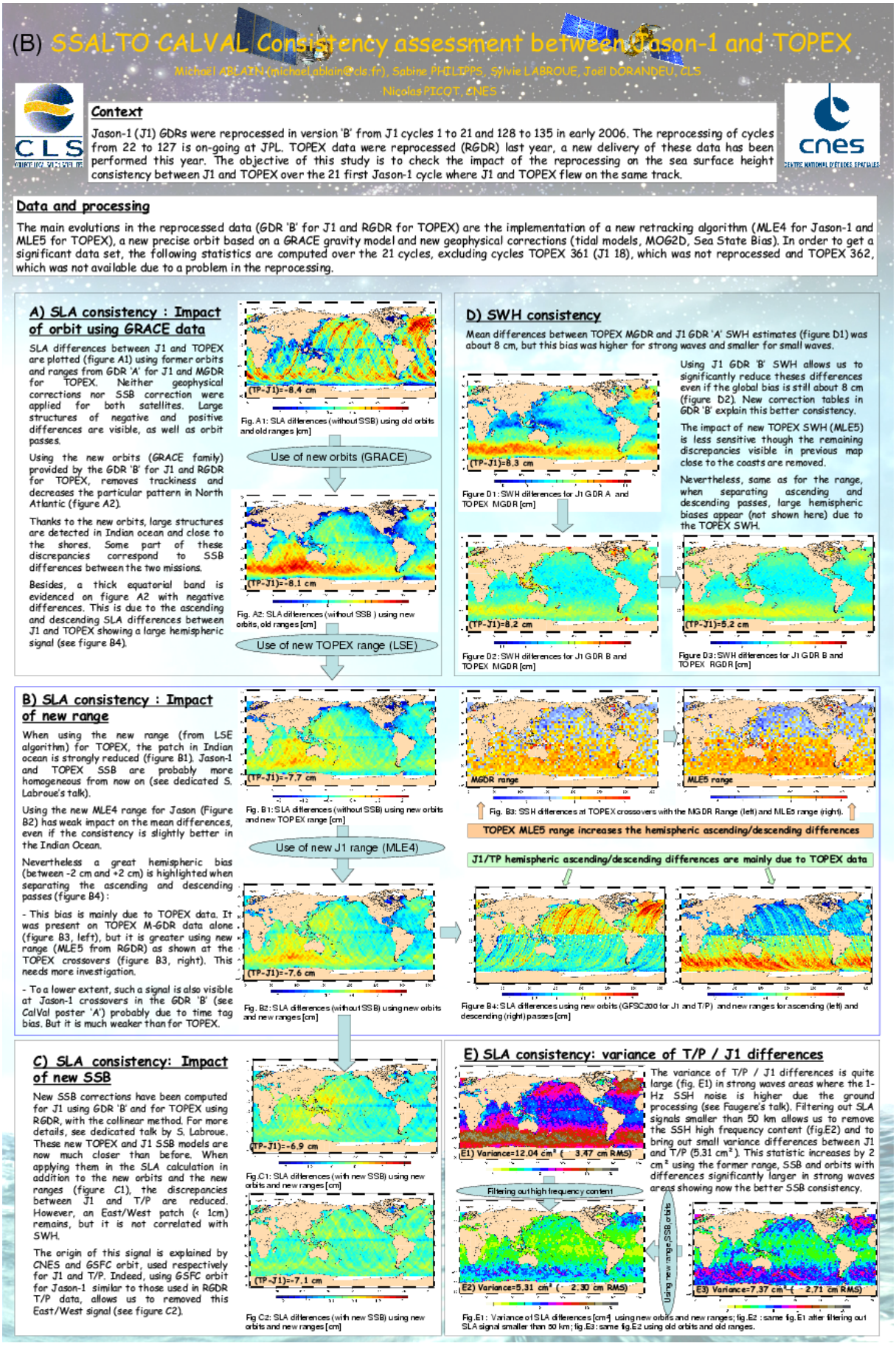

Figure 64: *Poster presented at OSTST meeting, Hobart 2007*

10.2 Study on High frequency content

10.2.1 Introduction

The aim of this study is to compare the high frequency content for Jason-1 and Envisat missions in order to raise differences of instrumental or processing behaviours for high frequencies.

Actually, the high frequency content includes instrumental noise, processing errors, residual geophysical signals... Because the spectra are analysed in relative and not in absolute (between missions or for different selection), differences are analysed on uncorrelated SLA, the rawest altimetric data.
Previous studies ([28] and [18]) showed for instance that the evolution of GdrA to GdrB including various algorithmic modifications enabled to obtain more consistent high frequency content between Envisat and Jason-1. The main results of this previous study will be shown again and completed in this document. This document is organized in 7 parts:

- The first part presents the data and methods used to perform the High Frequency analysis.
- The second part recalls the main results of a previous study on HF Content and the questions it raises are listed.
- The third part focuses on the effect of a selection on the apparent mispointing values and underlines the possible causes of such effect.
- The fourth part studies the meanings of zones edited on apparent mispointing criterion.
- The fifth part is a comparison between compression editing and evaluates the impact on spectral analysis.
- The sixth part focuses on the effect of a selection on the wave height.
- Conclusions are proposed in the last part.

10.2.2 Data and methods

The High Frequency Content of Jason-1 and Envisat missions is analysed different algorithms of parameters estimation. It is analysed through a spectral analysis method. The different estimation algorithms, data used, as well as the method of HF extraction are presented hereafter.

10.2.2.1 Data used

The parameters estimation is based on a Least Square fitting of the measured echo by a model with 3, 4 or 5 parameters. This mean square fitting is derived from a Maximum Likelihood Estimator [Ref 2].
- **MLE3** is an acronym to define the Least Square fitting of the measured echo by a model with 3 parameters: Sigma 0, Range and Significant Wave Height (SWH).
- **MLE4** is an acronym to define the Least Square fitting of the measured echo by a model with 4 parameters, the additional parameter being the mispointing of the waveform.

Envisat Gdr (MLE3) and Jason-1 GdrA (MLE3) and GdrB (MLE4) are used for this study. Both missions are analysed on 1Hz and 20Hz data.
- 1Hz Envisat/Jason-1 GdrB comparison is performed over the periods 7 to 26 September 2006.
- 1Hz Envisat/Jason-1 GdrA and Jason-1 GdrA/GdrB comparison is performed over the periods 5 to 14 September 2005.
- 20Hz Envisat/Jason-1 GdrB comparison is performed over the periods 7 to 8 September 2006.
- 20Hz Envisat/Jason-1 GdrA and Jason-1 GdrA/GdrB comparison is performed over the periods 5 to 6 September 2005.

10.2.2.2 Spectral analysis method

The spectral analysis enables to identify the location of the energy contained in a given bandwidth.
If the spectrum is modelled as a signal added to noise, the spectrum can be seen (cf. Figure 65) as a decreasing spectrum added to a white noise spectrum that is a uniform plateau (energy equally distributed on all frequencies).
The high frequency plateau can therefore be interpreted as the noise level of the data.

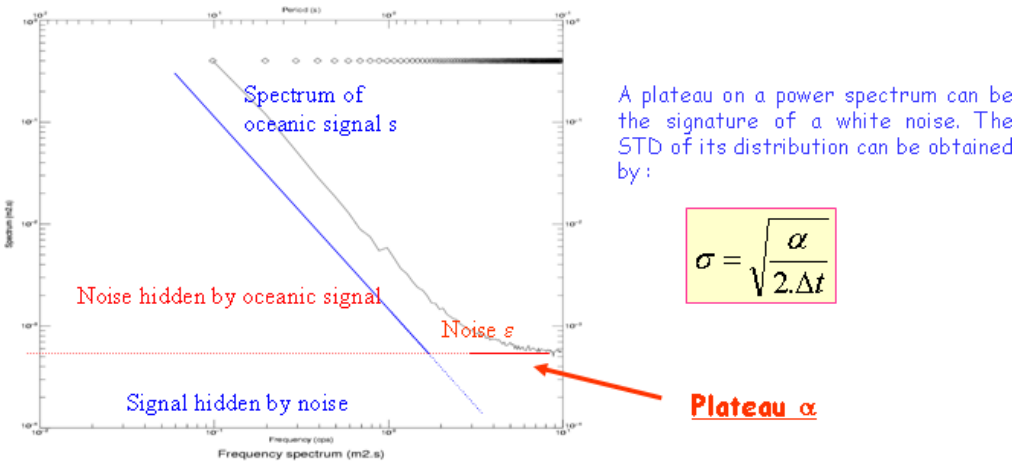

Figure 65: *The spectral method.*

The method used to plot spectra is based on the spectrogram method which consists in averaging N Fast Fourier Transform, calculated on samples constituted of M points along track. The length of the samples is 300 points or 15 seconds for 20Hz data and 160 seconds for the 1Hz data.

The bandwidth analysed with this method concerns frequencies between the inverse of the spectrogram window's size and Shannon frequency (inverse of the sampling period). These frequencies can also be converted into distances with the relation:

$$Distance = Ground\_Satellite\_Speed * Frequency \quad (1)$$

Where Ground_Satellite_Speed = 7km/s.

For **1hz data**, analysed frequencies are:
- between 2 and 160 seconds.
- between 0.006 Hz (1/160 seconds) and 0.5 Hz (1Hz/2).

- between 14 km and 1120 km.

For **20hz data**, frequencies analysed are:
- between 0.1 and 15 seconds.
- between 0.07 Hz (1/15 seconds) and 10 Hz (20Hz/2).
- between 700 m and 105 km.

Because the Fourier Transform needs continuous samplings, managing gaps of data is a major issue in this method. Here, holes are filled up by an average value in order to have continuous samples. The number of missing data as well as the amount of consecutive missing data can be chosen. For this study, depending on the study, we allowed:
- 10% missing points and 7 consecutive missing points or
- 50% missing points and 7 consecutive missing points.

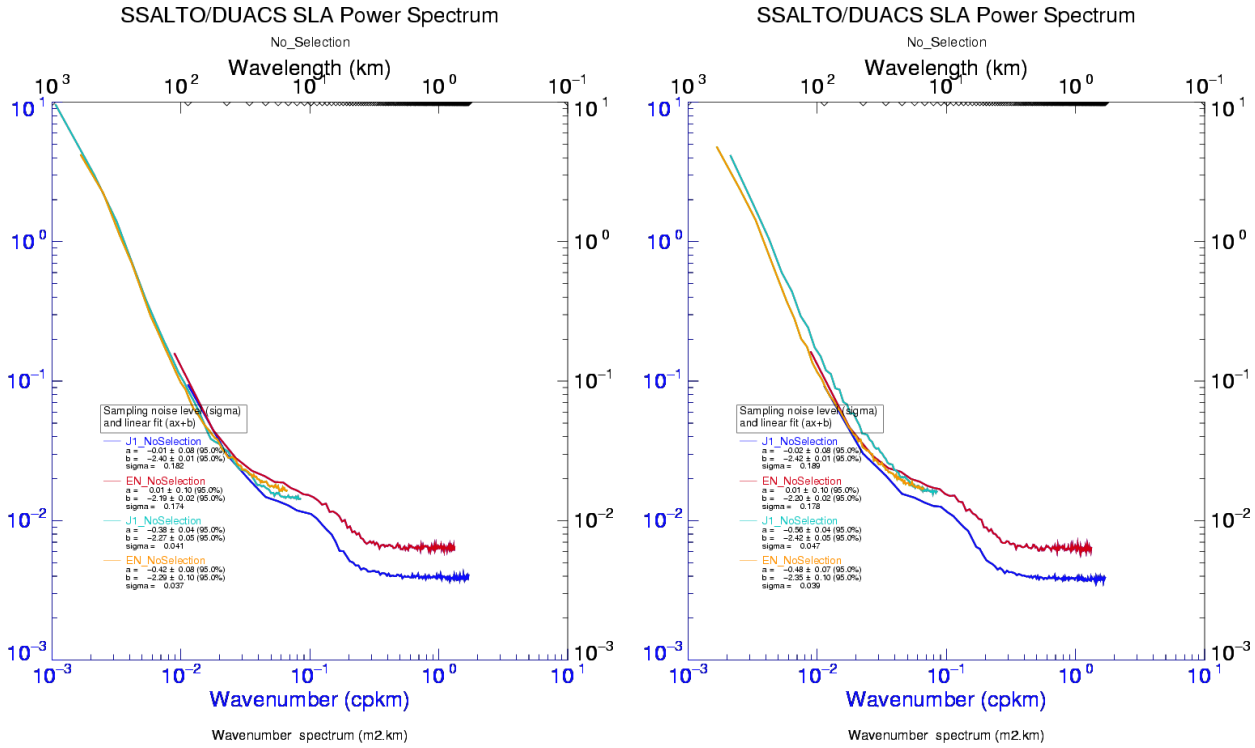

Figure 66: *1Hz and 20Hz spectrums versus km for 10% missing points allowed (left) and for 50% missing points allowed (right). No selection applied on data (only Ocean validity and Latitude lower than 66°.*

Allowing 50% of missing points enables to have more data and to have smoother spectra but Figure 66 shows that allowing 50% of missing points instead of 10% can impact the spectra's shape (see the 1Hz Jason-1 spectrum). In this document, the number of valid Fast Fourier Transform samples are usually unsufficient to give smooth spectra with 0% missing points allowed but they are sufficient if 10% are allowed. Therefore, results are all shown with this criteria. One exception is made for the red and blue curves of Figure 75 where 50% were allowed in order to reduce a too high noise.

10.2.2.3 SLA frequency content

SLA is a difference of Orbit, Range, Corrections and Mean Sea Surface (MSS) :

$$SLA = Orbit - Range - MSS - Corrections \tag{2}$$

It can also be seen as an uncorrected SLA term - corrections :

$$SLA = UncorrectedSLA - Corrections \tag{3}$$

Where the sum of correction is:

$$Corrections = ssb.cls + iono.smooth + dry\_tropo.ecmwf + wet\_tropo.ecmwf\_G + inv\_baro.mog2d + ocean\_tide.got00V2\_S1\_S2 + solid\_tide + pole\_tide \tag{4}$$

All SLA components are available at 1Hz. Orbit and Range are also available at 20Hz. Corrections are supposed to sign at low frequencies. Thus, the 20Hz corrections are a duplication of 1Hz correction, only the MSS which contains strong gradient in several part of the globe is interpolated using a spline technique at 20Hz.

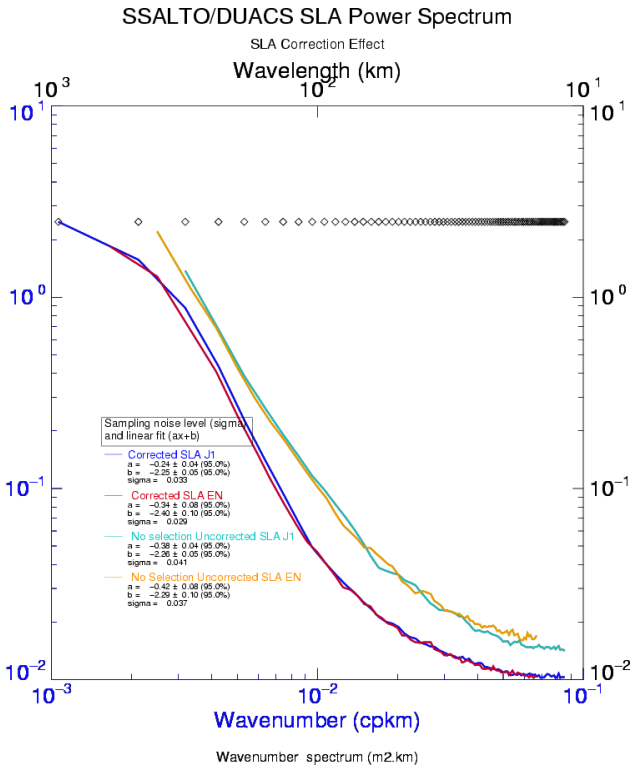

Figure 67: *Correction effect on SLA spectrum (right).*

Figure 67 illustrates the fact that the high frequency energy included in the corrections are small and do not change much the SLA spectra. In the following analysis, in order to have consistent 20Hz and 1Hz data,

spectra are performed using uncorrected SLA.

10.2.3 Difference of High Frequency content using MLE4 instead of MLE3

Thanks to Jason-1 reprocessing from GdrA to GdrB, differences of behaviour could be analysed between a SLA using a Range estimated with MLE3 or MLE4. In term of high frequency content, big differences were observed.

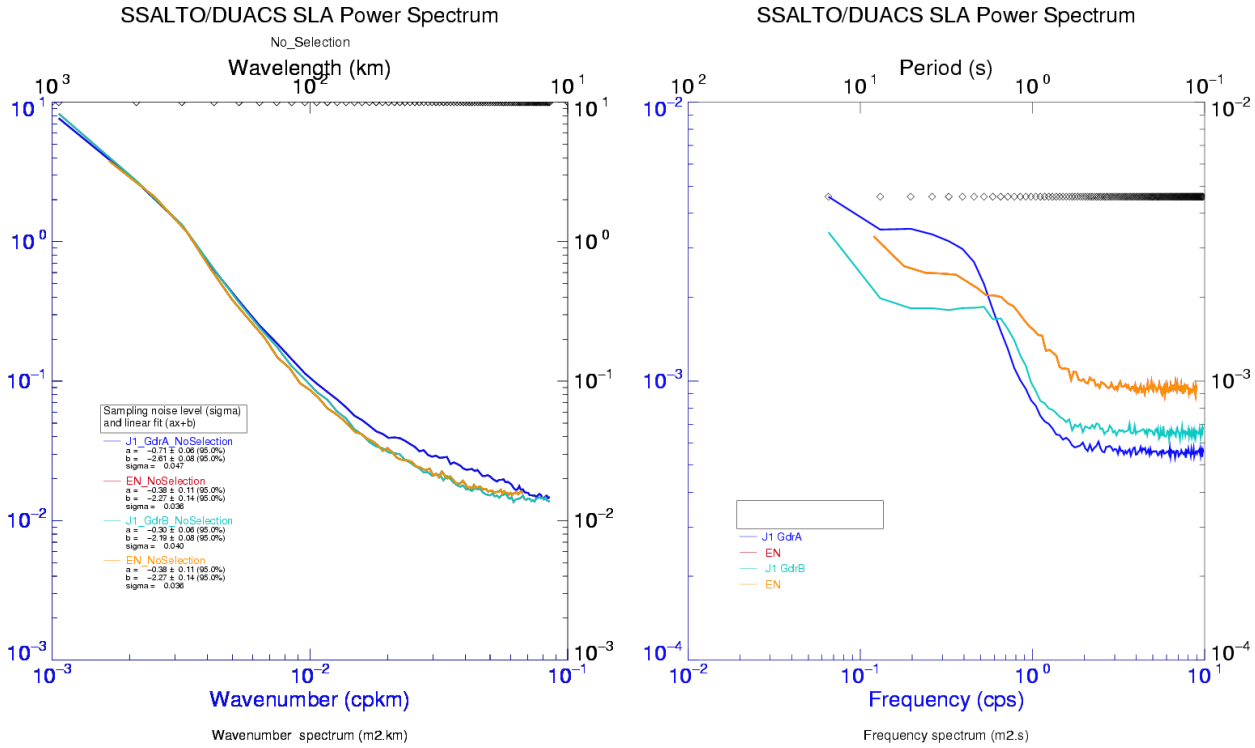

Figure 68: *1Hz versus km (left) and 20Hz versus seconds (right) Spectrums using MLE3 (GdrA) or MLE4 (GdrB). No selection.*

Figure 68 and Figure 69 show the impact of changing the estimation algorithm on Jason-1 with GdrA, GdrB and on Envisat.

Figure 68 (left) shows that Jason-1 GdrB 1Hz data are more consistent with Envisat data although the estimating algorithm is different. Unlike with Jason-1 GdrA, GdrB spectrum is almost super-imposed to Envisat's and it now presents a flat part corresponding to the so called 1Hz noise which is slowly higher for Envisat than for Jason-1.

For frequencies greater than 1Hz, Figure 68 (right) also shows a better consistency between Jason-1 GdrB and Envisat than between GdrA and Envisat. The noise level is increased on GdrB compared to GdrA because the estimation of a 4th parameter in a MLE increased noise. However, the difference between MLE3 and MLE4 is that the mispointing is estimated in the latter, in addition to the three others (range, waves and sigma0). Therefore, those spectra show that estimating the apparent mispointing more precisely

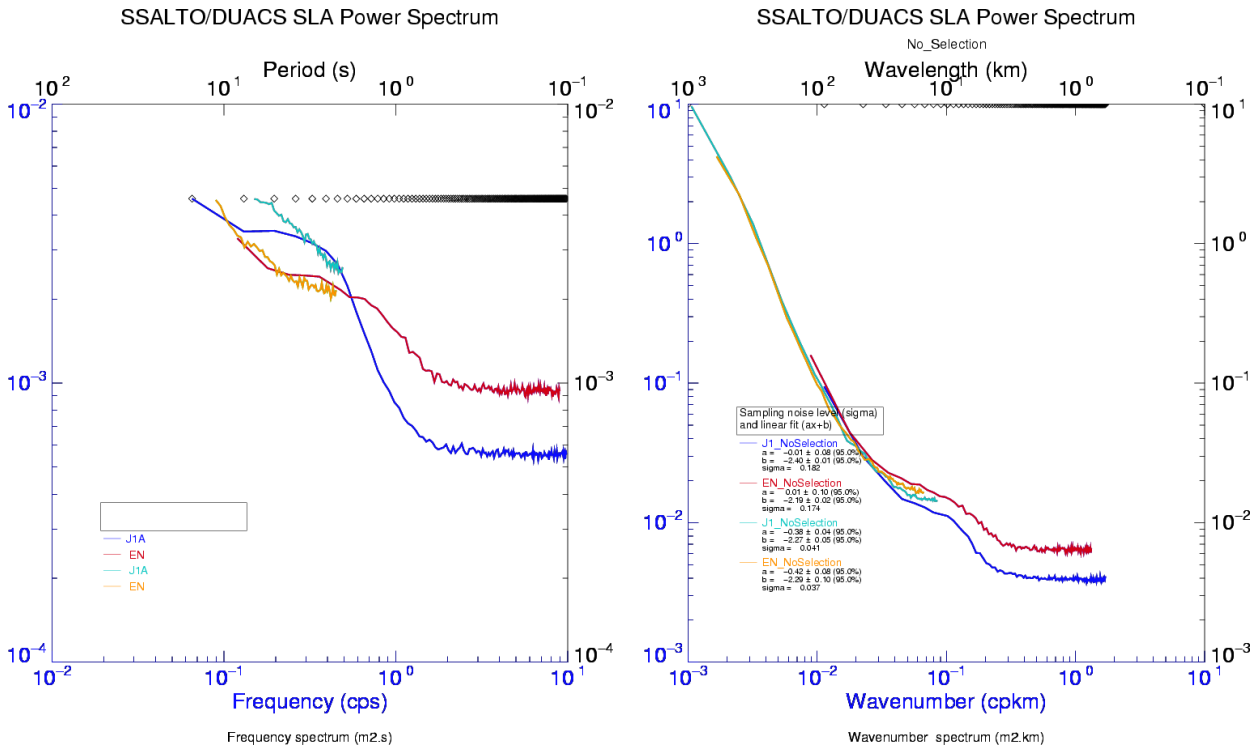

Figure 69: *1Hz and 20Hz Spectrums using MLE3 (GdrA) versus seconds (left) or MLE4 (GdrB) versus km (right). No selection.*

reduces the bump observed for the frequencies between 0.1-0.4Hz (between 20km and 70km).

The MLE4 seems to decorrelate the high frequency signal (increase of high frequency 20Hz plateau) and to correlate a signal signing in a frequency bandwidth of 20km to 70km.

On Figure 69, 1Hz and 20Hz spectra are plotted on the same graph. This underlines that the 1Hz frequency of the 20Hz spectrum is not totally superimposed to the 1Hz frequency of the 1Hz spectrum.

In order to localise the geographical zones where Envisat and Jason-1 are consistent in term of noise, the SLA was high pass filtered with a 20km cut off distance. The difference of variance calculated per 2deg/2deg boxes is plotted on Figure 70. It shows that Envisat and Jason-1 are more consistent in term of noise at low latitudes and mainly in wet areas (from $5cm^2$ to $0.5cm^2$ in western pacific and altantic basins) but the difference remains rather high in the circumpolar zone (still around $2cm^2$).

Four points are therefore raised:

1. Contrarily to the theoretical ocean spectrum which is mostly a low frequency signal + high frequency noise, Envisat and Jason spectrum present a bump in a frequency bandwidth of 20km to 70km. What causes this unexpected energy?

2. The bump on Jason-1 spectrum is smaller when the apparent mispointing is estimated (GdrB) than when it is not (GdrA).

3. At 1Hz and 20Hz, Envisat MLE3 spectrum is more consistent with Jason-1 MLE4 (GdrB) spectrum than with Jason-1 MLE3's (GdrA). Can this be explained?

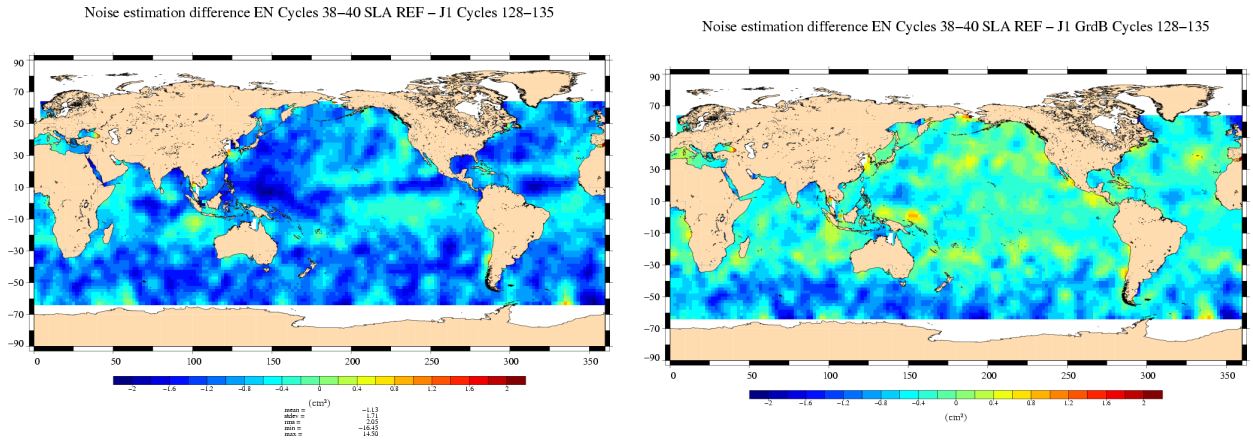

Figure 70: *Difference of Variance Envisat - Jason-1 GdrA (left) and Envisat - Jason-1 GdrB (right).*

4. Plotting both 1Hz and 20Hz spectra on the same Figure 69 underlines that the 1Hz frequency of the 20Hz spectrum is not totally superimposed to the 1Hz frequency of the 1Hz spectra. Does it reveal a problem of compression in the 1Hz data?

10.2.4 Apparent mispointing selection impact on spectra

The main difference between the two estimating algorithms MLE3 and MLE4 is the estimation or not of the mispointing of the waveform. This parameter estimated the slope of the waveform's trailing edge which can be distorted for 2 possible causes:
- either a real mispointing (this is almost never the case on Envisat data)
- or a change in the sea surface roughness (on rainy zones for instance).
For this reason, the mispointing estimated on the waveform will now be called *apparent mispointing*.
Extreme values of apparent mispointing can come from an over-estimation due to the impact of speckle on the estimation phase or from a real distortion of the trailing edge of the waveform. In both cases the waveform differs from its expected ocean like shape. This can have an impact on the range estimation but in a weaker way when using MLE4 because it decorrelates the estimated parameters.
This part focuses on the effect of the apparent mispointing selection on spectra.
Figure 71 shows that the apparent mispointing repartition is larger for Jason-1 (standard deviation of 0.018deg2) than for Envisat (standard deviation of 0.027deg2). It also show that Jason-1 has more extreme values than Envisat.

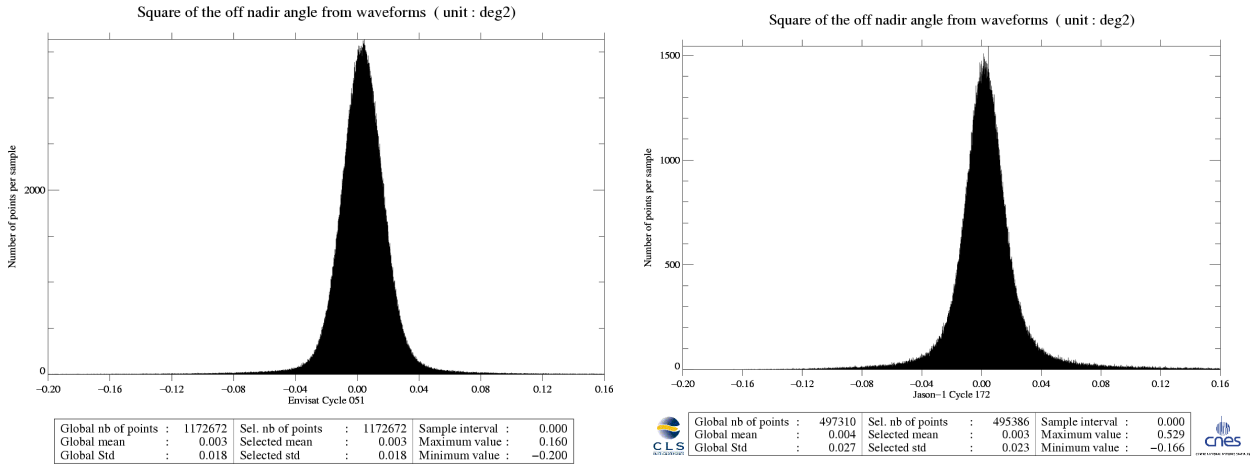

Figure 71: *Square Mispointing Histogram for Envisat (left), Jason (right).*

In order to isolate those extreme values, a threshold was applied on the absolute value of the apparent mispointing centered. Three cases were analysed:
- Centered absolute mispointing lower than 0.02deg2
- Centered absolute mispointing lower than 0.06deg2
- Centered absolute mispointing greater than 0.02deg2

The zone edited by the threshold on the absolute value of apparent mispointing are plotted on Figure 72, 73 for low apparent mispointing and Figure 74 for high apparent mispointing. Those maps represent the percentage of data used, averaged on 2° by 2° boxes relatively to a reference grid of valid ocean points, with bathymetry greater than 1000m.
Purple boxes represent the zones were less than 40% of the data are selected for the spectral analysis. Red boxes represent the zones were 100% of the data are selected for the spectral analysis. These maps show that high mispointing are mostly placed in humid zones but also randomly spread on all oceans.

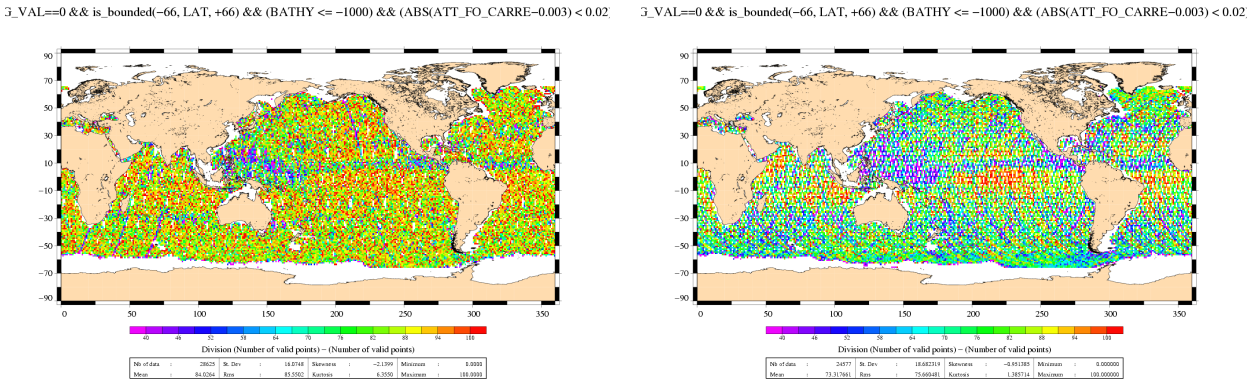

Figure 72: *Centred apparent mispointing smaller than 0.02. Percentage of points used for the analysis on Envisat:* ***84%*** *(left) and Jason-1:* ***73%*** *(right).*

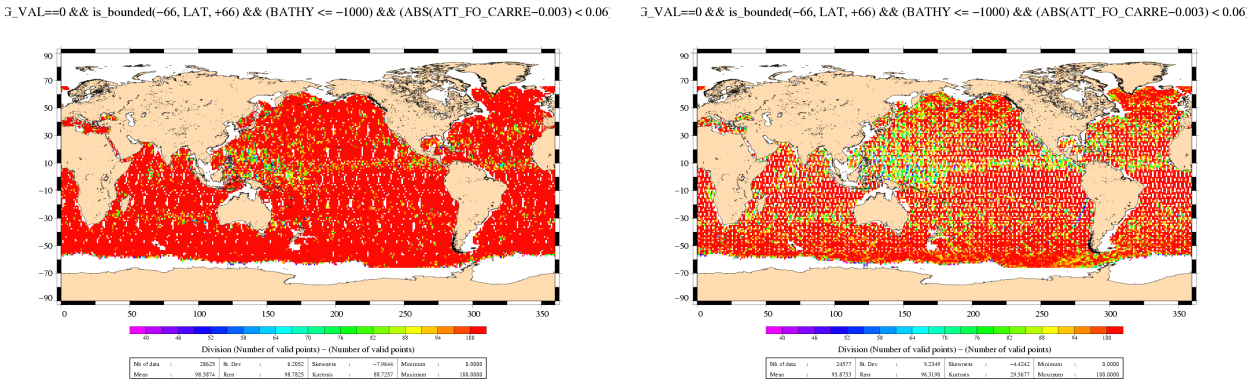

Figure 73: *Centred apparent mispointing smaller than 0.06. Percentage of points used for the analysis on Envisat:* ***98.5%*** *(left) and Jason-1:* ***96%*** *(right).*

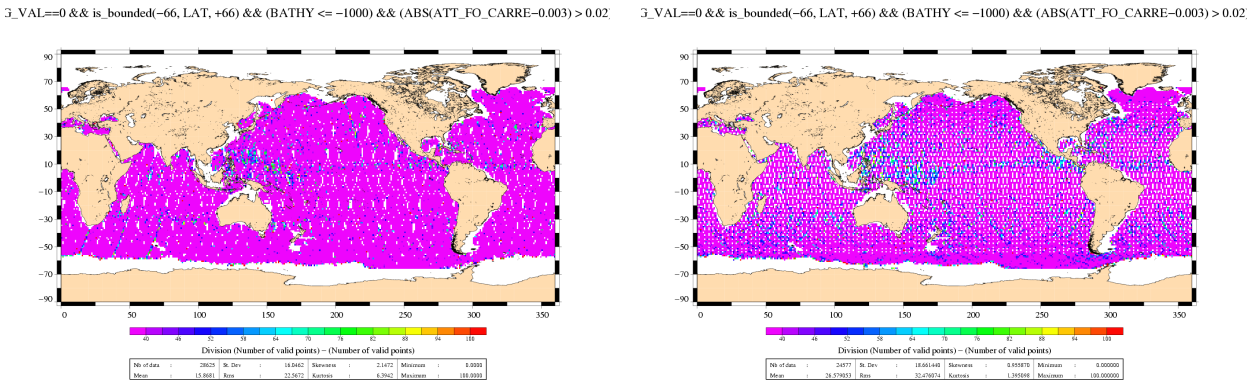

Figure 74: *Centred apparent mispointing greater than 0.02. Percentage of points used for the analysis on Envisat:* ***16%*** *(left) and Jason-1:* ***26%*** *(right).*

Figures 75 show the impact of such selections on the spectra at 1Hz and 20Hz. The first figure corresponds to data with only extreme values of absolute apparent mispointing (centred apparent mispointing greater than 0.02deg2 that is greater than the standard deviation of the histograms). The second one is con-

versely built with low apparent mispointing zones.

These spectra drive us to the conclusion that when selecting only high apparent mispointing zones, the spectrum figures a strong signal in the zone 0.1-0.4Hz (Figure 75 C-D) and the noise level is much decreased for both missions. On the contrary, the 0.1-0.4Hz bump disappears for low apparent mispointing (Figure 75 A-B) and the noise level remains unchanged.
Those figures also show that Envisat and Jason-1 1Hz spectra are superimposed for low apparent mispointing selection.

It is seen on Figure 76 that for both mission, the higher the apparent mispointing, the stronger the bump. The threshold has to be quite small to remove the bump: for instance, a 0.06deg2 threshold is not sufficient. The noise noticed on Envisat spectrum compared to Jason-1 is due to the small amount of data used for high mispointing selection (16% and 26% see Figure 74). On Figure 75 B, the noise is reduced for the 20Hz spectrum with selection because 50% of data missing per sample was allowed instead of 10% elsewhere. A special caution must be given to that spectrum because low frequency is different than other. It may mean that the signal sampled is different in both cases.

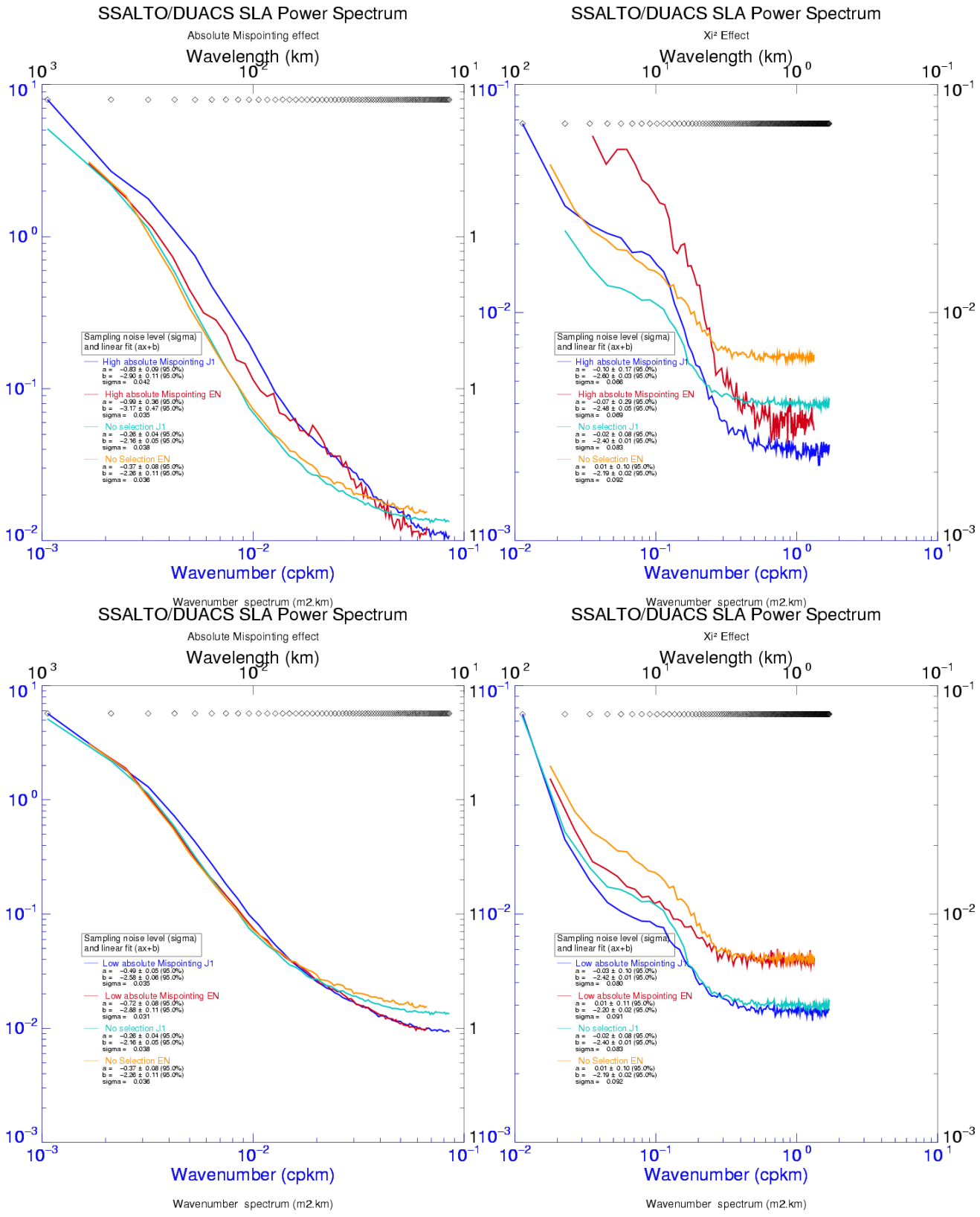

Figure 75: *Spectrums using high apparent mispointing Selection or not for 1Hz A (top left) and B 20Hz (top right). Spectrums using low apparent mispointing Selection or not for 1Hz C (bottom left) and 20Hz 50% of gaps allowed D (bottom right).*

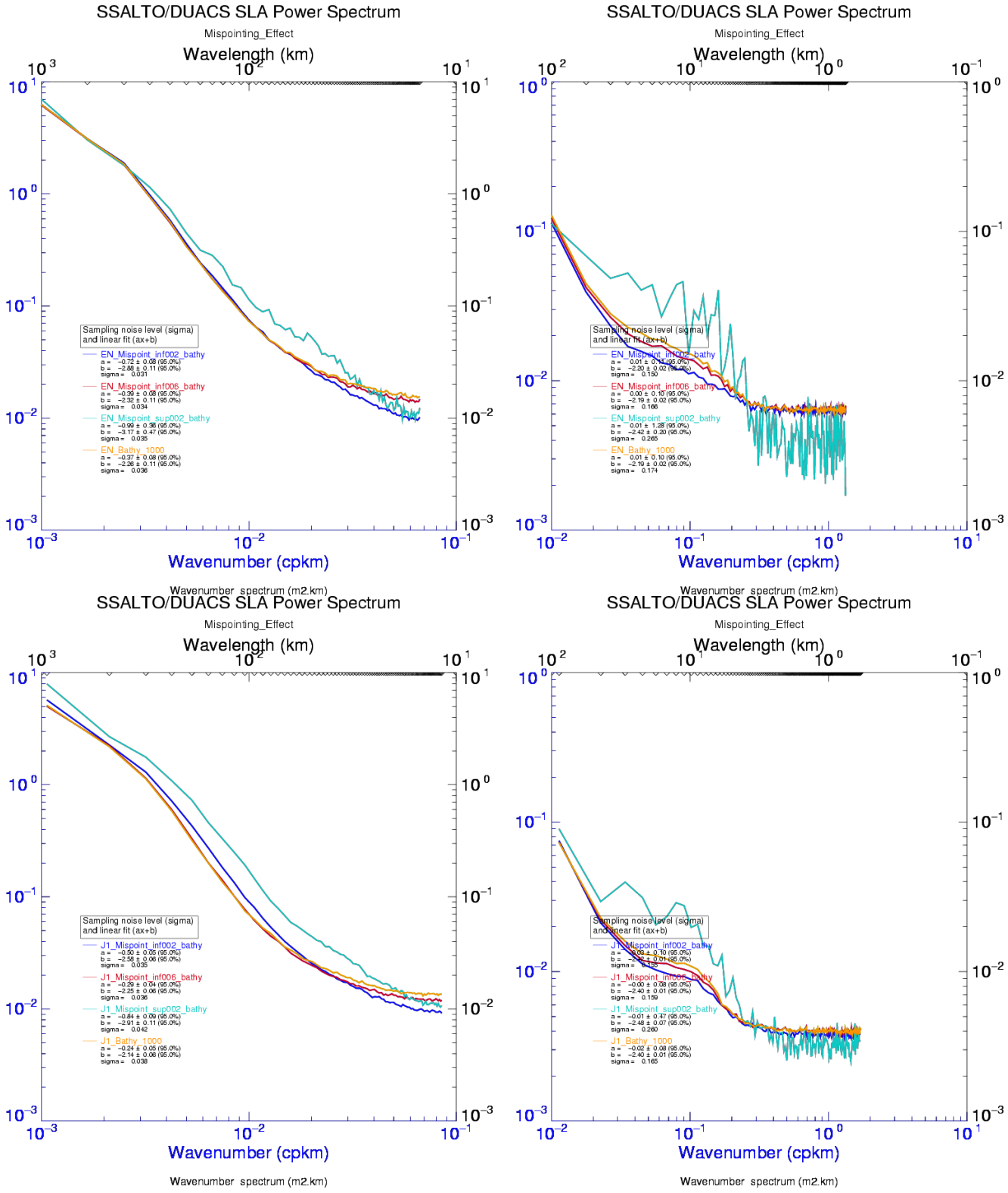

Figure 76: *Impact of selection on apparent mispointing on spectra for Envisat 1Hz A (top left) and 20Hz B (top right) and for Jason-1 20Hz C (bottom left) and 1Hz D (bottom right).*

On Figure 77, the continuity of 20Hz/1Hz spectra is specifically looked at. They show that with only the bathymetric selection or with an apparent mispointing lower than 0.06deg2 (Figure 77 A and C), 20Hz/1Hz spectra are not continuous. For an apparent mispointing lower than 0.02deg2 (Figure 77 B), Jason-1 spectrum are continuous unlike Envisat's. And for a high apparent mispointing greater than 0.02deg2, none of the missions have continuous 20Hz/1Hz spectra.

.

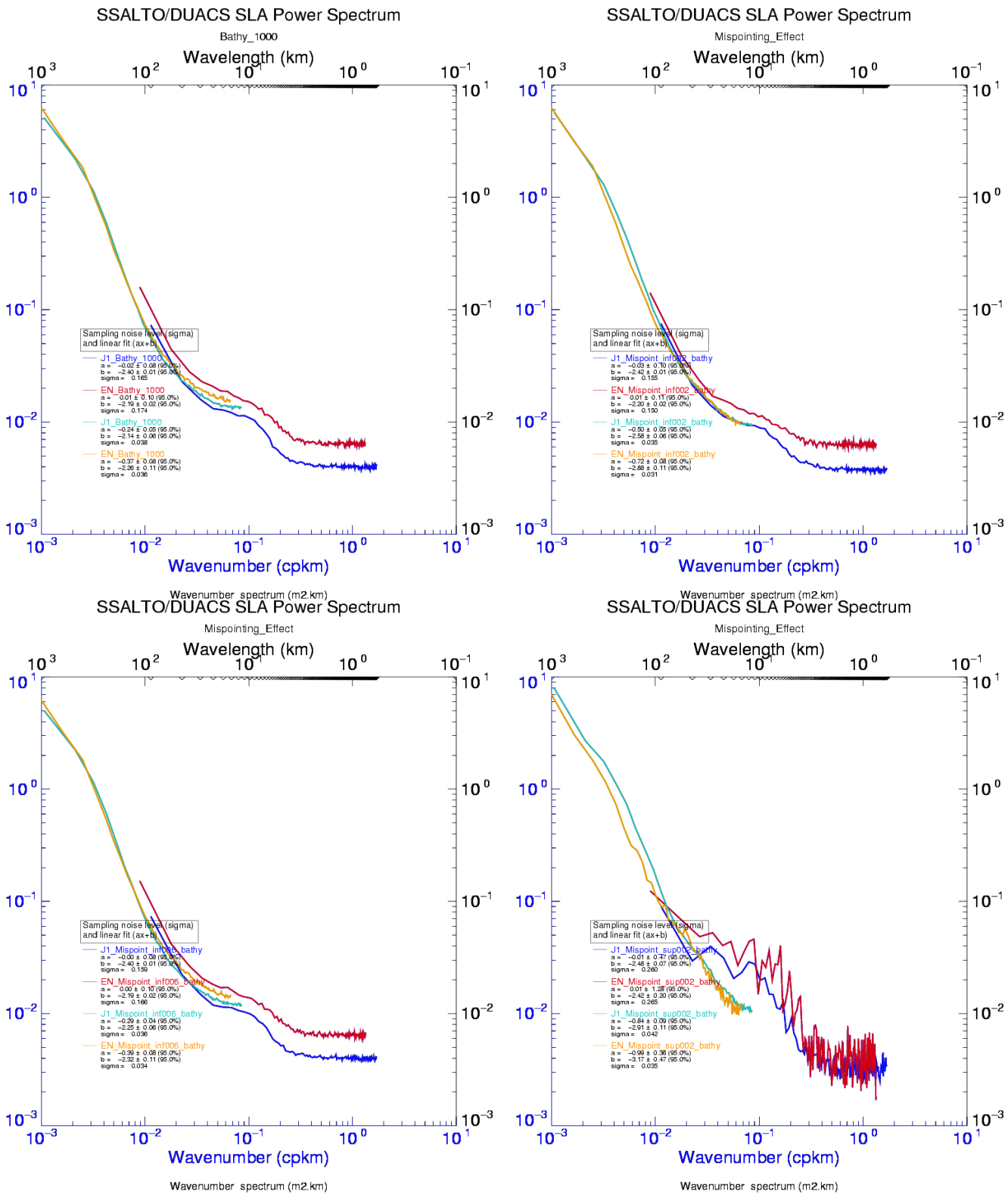

Figure 77: *Impact of selection on valid number per second on Envisat and Jason-1. Only Bathy selection A (top left), apparent mispointing lower than 0.02deg2 B (top right), apparent mispointing lower than 0.06deg2 C (bottom left), apparent mispointing greater than 0.02deg2 D (bottom right)*

Conclusion: These spectra drive us to the conclusion that when selecting only high apparent mispointing zones, the spectrum figures a strong signal in the zone 0.1-0.4Hz (20-70km) and the noise level is much decreased for both missions. On the contrary, the 0.1-0.4Hz bump disappears when sufficiently low apparent mispointing (lower than 0.02deg2) are selected, the noise level remains unchanged and Envisat and Jason-1 1Hz spectra are superimposed.

Therefore, high frequency content of SLA concerning the frequencies between 0.1-0.4Hz (between 20km and 70km) is (indirectly) correlated to high apparent mispointing zones. This bump is likely to be due to a particular answer of the range estimated in these zones.

Link with Figure 68: Figure 68 showed that the bump on the Jason-1 spectrum was significantly reduced when the apparent mispointing was estimated by the MLE4 (GdrB) compared of MLE3 (GdrA). Figures 75 now show that estimating the range on high apparent mispointing zones still provokes a signal on the range at a frequency of 20km -70km. Note that this size is typically the size of rain cells.

What do the high apparent mispointing zones correspond to? This is detailed in next part.

10.2.5 Meaning of the high apparent mispointing zones

Maps of high apparent mispointing show that high mispointing are mostly placed in humid zones but that they are also irregularly spread on all oceans. The high mispointing zones are looked at more precisely and related to physical data such as rain flags (Figure 78 right), sigma 0 value (Figure 80 left) or liquid water content (Figure 80 right).

Figure 78 (left and right) shows that a high apparent mispointing does not correspond systematically to an active rain flag.

Figure 79 (left and right) shows that on the points of high apparent mispointing,a high variability is observed on the range parameter.

And figure 80 (left and right) shows that high apparent mispointing points correspond to high values of liquid content and high sigma zero values.

The variability of those different parameters compared to the high apparent mispointing zones enables to conclude that in the high apparent mispointing zones, the waveforms seem to be polluted by a particular sea surface state (sigma bloom or rainy zone) which are not entirely identified by the current rain flag.

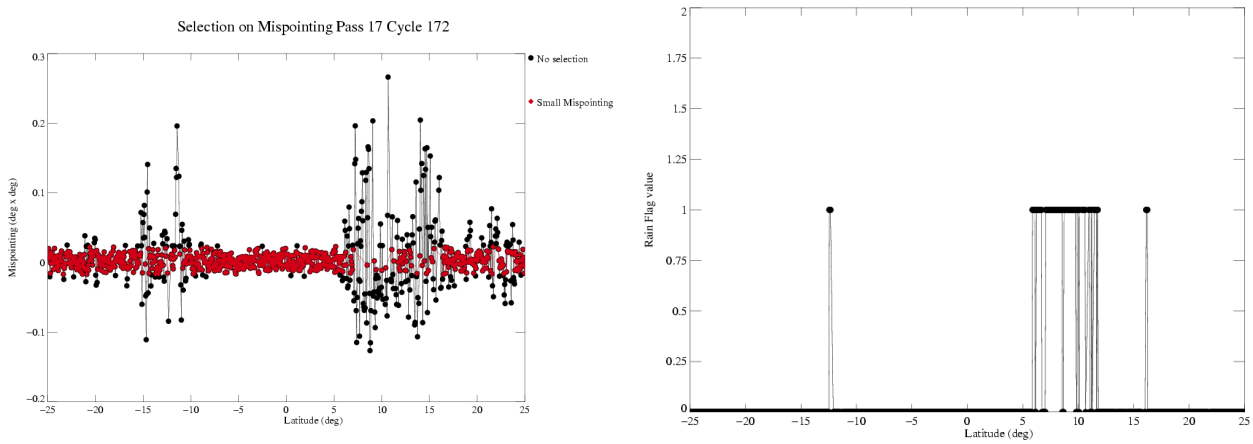

Figure 78: *Selection on apparent mispointing (left) small apparent mispointing red, high apparent mispointing black compared to the Rain flag value (right).*

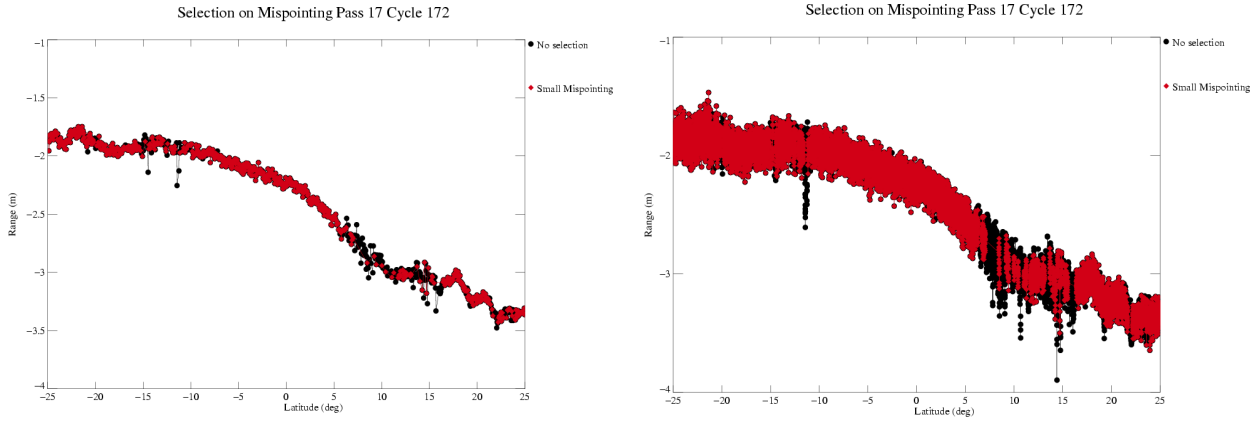

Figure 79: *Selection on apparent mispointing: on Range 1Hz (left), Range 20Hz (right).*

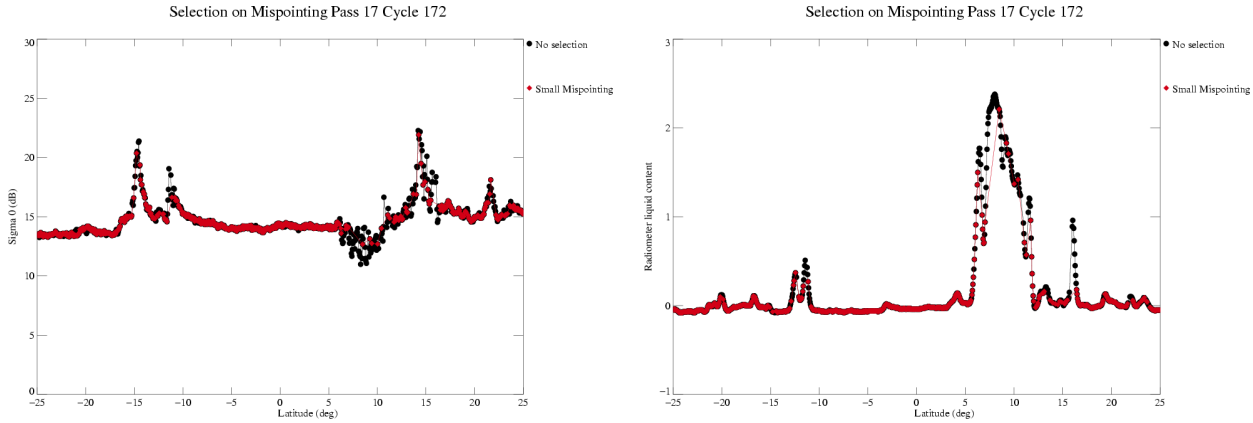

Figure 80: *Selection on apparent mispointing: on Sigma 0 (left), on Radiometer liquid content (right).*

The following selection applied on data before this new spectral analysis enables to show is a selection on rainy zones is equivalent or not to an editing on high mispointings. Three selections are applied on data:
- not rain flagged data, water content lower than 1, sigma0 greater than 17 (Figure 82)
- not rain flagged data, water content lower than 0.5, sigma0 greater than 17 (Figure 83)
- not rain flagged data, water content lower than 1, sigma0 greater than 17 and high mispointings selected in addition(Figure 84).

The third one (Figure 84) enables to see the impact of the high mispointing zones NOT situated in humid zones.

Figure 81 shows the corresponding spectrum. The two first editings enable to keep more than 90% of the data and do not change much the spectrum. But the third one enables to see that throughout the percentage (14% for Envisat and 26% for Jason-1) of data with a apparent mispointing higher than 0.02, less than 20% are situated in rainy zones, the rest being spread on all oceans ($\frac{(16-14)}{14}$=14% for Envisat and $\frac{(26-21)}{26}$=20% for Jason-1, see Figures 74).

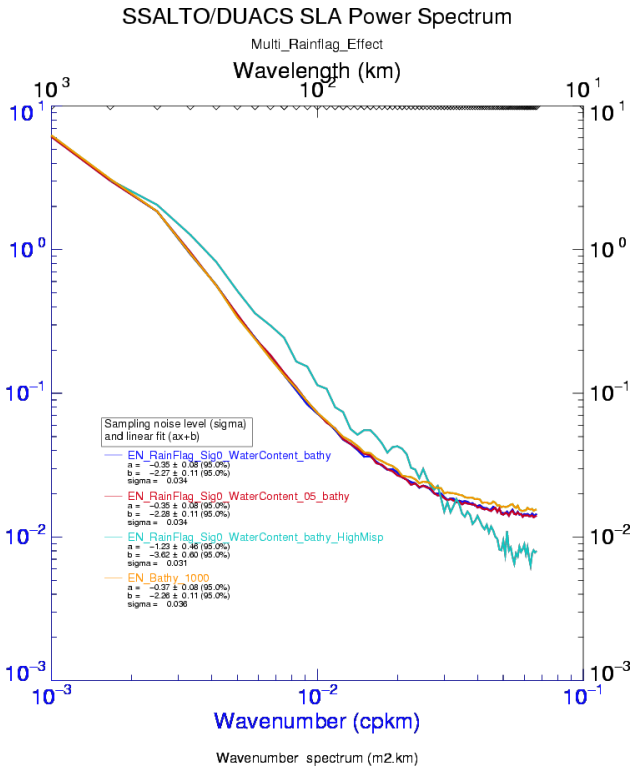

Figure 81: *Rain flag off, Water content lower than 1, Sigma0 greater than 17 effect.*

This test enables to show that the selection on these parameters is not equivalent to an editing on high mispointing because the 1Hz spectrum is unchanged with this selection unlike with the apparent mispointing threshold of 0.02.

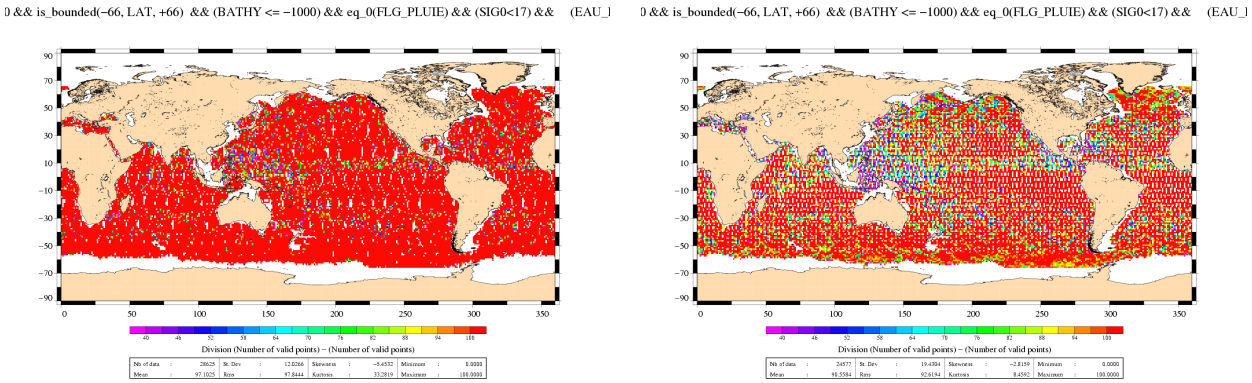

Figure 82: *Rain flag off, Water content lower than 1, Sigma0 greater than 17. Percentage of points used for the analysis on Envisat:97% (left) and Jason-1: 90.5% (right).*

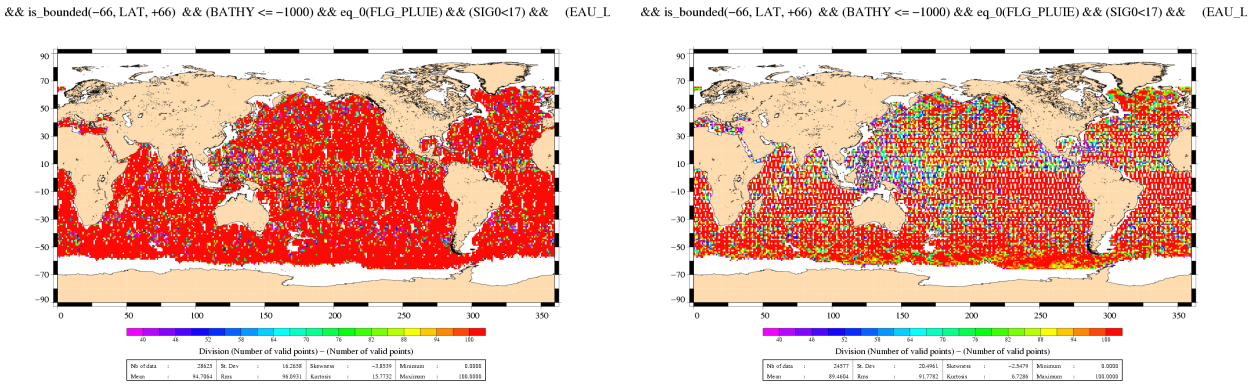

Figure 83: *Rain flag off, Water content lower than 0.5, Sigma0 greater than 17. Percentage of points used for the analysis on Envisat:95% (left) and Jason-1: 89.5% (right).*

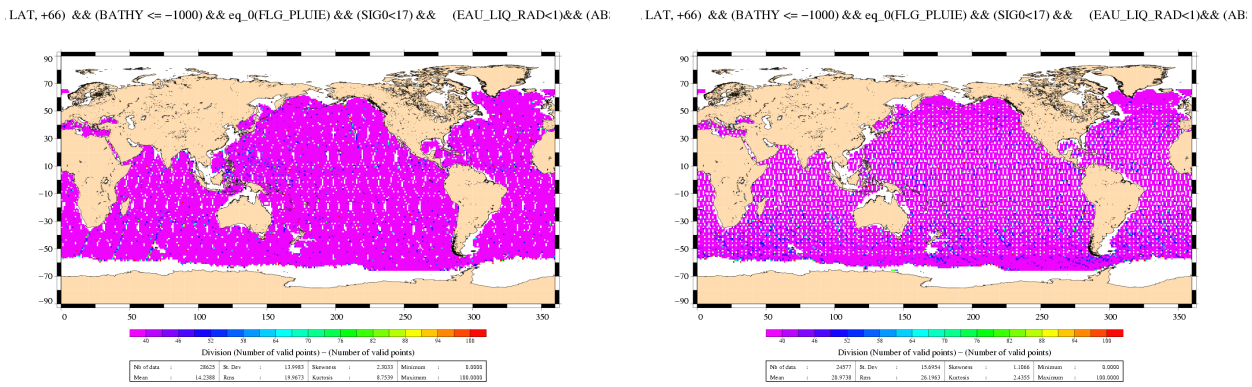

Figure 84: *Rain flag off, Water content lower than 1, Sigma0 greater than 17 and high mispointing (greater than 0.02). Percentage of points used for the analysis on Envisat:14% (left) and Jason-1: 21% (right).*

Conclusion: Envisat and Jason-1 are more consistent when mispointing is estimated on Jason-1. Furthermore, the energy bump around 0.1-0.4Hz disappears when high mispointing zones are excluded and increases when small mispointing zones are excluded.
High apparent mispointing zones seem to coincide with zones of high Sigma 0, high liquid content. However, a selection on these parameters is not equivalent to an editing on high mispointing in terms of 1Hz spectrum content.
More generally, high apparent mispointing zones seem to coincide with zones where waveforms differ from the ocean model and for the moment, no equivalent editing could be identified.

Remark: The rain flag used here is not properly adapted to these data. Actually, this flag is computed with parameters (sigma 0 among others) estimated with a MLE3 whereas the data studied are derived from a MLE4 estimator. The efficiency of the rain falag might be affected.

Furthermore, Envisat and Jason-1 are more different on high mispointing zones than elsewhere at 1Hz. This means that both missions show differences in the processing of such atypical waveforms on Envisat and Jason-1 missions. A difference of processing is their editing, more 20Hz data are considered as valid on Envisat than on Jason-1. Next part deals with the comparison of editing for both missions, specifically on high apparent mispointing zones.

10.2.6 Compression editing comparison of both missions and impact on spectral analysis

On Envisat, the number of valid points per second is almost always 20.
Contrarily, on Jason-1, the number of valid points per second varies more, between 15 and 20, depending on the zone.

Figures 85 show that the zones where the number of valid data is weaker for Jason-1 than for Envisat also corresponds to the zones where apparent mispointing takes its extremes values.

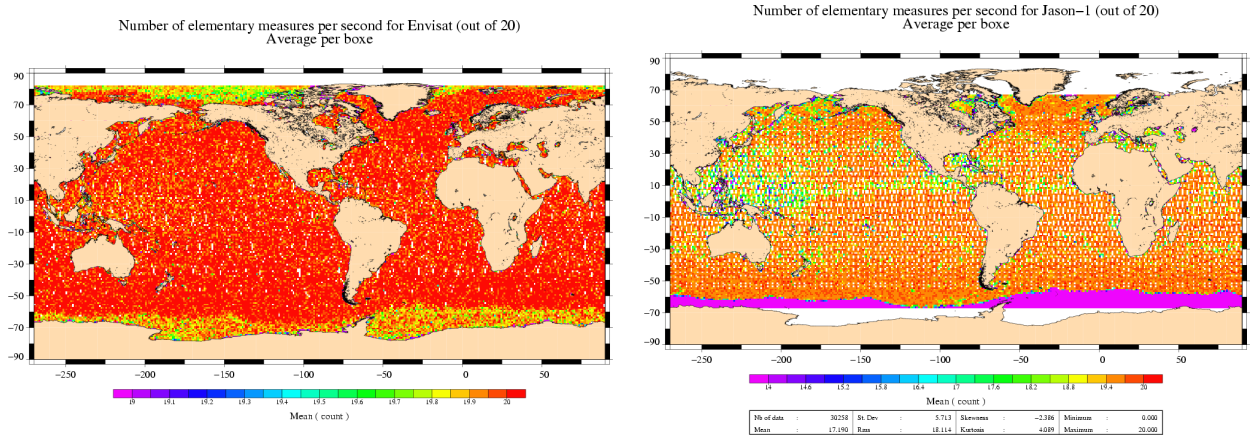

Figure 85: *Number of valid points per second averaged per 2°*2° boxes for Envisat (left), Jason (right).*

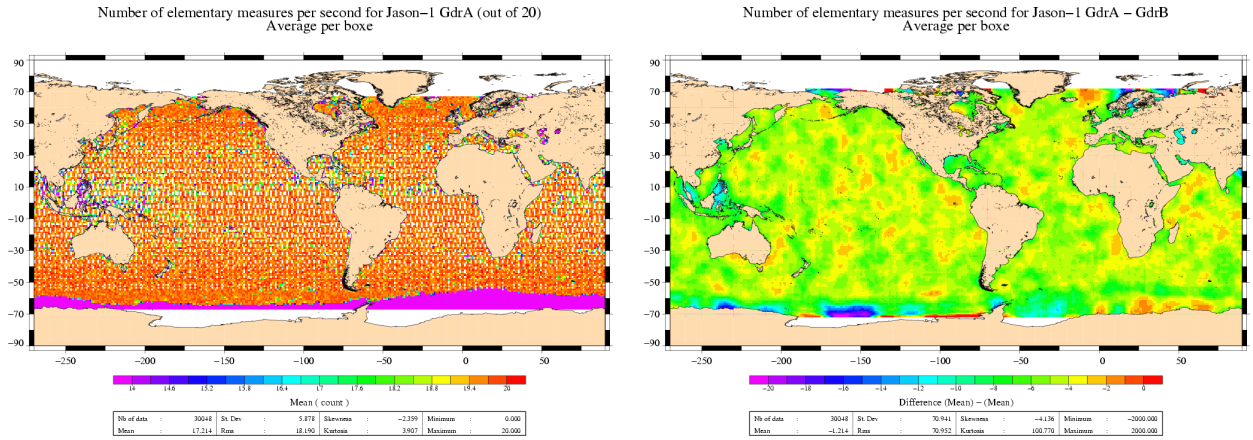

Figure 86: *Percentage of valid points greater than 17 out of 20 per second averaged per 2°*2° boxes for Jason-1 GdrA (left), GdrA-GdrB (right). Cycle 100.*

This may have an impact during the compression step (average of the elementary measurements to 1Hz) as the number of data out of 20 used for the average is different for both missions. However, when comparing the number of valid data per second between Jason-1 GdrA-GdrB on cycle 100 where both GdrA and B

exist (Figure 86) it is seen that the increasing of valid data per second is geographically homogeneous. This means that the noise reduction does not directly come from the increasing of valid data per second.

To find out the impact of the number of valid data per seconds on the high frequency content, a spectral analysis was performed with three selections: number of valid data per seconds out of 20 greater than 17, 18 and 19 (that is to say equal to 20).
Figures 87 to 89 show the repartition of values taken for the analysis.

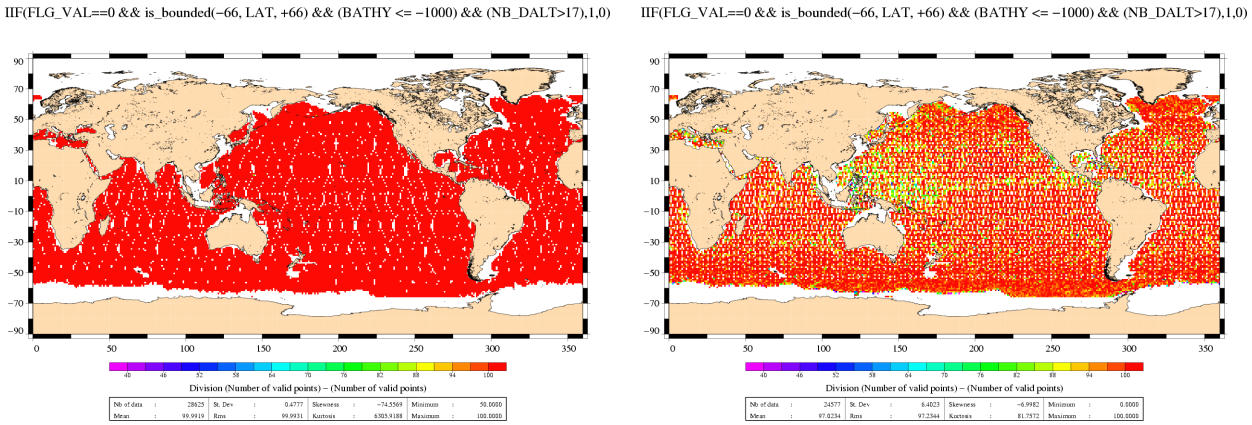

Figure 87: *Number of valid data per second greater than 17. Percentage of points used for the analysis on Envisat: 99.99% (left) and Jason-1: 97% (right).*

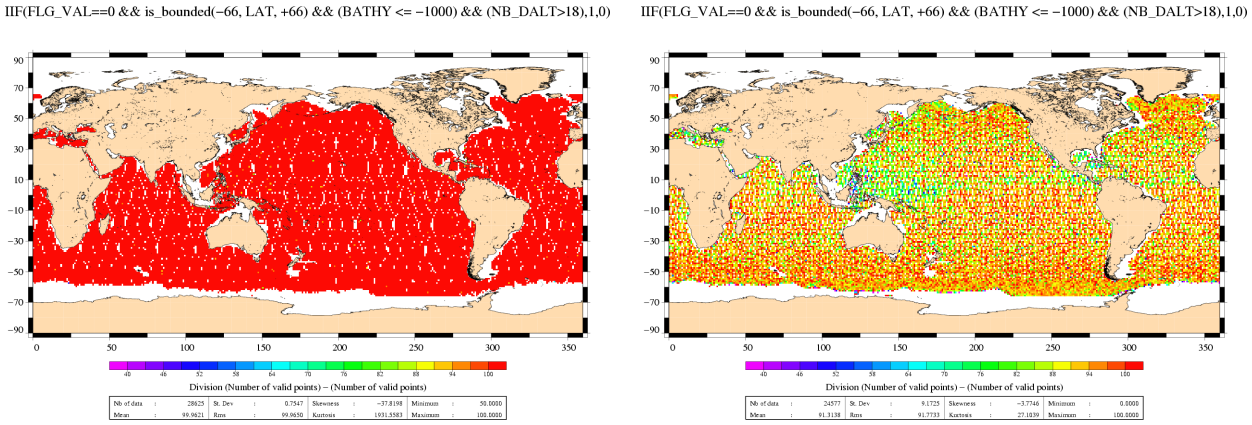

Figure 88: *Number of valid data per second greater than 18. Percentage of points used for the analysis on Envisat: 99.96% (left) and Jason-1: 91% (right).*

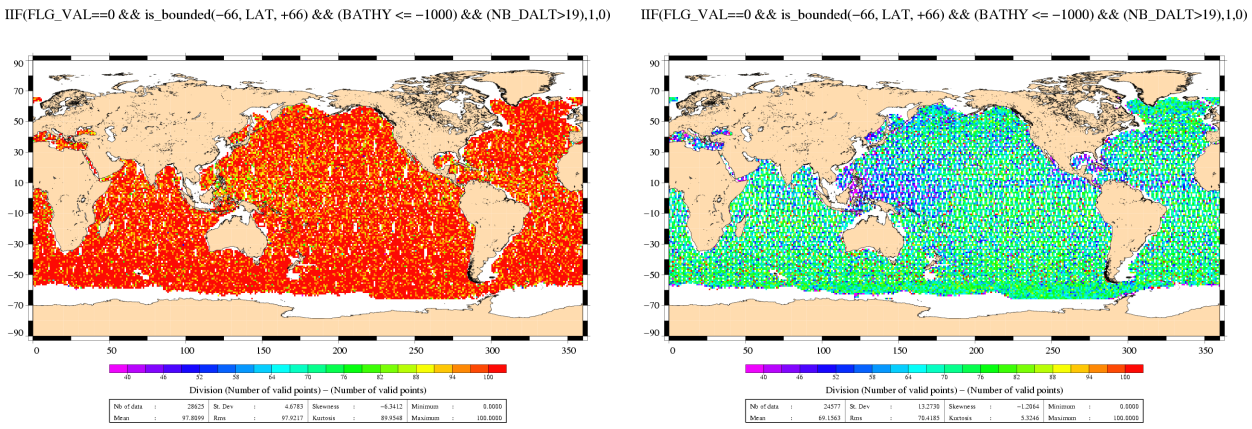

Figure 89: *Number of valid data per second greater than 19. Percentage of points used for the analysis on Envisat: 98% (left) and Jason-1: 69% (right).*

Figures 90 show the impact of the selections on the spectra. It is seen that the selection on valid number per second is important for Jason-1, and has no impact on Envisat.

Figures 90 show that the highest the threshold the closer the 1Hz and 20Hz spectra and on Figure 90 D, it is also seen that the shape of Jason-1 spectrum is similar to the one done with mispointing higher than 0.02 (Figure 90 C-D). This is probably due to the fact that high mispointing zones also have a lower rate of valid number per second.

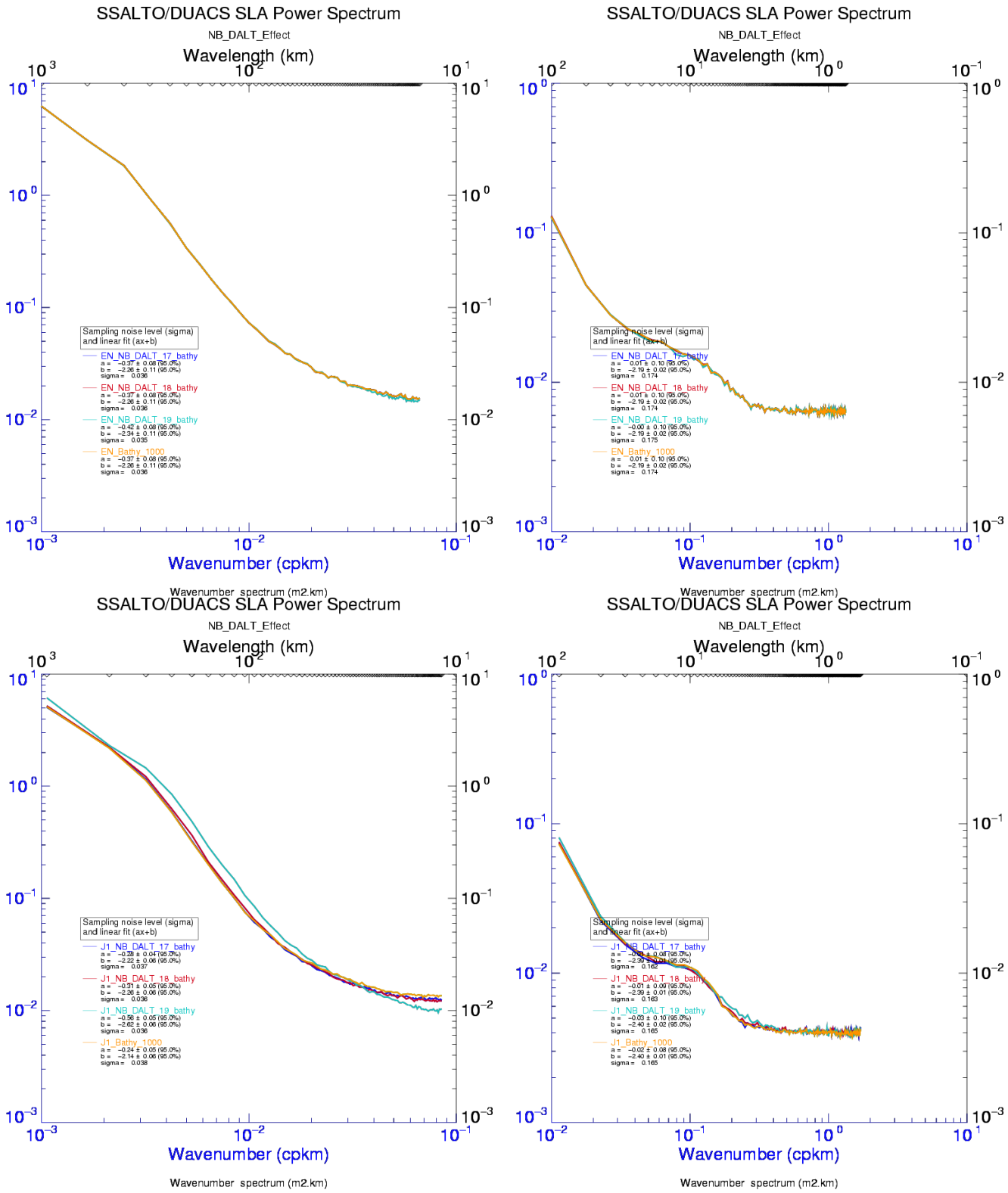

Figure 90: *Impact of selection on valid number per second on spectra for Envisat 20Hz A (top left) and 1Hz B (top right) and for Jason-1 20Hz C (bottom left) and 1Hz D (bottom right).*

Conclusion: The number of valid number of data per second has no impact on Envisat, unlike on Jason-1 where a selection of 20 valid values per seconds enables to obtain a spectrum similar to the one obtained with mispointing higher than 0.02.
This means that the 20Hz editing is different on both missions and that this impacts the high frequency content.

Two questions are raised:
- Why is the number of data lower on Jason-1 than on Envisat? Do Jason-1 aquire fewer data? or does its processing edit more data?
- For the points where few data are kept: is the 1Hz average less robust because there is less data? or are the remaining waveform still degraded which unvalidates the retracking?

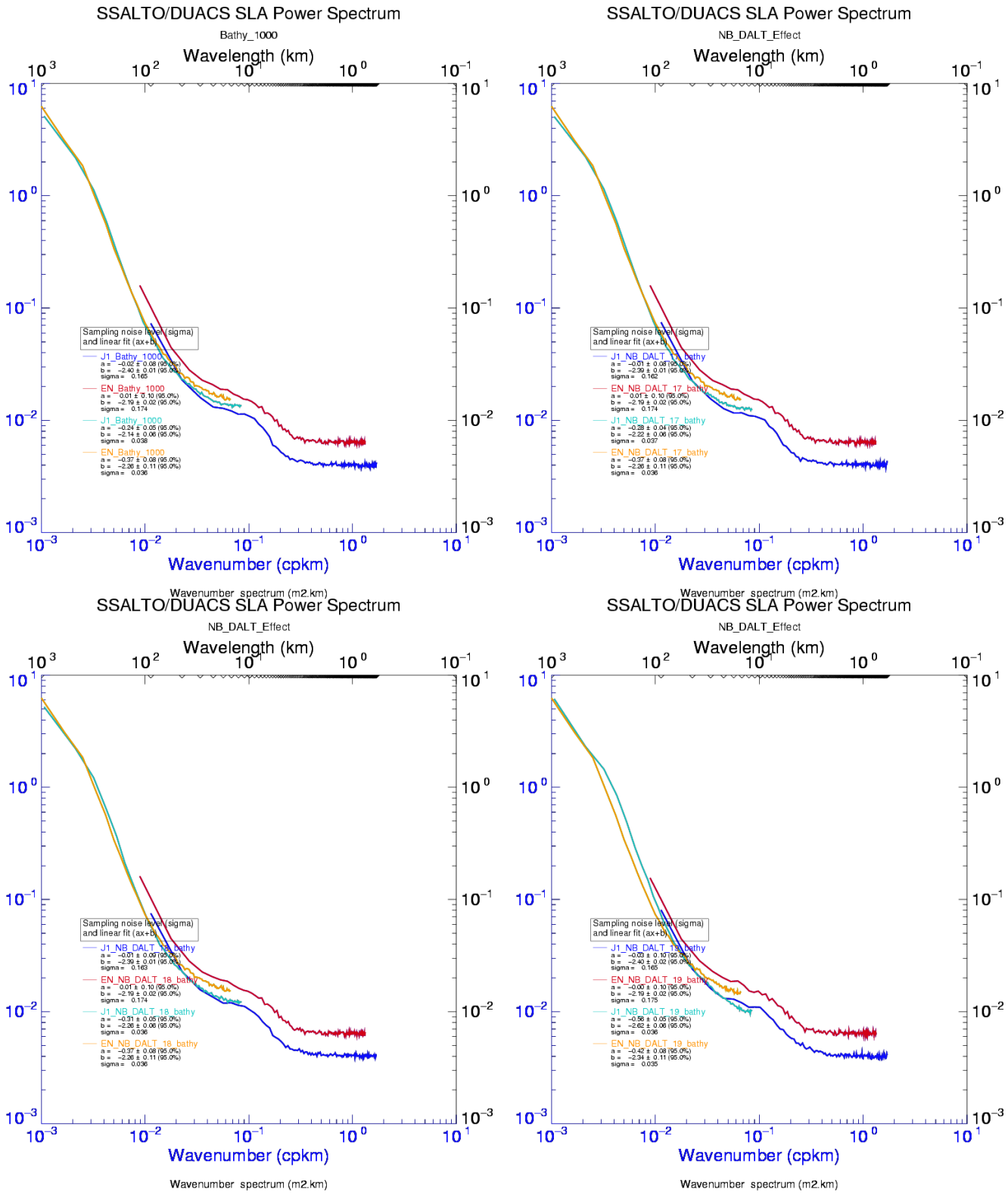

Figure 91: *Impact of selection on valid number per second on spectra for Envisat and Jason-1. Only Bathy selection A (top left). More than 17 values per seconds B (top right). More than 18 values per seconds C (bottom left), More than 19 values per seconds D (bottom right).*

10.2.7 SWH effect

The high frequency content of SLA is well known to be related with the noise level, itself related to the wave height. It is known that the higher the waves, the greater the noise because the retrodiffusion on a stormy sea is more affected by speckle than a calm sea and because the speckle of the sea is related to the noise of the oceanic parameters estimation.

Because small wave areas are also correlated with wet zones (like high apparent mispointing), a spectral analysis is performed with selections on waves. Spectra are plotted for three classes of waves:
- High waves (between 3 and 11m)
- Average waves (between 1.5 and 3m)
- Small waves (between 50 cm and 1.5m)

Figures 92 to 94 represent the amount of data selected for each class of waves. Each class represents a percentage of the data which can be very small concerning the small waves (10 and 14%) but the impact on spectra quality is less important than for apparent mispointing selection because the samples selected are much more continuous, due to the physic continuity of wave series.

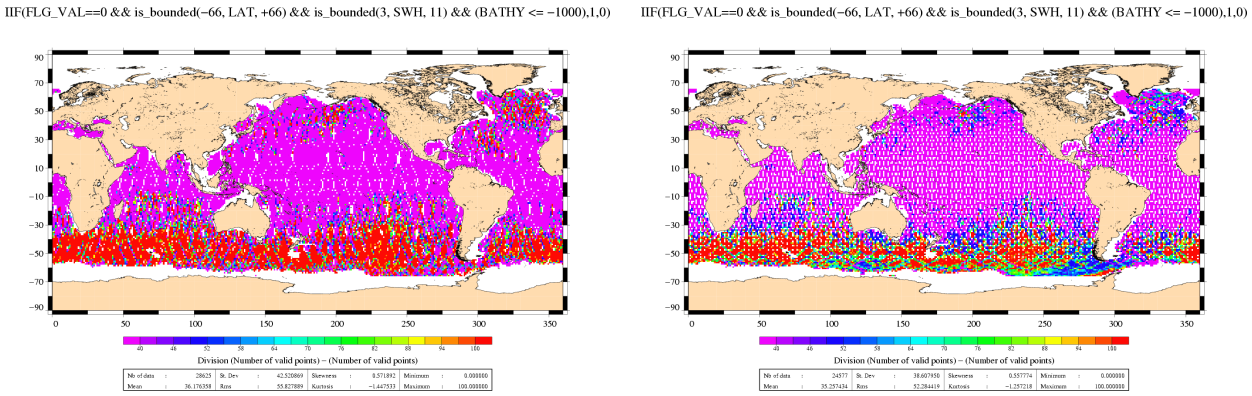

Figure 92: *High waves (between 3 and 11m). Percentage of points used for the analysis on Envisat 36% (left) and Jason-1 35% (right).*

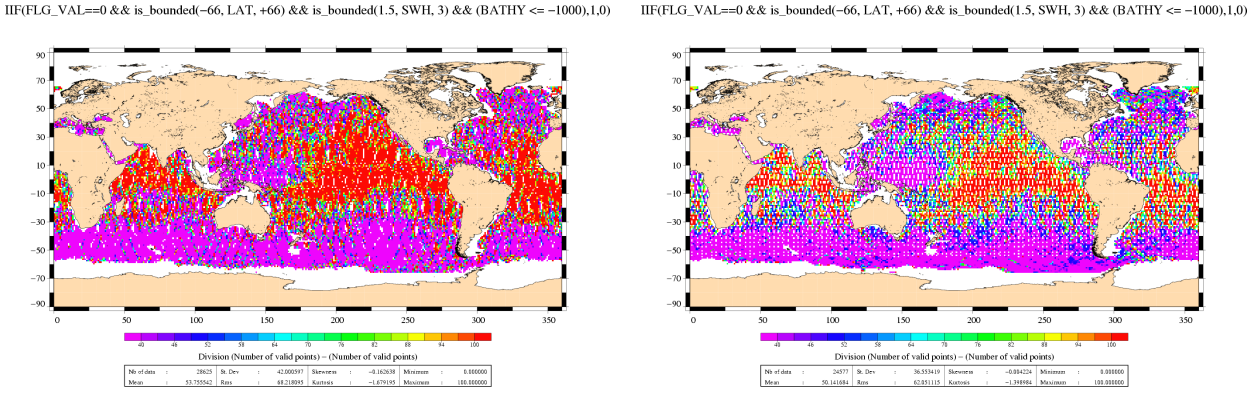

Figure 93: *Average waves (between 1.5 and 3m). Percentage of points used for the analysis on Envisat 54% (left) and Jason-1 50% (right).*

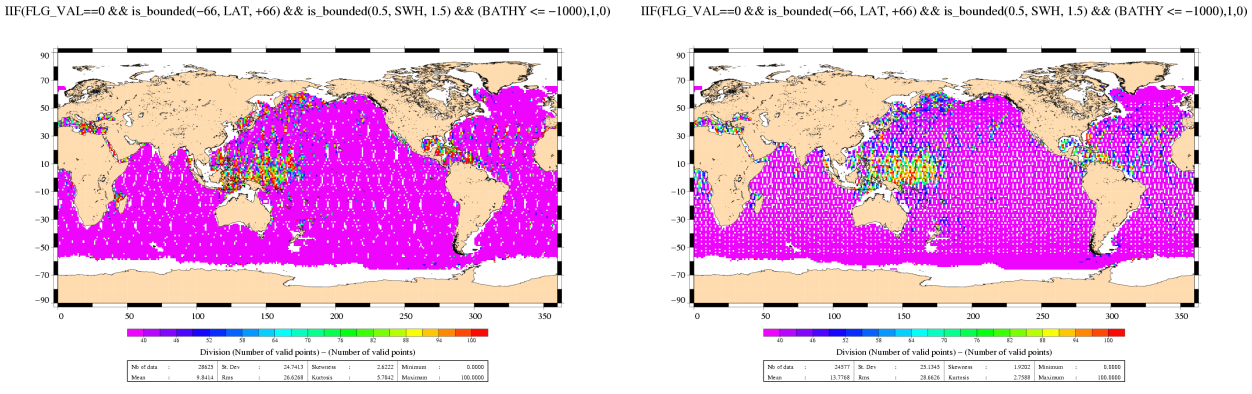

Figure 94: *Small waves (between 50cm and 1.5m). Percentage of points used for the analysis on Envisat 10% (left) and Jason-1 14% (right).*

The impact of wave selection on spectra is seen on Figures 95. Without any surprise, it shows that the higher the waves the higher the noise. But it is also seen on Figure 96 that for both missions, small waves are more correlated at 20-70km frequency than high waves. On Envisat, this phenomenon is even stronger.

The remark must be taken cautiously because of the small amount of data concerned (10%) but the same tendency is also observed on other selection because average waves are also more correlated at 20-70km frequency than high waves.

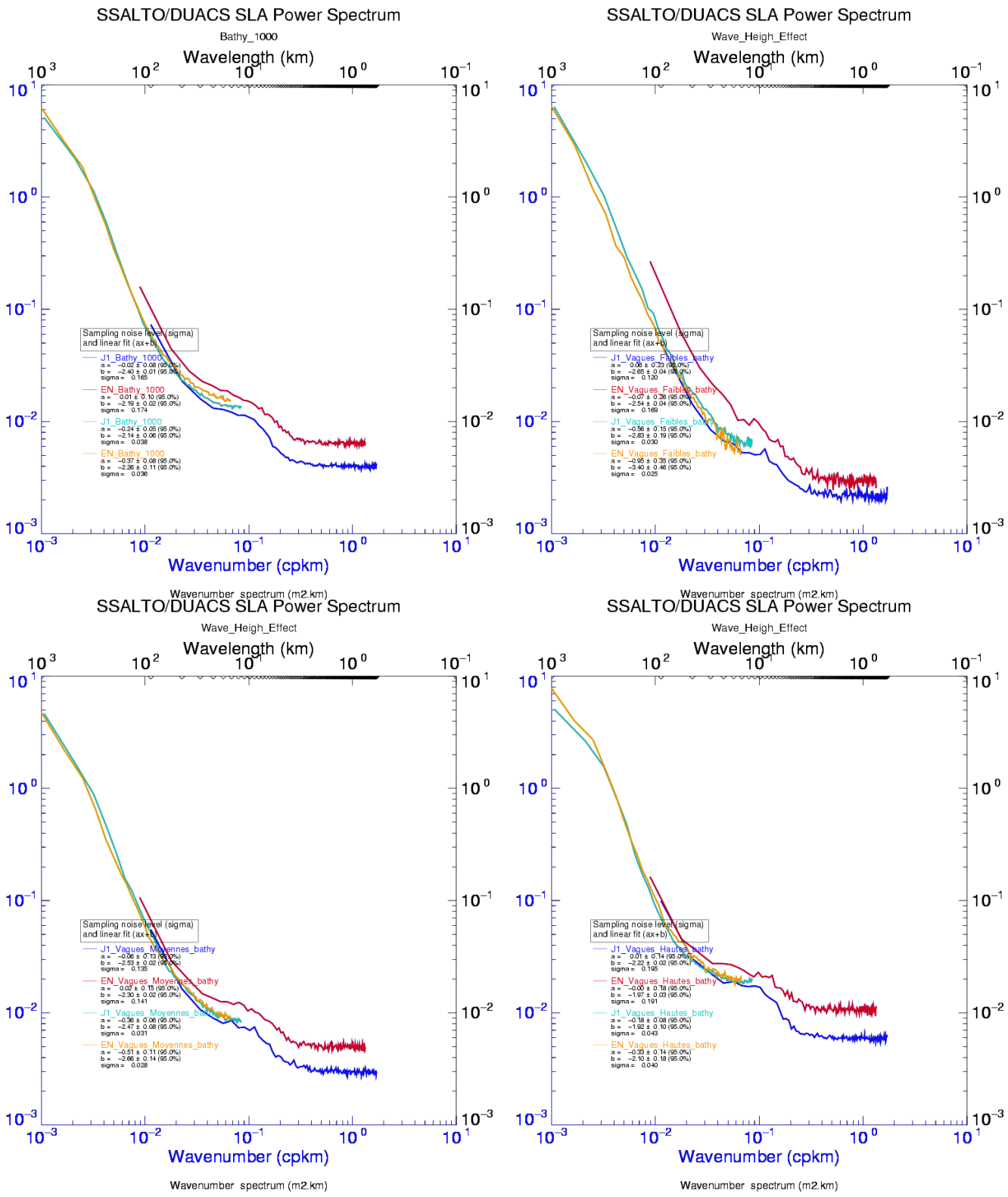

Figure 95: *Impact of selection on Wave height on Envisat and Jason-1. No Selection A (top left). Small waves (between 50cm and 1.5m) B (top right).Average waves (between 1.5 and 3m) C (bottom left). High waves (between 3 and 11m) D (bottom right)*

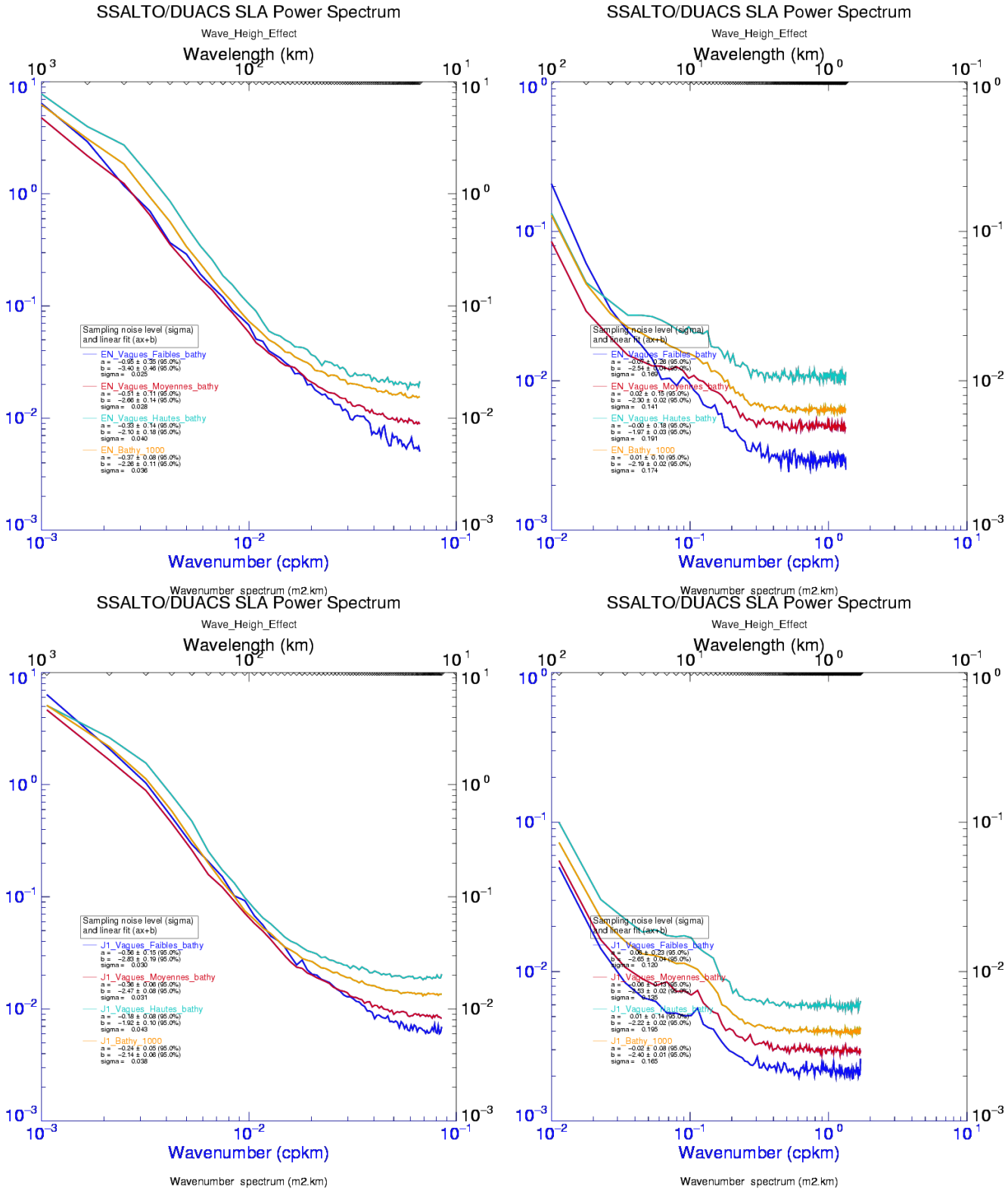

Figure 96: *Impact of selection on Wave height on spectra for Envisat 20Hz A (top left) and 1Hz (top right) and for Jason-1 20Hz C (bottom left) and 1Hz D (bottom right).*

Concerning the 20Hz noise level, it is seen that the dependency in wave class is slightly different for Envisat and Jason-1. Figure 97 confirms that Envisat and Jason do not have exactly the same dependency in wave height. Envisat (red dotted line) increases faster than Jason (blue dotted line). This can explain the difference of noise level observed on Figures 96.

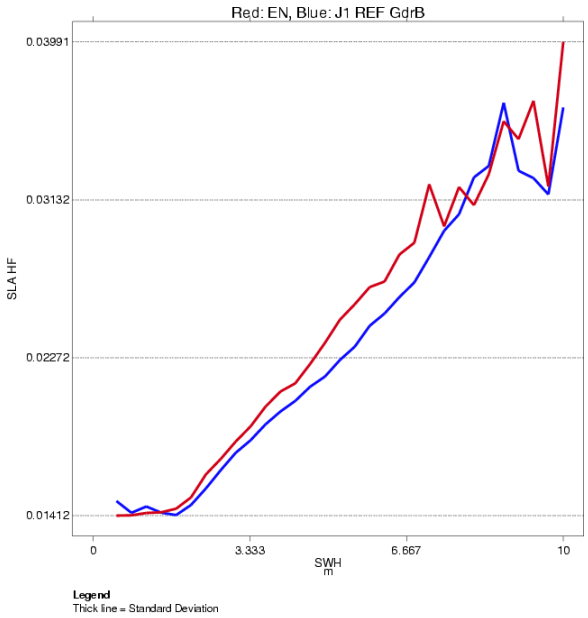

Figure 97: *Dispersion diagram of SLA high frequency as a function of wave height.*

Conclusion: The spectral analysis performed with wave selection shows that the selection on small wave reduces the 0.1-0.4Hz bump on SLA spectra but in the meanwhile, it reduces the noise plateau. Even if the small wave zones coincidate with the humid zones, and more or less to high mispointing zones, spectra are not equivalent. An interesting point is however that for Jason-1, a very located peak appears for average and small waves at precisely 10km wavelength.

10.2.8 Conclusion

This document is a comparison of the high frequency observed by Envisat and Jason-1 missions, with 20Hz and 1Hz data. Preliminary studies had shown that the high frequency content was different on both missions and concerning Jason-1, different when analysing GdrA or GdrB. This new study enables to precise the questions raised by that these analysis.

Contrarily to the theoretical ocean spectrum which is mostly a low frequency signal + high frequency noise, Envisat and Jason spectrum present a bump in a frequency bandwidth of 20km to 70km which is likely to be due to a signal appearing or disappearing with this frequency. It is shown that Envisat and Jason-1 are more consistent when apparent mispointing is estimated on Jason-1. Furthermore, the energy bump around 0.1-0.4Hz disappears when high apparent mispointing zones are excluded and increases when small apparent mispointing zones are excluded.

High apparent mispointing zones seem to coincide with zones of high Sigma 0, high liquid content. However, a selection on these parameters is not equivalent to an editing on high mispointing in terms of 1Hz spectrum content. This seems to be confirmed by three points:
- editing humid zones (by flag and sigma0) does not give the same results as editing high mispointing.
- editing high mispointing except humid zones gives the same results as editing high mispointing alone.
- editing small wave height (which is another way of avoiding humid zones) does not give the same results as editing high mispointing.

More generally, this document shows that the bump seems to be due to data localised on zones where waveforms differ from the ocean model. This seems to be confirmed by the fact that:
- applying a selection of 20 valid values per seconds for Jason-1 enables to obtain a spectrum similar to the one obtained with mispointing higher than 0.02.

Unlike Jason-1, editing Envisat valid values per seconds does not enable to edit atypical waveforms. The difference of valid values per seconds for both data raise two questions:
- Why is the number of data lower on Jason-1 than on Envisat? Do Jason-1 aquire fewer data? or does its processing edit more data?
- For the points where few data are kept: is the 1Hz average less robust because there is less data? or are the remaining waveform still degraded which unvalidates the retracking?

For the moment, no physical editing of atypical waveforms could be identified although the apparent mispointing or the number of valid values per seconds (for Jason-1) are good candidates.

Further analysis would be needed to understand the processing of atypical waveforms:
- the differences of editing on both missions must be analysed in order to understand why more data are edited on Jason-1 than Envisat.
- the waveforms situated on zones where the mispointing is high and where the number of valid data per second is low must be looked at more precisely in order to identify the causes of the range instability which seems to cause the bump.